JSCSEN 73(6)597–681(2008)

Journal of the Serbian Chemical Society

Electronic version

VOLUME 73

NO 6

BELGRADE 2008

Available on line at

www.shd.org.rs/JSCS

The full search of JSCS is available through

DOAJ DIRECTORY OF OPEN ACCESS JOURNALS

www.doaj.org

Journal of the Serbian Chemical Society
JSCS@tmf.bg.ac.yu • www.shd.org.yu/JSCS

J. Serb. Chem. Soc. Vol. 73, No. 6 (2008)

CONTENTS

Published by the Serbian Chemical Society
Karnegijeva 4/III, 11120 Belgrade, Serbia
Printed by the Faculty of Technology and Metallurgy
Karnegijeva 4, P.O. Box 35-03, 11120 Belgrade, Serbia

www.shd.org.rs

Journal of the Serbian Chemical Society

JSCS@tmf.bg.ac.yu • www.shd.org.rs/JSCS

J. Serb. Chem. Soc. 73 (6) 597–607 (2008) UDC **Sempervivum marmoreum* L.+66.061:615.28
JSCS–3742 *Original scientific paper*

Comparative screening of the anti-oxidant and antimicrobial activities of *Sempervivum marmoreum* L. extracts obtained by various extraction techniques

SAŠA S. STOJIČEVIĆ[1], IVANA T. STANISAVLJEVIĆ[1#], DRAGAN T. VELIČKOVIĆ[2], VLADA B. VELJKOVIĆ[1#] and MIODRAG L. LAZIĆ[1*#]

[1]*Faculty of Technology, Bulevar oslobodjenja 124 and* [2]*Zdravlje-Actavis, Vlajkova 199, 16000 Leskovac, Serbia*

(Received 10 September, revised 31 December 2007)

Abstract: This paper presents a comparative study of the anti-oxidant and anti-microbial activities, total phenolic compounds and total flavonoids in extracts obtained from houseleek (*Sempervivum marmoreum* L.) leaves by the classical (maceration), ultrasonic and Soxhlet extraction (CE, UE and SE, respectively). The extract obtained by the CE contained higher amounts of phenolic and flavonoid compounds and showed a better antioxidant activity than those obtained using other two techniques. All the extracts, independent of the extraction technique applied, showed antimicrobial activities against *Aspergillus niger* and *Candida albicans* only but not against the tested bacteria.

Keywords: antimicrobial activity; anti-oxidant activity; extraction; houseleek; *Sempervivum marmoreum* L.; ultrasound.

INTRODUCTION

Houseleek (*Sempervivum marmoreum* L., syn. *S. erytreum, S. italicum*) is an evergreen endemic plant on the Balkan Peninsula.[1] The genus *Sempervivum* contains about 50 species which occur predominantly in rocky places and at higher altitudes.[2] Therapy with preparations of *Sempervivum* species can be traced back to the origins of antique herbal medicine but the extracts of their leaves have not yet been introduced into medical practice. The earliest publications concerning the therapeutic use of this drug deal with its influence on pharingitis, tracheitis, thrush, combustion and otitis.[3] Strewn over wounds, sores, burns, abscesses or painful areas, the fresh juice from squeezed leaves of *S. tectorum* is used as a refrigerant and astringent, a sure remedy for insect bites, as well as to ease ear pains and inflammations, while the tea prepared from its leaves is recommended for ulcer treatment.[4]

Serbian Chemical Society member.
* Corresponding author. E-mail: lmiodrag@yahoo.com
doi: 10.2298/JSC0806597S

The benefits of juice and tea prepared from the leaves of *S. tectorum* can be attributed to the presence of many bioactive compounds, such as oligomeric and polymeric polyphenols, phenol carboxylic acids, ascorbic, citric malic acids, flavones- and flavonol-mono- and diglycosides with kaempferol and quercetin as aglycones, tannins, coumarines, oligo- and polysaccharides.[3,5,6] Polyphenols are present in 4.2 %, flavonoids in 0.70 % and polysaccharides in 11.2 %.[7] Glycosides of kaempferol, quercetin, isorhamnetin, scutellarein, myricetin, herbacetin, proanthocyanidins (prodelphinidin and procyanidin) and delphinidol were isolated from *Sempervivum* sp. extracts.[2,4] Rhamnose, arabinose, xylose, mannose and galactose are characteristic monosaccharides.[3] The extract of *S. tectorum* exhibited a genuine superoxide scavenger activity in a cell-free system, which suggested that this extract might also act as a direct scavenger of O_2^- in biological samples.[8] The antioxidant activity and antinociceptive effect of *S. tectorum* extracts were shown both *in vivo* and *in vitro*.[3,9] It was also found that *S. tectorum* extracts had a lipid-lowering effect in rats,[7] free radical scavenger, membrane stabilizing, and antimicrobial activity against *Staphylococcus aureus, Bacillus cereus, Enterococcus faecalis* and *Geotrichum* sp., while the growths of *Escherichia coli, Proteus morgani* and *Saccharomyces cerevisiae* were slightly inhibited.[4] The dominant cations are Ca (76.2 mg/g), K (40.47 mg/g) and Mg (817.85 mg/g),[3] while no toxic elements were detected in *S. tectorum* extracts.[10]

Recently, it was shown that ultrasound-assisted extraction (UE) is an efficient alternative to conventional extraction techniques.[11] The main benefits of the use of ultrasound are an increased extraction yield, a faster process and even an improved quality of the extracts. Ultrasound can also reduce the operating temperature, allowing the extraction of thermolabile compounds. UE has already been employed in the extraction of bioactive compounds of interest to the pharmaceutical and food industries, such as a phenolic component of coconut shell,[12] flavonoids from *Hypericum perforatum* L.[13] and anti-oxidants from *Rosmarinus officinalis*.[14]

To the best of our knowledge, there have been no reports on the extraction efficiency and kinetics of extractive substances (ES) from *S. marmoreum* leaves. Furthermore, no comparative study of the anti-oxidant and antimicrobial activities of its extracts obtained by different extraction techniques has hitherto been reported. To date, the extracts of *Sempervivum* sp. leaves have been prepared only by a two-step stirring-assisted maceration at room temperature, using methanol as the extracting solvent.[4]

In the present study, the extraction of ES from fresh leaves of *S. marmoreum* L. by UE, classical solvent extraction (CE) and Soxhlet extraction (SE) using methanol as the extracting solvent was investigated. The main goal was to compare the anti-oxidant and antimicrobial activities of the extracts obtained by the different extraction techniques. In addition, the yields of ES, total phenolic com-

pounds and flavonoids in the extracts obtained by the different methods were compared. The potential of methanolic extracts of *S. marmoreum* leaves for practical applications has not previously been studied in detail, thus this study provides important information concerning the natural anti-oxidants and antimicrobials present in the leaves of *S. marmoreum*.

EXPERIMENTAL

Materials

The plant material was harvested by hand in the morning, before the blooming period (South Serbia, Mt. Suva Planina, 1500 m, in the second half of May, 2006). The leaves were removed from the rosette and roots, washed, dried in the shadow, chopped and used immediately. The moisture content, determined by drying at 105 °C to constant weight, was 88.1 %.

Methanol was from Zorka-Pharma (Šabac, Serbia). Folin-Ciocalteu reagent, 2,2-diphenyl-1-picrylhydrazil (DPPH), gallic acid and rutin were obtained from Sigma (St. Louis, MO). Sodium carbonate, potassium acetate and aluminum chloride were purchased from Merck-Alkaloid (Skopje, FYR Macedonia).

Seven microorganisms were selected to test the antimicrobial activity: *Escherichia coli* ATCC 25922, *Pseudomonas aeruginosa* ATCC 9027, *Bacillus subtilis* ATCC 6633, *Staphylococcus aureus* ATCC 6538, *Candida albicans* ATCC 10231, *Saccharomyces cerevisiae* ATCC 9763 and *Aspergillus niger* ATCC 16404 (Oxoid, England). The tested bacteria were grown on Trypton soya agar (TSA, Merck), while Sabouraud dextrose agar (SDA, Merck) was used to grow the yeast and the mould. Plate count agar (Merck) was used for determining the total number of microorganisms (CFU/ml).

Soxhlet extraction

Chopped fresh leaves (10 g) and methanol (100 ml) were put into a Soxhlet apparatus. The solvent was boiled and refluxed for a period of 150 min (eleven extraction cycles). The liquid extract was evaporated under vacuum at 40 °C to constant weight. This yield of ES (g/100 g of fresh plant material) was taken to represent the content of ES in the plant material.

Classical extraction

Chopped fresh leaves (5.0 g) and methanol (50 ml) were put into Erlenmeyer flasks and placed in a thermostated water bath. The extraction was performed at 25±0.1 °C for 2.5, 5, 10, 20, 40 and 60 min. At the end of the extraction cycle, the liquid extract was separated from the solid residue by vacuum filtration. The solid residue was washed twice with fresh solvent (20 ml). The filtrates were collected and the solvent was evaporated in a rotary vacuum evaporator at 40 °C.

Ultrasonic assisted extraction

Chopped fresh leaves (5.0 g) and methanol (50 ml) were put into Erlenmeyer flasks (100 ml), which were then placed into an ultrasonic cleaning bath (Sonic, Niš, Serbia; total nominal power: 3×50 W and internal dimensions: 30 cm×15 cm×20 cm) operating at 40 kHz frequency. The sonication was performed for 2.5, 5, 10, 20, 40 and 60 min. The bath was filled with distilled water up to 1/3 of its volume (about 2.5 l). The extraction was carried out at 25 °C. The temperature was controlled and maintained at the desired level (±0.1 °C) by water circulating by means of a pump from a thermostated bath. The separation and further treatment of the filtrates were the same as described for the classical extraction.

Hydroxyl radical assay

Hydroxyl radicals were obtained by the Fenton reaction in the following system: 0.20 ml 10 mM H_2O_2, 0.20 ml 10 mM $FeCl_2$ and 0.20 ml 0.30 M DMPO as the spin trap and 0.20 ml DMF ("blank"). The influence of the extracts on the formation and transformation of hydroxyl radicals was investigated by adding a DMF solution of the extracts to the Fenton reaction system in the concentration range between 0.25 to 2.5 mg ml^{-1}. The ESR spectra were recorded after 5 min on a Bruker 300E ESR spectrometer (Rheinstetten, Germany) under the following conditions: field modulation, 100 kHz; modulation amplitude, 0.512 G; receiver gain, 5×10^5; time constant, 81.92 ms; conversion time, 163.84 ms; center field, 3440.00 G; sweep width, 100.00 G; *x*-band frequency, 9.64 GHz; power, 20 mW; temperature, 23 °C. The magnetic field scanning was calibrated using Fremy's salt (peroxylamine disulfonate).[15] Splitting constants were calculated from computer-generated second derivatives of the spectra, after optimizing the signal-to-noise ratios, and were verified by computer simulations. The scavenging effect, %, of the extract was defined as:

$$\text{Scavenging effect} = 100\frac{h_0 - h_x}{h_0}$$

where h_0 and h_x are the height of the second peak in the ESR spectrum of the DMPO–OH spin adduct of the blank and the sample, respectively. Butylated hydroxyanisole (BHA) was used as the reference compound (EC_{50} = 0.115 mg ml^{-1}).

DPPH photometric assay

The free radical-scavenging activity of the plant extracts was evaluated using the stable radical DPPH.[16] A series of extracts with different concentrations (1.00–0.01 mg ml^{-1}, seven different concentrations) were prepared in methanol. Then, 2.5 ml of the extract and 1.0 ml of a 3.0×10^{-4} M DPPH solution in methanol were mixed and placed in the dark at the room temperature for 30 min. The absorbance of each sample of the plant extract containing DPPH (A_s) was measured at 517 nm using a Varian Cary-100 spectrophotometer. Methanol (1.0 ml) plus the plant extract solution (2.5 ml) was used as the blank, while the DPPH solution plus methanol was used as the control. All determinations were performed in triplicate. The DPPH anti-radical-scavenging activity, *DPPH* (%), of each plant extract was determined using the following equation:

$$DPPH = 100\left(1 - \frac{A_s - A_b}{A_c}\right)$$

where A_s is the absorbance in the presence of the plant extract in the DPPH solution, A_c is the absorbance of the control solution (containing only DPPH) and A_b is the absorbance of the sample extract solution without DPPH. Ascorbic acid was used for comparison (EC_{50} = = 0.0039±0.0007 mg ml^{-1}).

Determination of total phenolic content

The total phenolic content in the *S. marmoreum* extracts was determined according to the Folin–Ciocalteu method,[17] using gallic acid as the standard. Samples (200 µl, 20 µg ml^{-1}) were introduced into test tubes and the Folin–Ciocalteu reagent was added and allowed to stand for 8 min at room temperature. Then, 0.80 ml of sodium carbonate (7.5 %) was added, mixed and allowed to stand for 30 min. The absorbance was measured at 765 nm. The total phenolic content was expressed as gallic acid equivalents (*GAE*), in mg/g of dry extract, as the mean ±*SD* of three replicate measurements:

$$A(765\ \text{nm}) = 12.722 c_{\text{gallic acid}}\ (\mu\text{g ml}^{-1}) + 0.0034,\ R^2 = 0.9994$$

Determination of total flavonoid content

The total flavonoid content was determined according to the aluminum chloride colorimetric method.[18] Each plant extract (2.0 ml, 5.0 μg ml^{-1}) in methanol was mixed with 0.10 ml of 10 % aluminum chloride, 0.10 ml of 1.0 M potassium acetate and 2.8 ml of deionized water. After 40 min incubation at room temperature, the absorbance of the reaction mixture was measured at 415 nm against a deionized water blank. Rutin was chosen as the standard and the total flavonoid content was expressed as milligram rutin equivalents (*RE*) per gram of dry extracts, as the mean±*SD* of three replicate measurements:

$$A(415\ \text{nm}) = 7.2328 c_{\text{rutin}}\ (\mu\text{g ml}^{-1}) - 0.2286,\ R^2 = 0.9919$$

Determination of antimicrobial activity

An agar well-diffusion method was employed for the determination of the antimicrobial activities of the extracts.[19] 0.10 ml of micro-organism suspension, formed during 24 h culture on agar with 10 ml sterile 0.90 % NaCl was suspended in 10 ml of the nutrition medium (*ca*. 10^6 CFU/ml). A Petri dish (86 mm internal diameter) was filled with this system. Wells (10 mm in diameter) were cut from the agar and 30 μl of extract solution (concentration 10 mg ml^{-1} in methanol) was delivered into them. Erythromycin (997 μg/mg; [114-07-8]; approx. 98 %; H_2O content 4 %; Sigma) and tylosin tartrate (950 μg/mg; [74610-55-2]; Sigma) were used as the positive controls (concentration in methanol 0.05 mg ml^{-1}). All extracts were filtrated using a 0.45 μm membrane filter (Sartorius, Germany) and tested three times. After incubation at 37 °C for 24 h, the agar plates were examined for any zones of inhibition. The diameters of the inhibition zones, mm, were measured using a Fisher Lilly Antibiotic Zone Reader (USA).

Statistical analysis

Each of the measurements described above was performed in three replicate experiments, except the extract yields which were in duplicate. Comparison of means was analyzed by the Student's *t*-test and differences were considered significant when $p < 0.05$.

RESULTS AND DISCUSSION

Kinetics of the extractions

The change of the ES yield from *S. marmoreum* during the CE and UE, using methanol at a leaves-to-solvent ratio (1 g:10 ml) and a temperature of 25 °C, are shown in Fig. 1. The obtained curves have the same shape as those for the extraction of ES,[20] flavonoids and active compounds[13] from St. John's wort (*Hypericum perforatum)*, pyrethrines from pyrethrum (*Chrysanthemum cineraria*) flowers[21] and ES from sage (*Salvia officinalis*).[22] Independent of the recovery technique, the extraction occurred in two main stages: first, dissolution of the material near the surface, characterized by a rapid increase in the ES yield at the beginning of the process (washing or fast extraction), and second, diffusion of the solute from the porous plant residue into the solution (slow extraction). The optimum time for both CE and UE was approximately 40 min, ensuring a near maximum ES yield.

The efficiency of UE exceeded that of CE. Fig. 1 shows that ultrasound improved both the ES yield and the rate extraction. The total ES yield obtained

by UE was 4.3 % higher than the one obtained by CE but it was only 82.8 % of the yield achieved by SE. This was explained by the higher extraction temperature and much longer extraction time in the case of the SE.

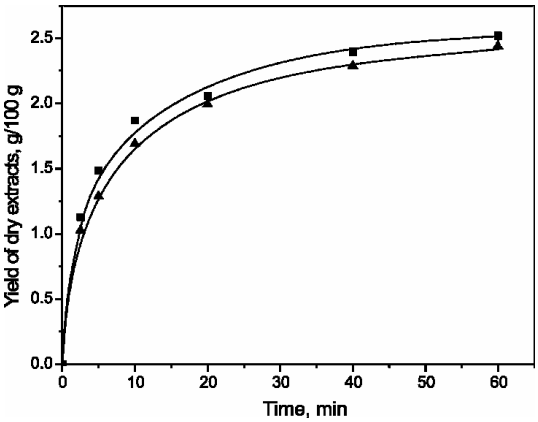

Fig. 1. Time course variation of the ES yield from *S. marmoreum* (CE: triangles; UE: squares).

Anti-oxidant capacity

The anti-oxidative effect of the houseleek extracts obtained by CE and UE was estimated by the ability of the extracts to scavenge hydroxyl radicals. This is very important because hydroxyl radicals are the major active oxygen species causing lipid oxidation.[15] Employing a spin trap, such as DMPO, it is possible to convert reactive hydroxyl radicals to stable nitroxide radicals (DMPO–OH adducts) with spectral hyperfine splitting that reflects the nature and the structure of these radicals. The relative intensity of free radical formation was determined by ESR spectroscopy, the height of the peaks being in proportion to the number of radical adduct molecules in the accumulating system.

As shown in Fig. 2, the reaction of Fe^{2+} with H_2O_2 in the presence of the spin trapping agent DMPO generated a 1:2:2:1 quartet of lines with hyperfine coupling parameters (aN = aH = 14.9 G). The intensity of the ESR signal, corresponding to the concentration of the formed free radicals, was decreased in the presence of the extracts of *S. marmoreum.*

The anti-oxidative activity of the *S. marmoreum* extracts obtained by different extraction techniques was also estimated by the ability of the extracts to scavenge the stable DPPH radicals. The DPPH method was chosen to evaluate the anti-oxidant activity because it is one of the most effective methods for evaluating the concentration of radical-scavenging materials effective as a chain-breaking mechanism.[23]

The percentage of DPPH and the hydroxyl radicals-scavenging activity are plotted against the plant extract concentration in Fig. 3. To calculate the concentration of the extract necessary to decrease DPPH radical concentration by 50 % (called EC_{50}), the relationships of *DPPH* and the hydroxyl radicals-scavenging

activities on the concentration of the extract solution were determined by non-linear (sigmoid) and linear regression methods, respectively. The EC_{50} value was used to measure the antiradical activity of the extracts: the lower the EC_{50}, the higher is the value of the antiradical activity.

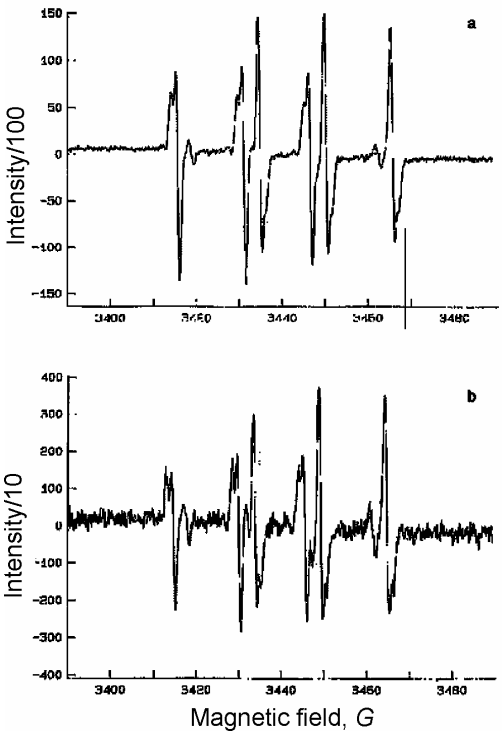

Fig. 2. ESR spectra of the DMPO–OH spin adduct recorded 5 min after mixing of a) 0.20 ml 0.30 M DMPO, 0.20 ml 10 mM H_2O_2 and 0.20 ml 10 mM Fe^{2+} (blank) and b) the same as the blank but with a DMF solution of *S. marmoreum* extract, 0.50 mg ml^{-1} (sample).

As it can be seen in Table I, the extract obtained by CE showed the highest anti-oxidant activity. This extract also contained the highest amount of total phenolic compounds and flavonoids. The differences observed between the anti-oxidant activity and the amounts of total phenolic compounds and flavonoids for all the extracts were statistically significant with a 95 % confidence level. The total amount of these compounds was accepted as an indication of the anti-oxidant potential because they acted as anti-oxidants, antimicrobials and photoreceptors in plants.[24]

It is believed that the observed reduction of phenolic and flavonoid compounds in the extract obtained by UE was the result of their degradation by interaction with the highly reactive hydroxyl radicals formed during sonication. The extractions were performed in methanol, a solvent which does not give rise to such a large proportion of radicals under cavitation,[25] but the water present in the fresh leaves of houseleek could.

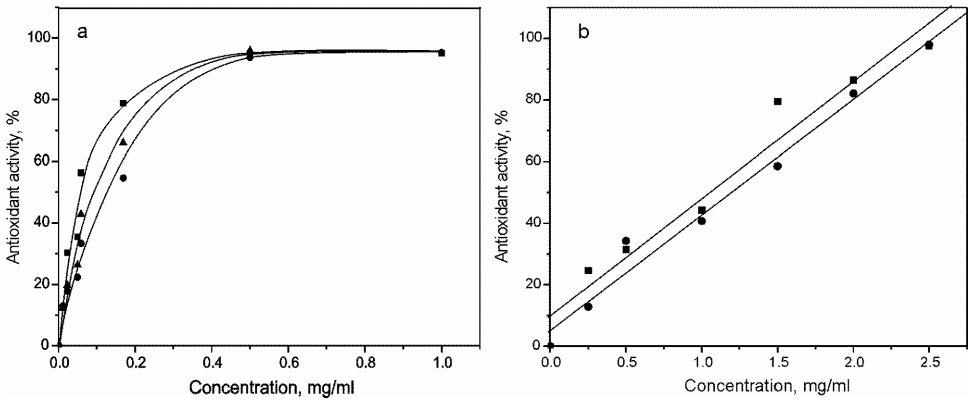

Fig. 3. Antioxidant activity against a) DPPH radical and b) hydroxyl radical for methanolic extracts of *S. marmoreum* obtained by different extraction techniques (CE: circles; UE: squares; Soxhlet extraction: triangles).

TABLE I. Yield of ES (g/100 g fresh plant material) obtained by the different extraction techniques, anti-oxidant capacity, total amount of phenolic compounds (mg gallic acid/g fresh plant material[a]) and flavonoids (mg rutin/g fresh plant material[a]) of *S. marmoreum* methanolic extracts

Extraction technique	Yield of ES	EC_{50} / mg ml^{-1}		Total phenolic content	Total flavonoids
		DPPH assay[a]	Hydroxyl radical assay		
CE[b]	2.3	0.06±0.01	1.08	0.73±0.005	0.62±0.003
UE[b]	2.4	0.09±0.01	1.26	0.59±0.005	0.58±0.011
SE[c]	2.9	0.12±0.04	ND[d]	0.56±0.004	0.51±0.006

[a]Data are expressed as the mean of three replicates ± standard deviation; [b]40 min, 25 °C; [c]150 min, T_b; [d]not determined

The total phenolic content was correlated to the anti-oxidant activity of the extracts (R^2 = 0.884), as can be seen in Fig. 4. Thus, the anti-oxidant activity of an extract could be predicted from its total phenolic content. Statistically significant relationships were also observed between the total phenolics and the anti-oxidant activity in the case of virgin olive oils (R^2 = 0.991),[26] flaxseed (R^2 = 0.963) and cereal products (R^2 = 0.905).[27]

Antimicrobial activity

The antimicrobial activities of the methanolic extracts of *S. marmoreum* are given in Table II. As expected, the control treatment (methanol) had no inhibitory effect on any of the tested micro-organisms. All extracts showed a lower antimicrobial activity than the control antibiotics. Independent of the extraction technique, the methanolic extracts from *S. marmoreum* showed antimicrobial activity against only two of the seven tested microorganisms, the mould *Aspergillus niger* ATCC 16404 and the yeast *Candida albicans* ATCC 10231, with the diameters of the zone of inhibition ranging between 15.9 and 16.9 mm.

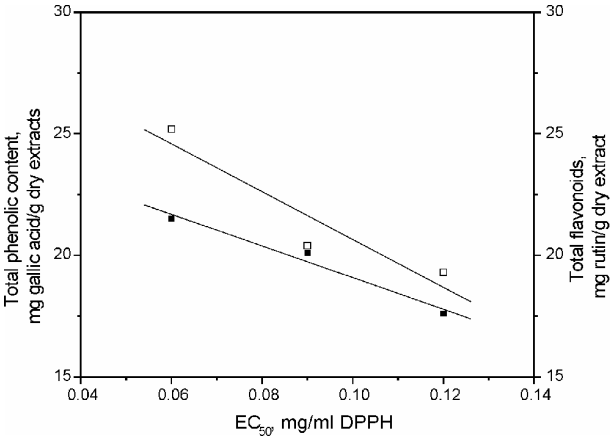

Fig. 4. Correlation between EC_{50} (determined by the DPPH method), total phenolic content (open squares) and total flavonoids (black squares) of methanolic extracts from *S. marmoreum.*

TABLE II. Antimicrobial activity of methanol extracts of *S. marmoreum* and antibiotic sensitivity of selected microorganisms to the extracts (zone size, mm)

Test microorganisms	Extracts (10 mg ml^{-1})			Antibiotics (0.05 mg ml^{-1})	
	UE[a]	CE[a]	SE[b]	Erythromycin	Tylosin tartrate
Escherichia coli ATCC 25922	–[c]	–	–	21.2±0.1	18.4±0.0
Pseudomonas aeruginosa ATCC 9027	–	–	–	24.1±0.8	17.6±0.1
Bacillus subtilis ATCC 6633	–	–	–	19.1±0.1	17.3±0.5
Staphylococcus aureus ATCC 6538	–	–	–	23.4±0.1	18.4±0.4
Candida albicans ATCC 10231	16.3±0.1	16.2±0.2	16.4±0.0	23.0±0.0	16.2±0.2
Saccharomyces cerevisiae ATCC 9763	–	–	–	–	–
Aspergillus niger ATCC 16404	16.9±0.3	16.4±0.4	15.9±0.3	20.5±0.5	18.1±0.1

Data are expressed as the mean of three replicates ± standard deviation; [a]10 mg ml^{-1}, 40 min, 25ºC; [b]150 min; [c]no antimicrobial activity

Independent of the tested micro-organism, there was no statistically significant difference (95 % confidence interval) in antimicrobial activities of the extracts obtained by UE and CE. The extract obtained by SE exhibited a slightly higher antimicrobial activity against *A. niger* and lower antimicrobial activity in the cases of *C. albicans*, than two other extracts.

The *S. marmoreum* extracts, similarly to *S. tectorum* extract,[4] had no antimicrobial activity against *Escherichia coli* and *Saccharomyces cerevisiae.*

CONCLUSIONS

The present study is a comparative study of the anti-oxidant and antimicrobial activities, total phenolic compounds and total flavonoids in the methanolic extracts obtained from houseleek (*Sempervivum marmoreum* L.) leaves by traditional (CE and SE) and novel (UE) extraction techniques. The extracts of *S. marmoreum* showed antimicrobial activity against the mould *Aspergillus niger* and the yeast *Candida albicans*, but not against the tested bacteria. The methanolic extract obtained by CE showed stronger anti-oxidant, but similar antimicrobial activities, compared to the extracts obtained by UE and SE. Thus, the study suggests that methanolic extracts of *S. marmoreum* are both potential sources of natural anti-oxidants and natural antimicrobial preparations.

Acknowledgements. This work was supported by the Ministry of Science of the Republic of Serbia, project OI 142073B.

И З В О Д

ПОРЕЂЕЊЕ АНТИОКСИДАТИВНОГ И АНТИМИКРОБНОГ ДЕЈСТВА ЕКСТРАКАТА *Sempervivum marmoreum* L. ДОБИЈЕНИХ РАЗЛИЧИТИМ ЕКСТРАКЦИОНИМ ТЕХИКАМА

САША С. СТОЈИЧЕВИЋ[1], ИВАНА Т. СТАНИСАВЉЕВИЋ[1], ДРАГАН Т. ВЕЛИЧКОВИЋ[2], ВЛАДА Б. ВЕЉКОВИЋ[1] и МИОДРАГ Л. ЛАЗИЋ[1]

[1]*Технолошки факултет, Булевар ослобођења 124 и* [2]*Здравље-Actavis, Влајкова 199, 16000 Лесковац*

Рад представља компаративну студију антиоксидативног, антимикробног дејства и садржаја укупних фенолних и флавоноидних једињења у екстрактима добијеним из листа чуваркуће (*Sempervivum marmoreum* L.) мацерацијом, ултразвучном екстракцијом и екстракцијом по Сокслету. Екстракт добијен мацерацијом садржи више фенолних и флавоноидних једињења и показује веће антиоксидативно дејство него екстракти добијени осталим техникама. Сви екстракти независно од примењене технике показују сличну антимикробну активност према *Aspergillus niger* и *Candida albicans* али не и према тестираним бактеријама.

(Примљено 10. септембра, ревидирано 31. децембра 2007)

REFERENCES

1. *Sempervivum marmoreum*, http://www.semper-vivum.de/kategorie/20/76/ (12 January, 2007)
2. J. F. Stevens, H. Hart, E. T. Elema, A. Bolck, *Phytochemistry* **41** (1996) 503
3. A. Blázovics, A. Lugasib, T. Keményc, K. Hagymásia, Á. Kéry, *J. Ethnopharmacol.* **73** (2000) 479
4. V. Abram, M. Donko, *J. Agric. Food Chem.* **47** (1999) 485
5. M. Šentjurc, M. Nemec, H. D. Connor, *J. Agric. Food Chem.* **51** (2003) 2766
6. A. Blázovics, R. Gonzáles-Cabello, I. Barta, P. Gergely, E. Fehér, Á. Kéry, G. Petri, *Phytother. Res.* **8** (1994) 33
7. Á. Kéry, A. Blázovics, N. Rozlosnik, J. Fehér, G. Petri, *Planta. Med.* **58** (1992) A661
8. A. Blázovics, L. Prónai, E. Fehér, Á. Kéry, G. Petri, *Phytother. Res.* **7** (1993) 95
9. 9. G. Kekesi, I. Dobos, G. Benedek, G. Horvath, *Phytother. Res.* **17** (2003) 1032
10. K. Szentmihályi, E. Fehér, P. Vinkler, Á. Kéry, A. Blázovics, *Toxicol. Pathol.* **32** (2004) 50

11. M. Vinatoru, *Ultrason. Sonochem.* **8** (2001) 313
12. S. Rodrigues, G. A. S. Pinto, *J. Food Eng.* **80** (2007) 869
13. A. Smelcerovic, M. Spiteller, S. Zuehlke, *J. Agric. Food Chem.* **54** (2006) 2750
14. S. Albu, E. Joyce, L. Paniwnyk, J. P. Lorimer, T. J. Mason, *Ultrason. Sonochem.* **11** (2004) 261
15. J. M. Canadanovic-Brunet, S. M. Djilas, G. S. Cetkovic, V. T. Tumbas, *J. Sci. Food Agric.* **85** (2005) 265
16. C. W. Choi, S. C. Kim, S. S. Hwang, B. K. Choi, H. J. Ahn, M. Y. Lee, S. H. Park, S. K. Kim, *Plant Sci.* **163** (2002) 1161
17. V. L. Singleton, J. A. Rossi, *Am. J. Enol. Vitic.* **16** (1965) 144
18. C. Chang, M. Yang, H. Wen, J. Chern, *J. Food. Drug Anal.* **10** (2002) 178
19. NCCLS (National Committee for Clinical Laboratory Standards), *Performance Standards for antimicrobial susceptibility testing*. 9th International Supplement, Wayne, PA, (1999), M100-S9.
20. V. Veljković, D. Milenović, *Hem. Ind.* **56** (2002) 60 (in Serbian)
21. M. Romdhane, C. Gourdon, *Chem. Eng. J.* **87** (2002) 11
22. D. T. Veličković, D. M. Milenović, M. S. Ristić, V. B. Veljković *Ultrason. Sonochem.* **13** (2006) 150
23. P. Maisuthisakul, M. Suttajit, R. Pongsawatmanit, *Food. Chem.* **100** (2007) 1409
24. P. Pietta, *J. Nat. Prod.* **63** (2000) 1035
25. L. Paniwnyk, E. Beaufoy, J. P. Lorimer, T. J. Mason, *Ultrason. Sonochem.* **8** (2001) 299
26. C. S. Sánchez, A. M. T. González, M. C. García-Parrilla, J. J. Q. Granados, H. L. García de la Serrana, M. C. L. Martínez, *Anal. Chim. Acta.* **593** (2007) 103
27. Y. S. Velioglu, G. Mazza, L. Gao, B. D. Oomah, *J. Agric. Food Chem.* **46** (1998) 4113.

Journal of the Serbian Chemical Society
JSCS@tmf.bg.ac.yu • www.shd.org.rs/JSCS
J. Serb. Chem. Soc. 73 (6) 609–618 (2008) UDC 599.735.5+591.436+66–946.1:591.478–035.57
JSCS–3743 *Original scientific paper*

Immobilization and characterization of bovine liver catalase on eggshell

ÖZLEM ALPTEKİN*, S. SEYHAN TÜKEL and DENİZ YILDIRIM

University of Çukurova, Faculty of Sciences and Letters, Department of Chemistry, Adana 01330, Turkey

(Received 12 September, revised 21 December 2007)

Abstract: Bovine liver catalase immobilized on eggshell particles was characterized and the reusability of the immobilized catalase was investigated in a batch type reactor. For immobilized catalase onto ground eggshell (ICATG), the optimum initial amount of catalase was 85 mg g^{-1} of eggshells, the optimum pH was 6.0 (75 mM citrate buffer) and the temperature was 30 °C. The V_{max} and K_m values of ICATG were determined as 29.1±1.2 U/mg of protein and 41.9±2.7 mM, respectively. The reusability of ICATG was tested and the remaining activity of ICATG was found to be 73 % of the initial activity after 80 cycles of batch operation. The amount of catalase bound onto the carrier was estimated by using the results of induced coupled plasma measurements. The catalytic efficiencies (k_{cat}/K_m) of free catalase and ICATG were found to be 1.4×10^6 and 2.8×10^3 dm^3 s^{-1} mol^{-1}, respectively. Catalase immobilization onto eggshell is economic and has good reusability. Hence, it can be concluded that eggshell is an efficient carrier for immobilizing catalase.

Keywords: catalase; eggshell; immobilization; glutaraldehyde; induced coupled plasma.

INTRODUCTION

Catalase (EC 1.11.1.6) is an abundant enzyme in nature decomposing hydrogen peroxide to water and molecular oxygen. Catalase from bovine liver (M_r = 240 kg mol^{-1}) is composed of four tetrahedrally arranged identical subunits. Each subunit consists of a single polypeptide chain, which associates with a prostetic group, ferric protoporphyrin IX. Immobilized catalase has useful applications in various industrial fields for the removal of hydrogen peroxide used as oxidizing, bleaching or sterilizing agent and in the analytical field as a component of hydrogen peroxide or glucose biosensor systems.[1–7] Catalase has been immobilized on numerous carrier materials, such as magnesium silicate, magne-

* Corresponding author. E-mail: alptekinozlem@yahoo.com
doi: 10.2298/JSC0806609A

tite, eggshell membrane, eggshell, gelatin, starch cellulose acetate, starch polycaprolactone blends, chitosan, cellulose, alumina, and agarose covalently; bioskin, kaolin and bentonite by adsorption; polyacrylamide gels and poly(isopropylacrylamide-co-hydroxyethyl methacrylate) (PNIPAM/HEMA) copolymer hydrogel by entrapment.[1,3–5,8–16]

In the present study, bovine liver catalase was immobilized onto hen eggshell by crosslinking with glutaraldehyde. Eggshell being an abundantly available and non-biodegradable waste product, unlike other supports which are expensive but commonly used, was selected as carrier.[17] Hen eggshell is a porous ceramic material mainly composed of calcium carbonate, known as calcite which is a more stable polymorph at room temperature. It has good mechanical strength and it is resistant to microbial attacks.[18]

In this paper, the immobilization of catalase onto eggshell and the characteristics of the immobilized catalase are reported.

EXPERIMENTAL

Materials

Hydrogen peroxide (aqueous solution, 30 % w/w), sulfuric acid (96.0 % w/w) were obtained from Merck AG (Darmstadt, Germany). Bovine liver catalase with a specific activity of 3090 U/mg of solid, glutaraldehyde solution (aqueous solution, 50 % w/w) and all other chemicals were obtained from Sigma (St. Louis, MO). Hen eggs were purchased from a local market.

Catalase immobilization

The hen eggshell was manually stripped from eggshell membrane after the albumen and yolk had been removed. Then eggshells were ground into pieces as small as possible in a mortar, kept in boiling water for 15 min, washed several times with acetone and dried in an oven at 60 °C. This type of carrier was considered as ground carrier. The immobilization method described by Chatterjee[9] was used with minor modifications. Briefly, 1.0 g of dried carrier was added to 8.5 ml of catalase solution in a final concentration of 5.0, 10.0, 15.0, and 20.0 mg ml^{-1} in 0.020 M, pH 6.8, potassium phosphate buffer and stirred for 15 min. Glutaraldehyde was added slowly with shaking to a final concentration of 1.2 % (w/v) to the mixture and the mixture incubated at 5 °C for 4 h. The resulting immobilized catalase (ICATG) was washed with the buffer until no catalase and glutaraldehyde were detected in the wash solution (filtrate). The ICATG samples were kept overnight at 5 °C in an incubator and then stored in closed glass tube.

Glutaraldehyde was detected according to Boratynski and Zal.[19] 200 µl of filtrate or a glutaraldehyde standard solution (8.0×10^{-6}–2.5×10^{-4} M) was mixed with 1.0 ml of phenol reagent (40 µl of an aqueous 5.0 % phenol solution was added to 10 ml of 70 % perchloric acid) and incubated at room temperature for 15 min. Absorbance was measured *vs*. the phenol reagent at 479 nm with a UV/Vis spectrophotometer.

The amount of catalase as a metalloenzyme in the filtrate was determined by induced coupled plasma (ICP, Varian Liberty Series II) using bovine liver catalase as the protein standard. Briefly, the filtrate was concentrated using a concentrator until the water had almost evaporated. 4.0 ml of sulfuric acid was added to the concentrated filtrate, then 3.0 ml of an aqueous H_2O_2 solution (30 %) was added and the solution was diluted to 25 ml with distilled water. To produce a calibration curve, the same procedure was applied for different amounts of catalase (2.5–25.0 mg). The iron content of the solvents used was also measured. The amount

of immobilized catalase was estimated by subtracting the amount of catalase determined in the filtrate from the total amount of catalase used in the immobilization procedure.

Enzyme activity assay

The catalase activity was determined according to Lartillot,[20] which is a modification of the method described by Bergmeyer.[21] The catalase activity was measured spectrophotometrically at 240 nm using a specific absorption coefficient of 0.0392 $cm^2/\mu mol$ H_2O_2. The reaction mixture containing 2.5 ml of substrate made up of 10 mM hydrogen peroxide in a 50 mM, pH 7.0, phosphate buffer and 2.78×10^{-4} mg of free catalase or 5.0 mg of immobilized catalase was used unless otherwise mentioned. The reaction was performed at 25 °C for 2 min and stopped by adding 0.50 ml of 1.0 M HCl. Eggshells alone and denaturated ICATG, kept in a boiling water bath for 1 h, were also used as controls to determine whether they decompose hydrogen peroxide. The activity of the free catalase is given as U/mg of protein and the activity of immobilized catalase is given as U/g of carrier or U/mg of protein.

Effects of pH, buffer concentration and temperature on the activity of free and immobilized catalase

Effect of pH. The dependence of the activity on pH was assayed using 50 mM acetate buffer for pH 5.0 and 5.5, 50 mM citrate buffer for pH 6.0, 50 mM phosphate buffer for pH 6.5, 7.0, 7.5 and 8.0 and 50 mM borate buffer for pH 9.0 for both the free catalase and the ICATG.

Effect of buffer concentration. The dependence of the activity of free catalase and ICATG on ionic strength was assayed using 25, 50, 75 and 100 mM buffer at pH 7.5 and 6.0, respectively.

Effect of temperature. The effect of temperature on the activity of free catalase and ICATG were investigated in the temperature range 10–60 °C.

Thermal, storage and operational stabilities

Thermal stability. An estimation of the thermal stability was performed by measuring the residual activity of free catalase and ICATG exposed to temperatures of 30, 35, 40, 50 and 60 °C. Samples were taken at 1, 3, 7 and 15 h time intervals during incubation and the residual activities were measured.

Storage stability. Free catalase and ICATG were stored at 5 °C and room temperature and the residual activities were measured.

Operational stability. To determine the operational stability, 1.0 g of ICATG was mixed with 5.0 ml of 10 mM hydrogen peroxide solution in a glass column reactor (diameter 1.1 cm and length 10 cm) for 2 min at room temperature. The solution was then immediately separated from the ICATG and the absorbance was measured at 240 nm. The same procedure using the same ICATG sample was repeated every 2 min eighty times.

Effect of immobilization on the kinetic constants

The effects of substrate concentration (2.5–25.0 mM H_2O_2) on the activities of free and ICATG were investigated. The Michaelis–Menten coefficients (K_m) and maximum velocities (V_{max}) were determined from Lineweaver–Burk plots and the catalytical efficiencies (k_{cat}/K_m) were calculated.

RESULTS AND DISCUSSION

Immobilization of catalase on eggshell

The activity of ICATG as a function of the total amount of catalase contacted with 1.0 g of ground eggshell during immobilization is shown in Fig. 1. On increasing the total amount of catalase used in the immobilization from 42.5 mg to

85 mg, the ICATG activity increased from 38 to 86 U/g of carrier. However, the ICATG activity decreased when the total amount of catalase used in the immobilization was increased above 85 mg. Therefore, the optimal initial amount of catalase for immobilization was determined as 85 mg/g of carrier.

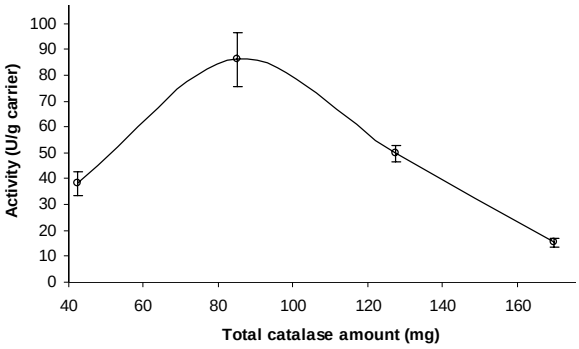

Fig. 1. Activity of ICATG as a function of the total amount of catalase contacted with 1.0 g of ground eggshell during immobilization.

In most of the immobilization studies, the enzyme load was measured by detecting the decreased amount of protein in the residual enzyme solutions. The biuret method, the Folin–Ciocalteu assay as modified by Lowry, the determination of Bradford with the dyestuff Coomassie brilliant blue or spectroscopic absorption measurements at 280 nm are frequently employed analyses. In the present study, it was not possible to obtain reproducible and reliable results for protein determination with the above-mentioned classical methods, probably due to the presence of glutaraldehyde in the filtrate, although in some studies it was reported that the protein content of the filtrate was determined using the Lowry method[9] and optical density measurement at 280 nm[17] even in the presence of glutaraldehyde. Therefore, the amount of catalase immobilized on the carrier was determined based on the iron content of catalase in the filtrate. The calibration curve for analysis of the iron content of the catalase solutions showed a linear correlation between the catalase concentration and the ICP iron signal, Fig. 2. In the present immobilization experiments, the amount of bound catalase ICATG was 82.3, mg/g of carrier, when 85 mg of total catalase was used per g of carrier.

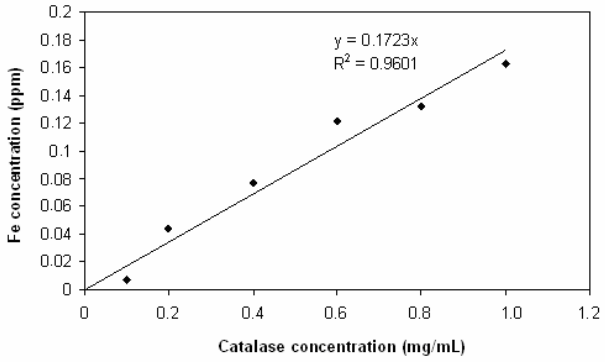

Fig. 2. The calibration plot for the determination of the amount of catalase using ICP. (The calibration plot shows the iron content of catalase *vs*. the concentration of bovine liver catalase).

Effects of pH, buffer concentration and temperature on the activity of free and immobilized catalase

Effect of pH. The effect of pH on the activity of free catalase and ICATG was studied in the pH range 5.0–9.0. The relative activities at different pH values are shown in Fig. 3. Free catalase and ICATG showed their maximum activity at pH 6.0 and 7.5, respectively. Chatterjee[9] reported that eggshell bound goat liver catalase showed two pH optima at 6.4 and 7.6. However, in this study only one pH optimum was determined. The maximum activity of catalase shifted in the acidic direction (pH 6.0) after immobilization on eggshell, as compared with that of free catalase. The relative activities of free catalase and ICATG were 18 and 56 % of maximal activity, respectively, at pH 5.0 (50 mM acetate buffer).

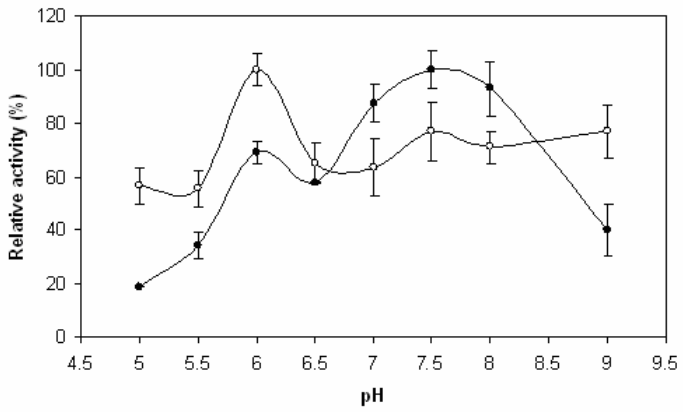

Fig. 3. Effect of pH on the activity of free catalase (●) and ICATG (○).

Effect of buffer concentration. The effect of buffer concentration (25, 50, 75 and 100 mM) on the activity of free catalase and ICATG were determined at pH 7.5 and 6.0, respectively. The results are presented in Fig. 4. The optimum buffer concentrations were determined as 50 mM and 75 mM for free catalase and ICATG, respectively. The ICATG activity was more significantly affected by the buffer concentration than that of free catalase. As the buffer concentration was increased gradually from 25 to 75 mM, the relative activity of ICATG also increased from 64 to 100 %. When the buffer concentration was increased from 75 to 100 mM, the relative activity of ICATG dramatically decreased from 100 to 33 %.

Effect of temperature. The effect of the temperature on the activity was investigated in the temperature range from 10 to 60 °C. The activities of free catalase and ICATG as a function of temperature are shown in Fig. 5, from which it can be seen that the maximum activities of free catalase and ICATG were 25 and 30 °C, respectively. At 60 °C, the relative activity of free catalase was only 13 %. However, the relative activities of ICATG at high temperatures (50–60 ºC) were higher than those of free catalase.

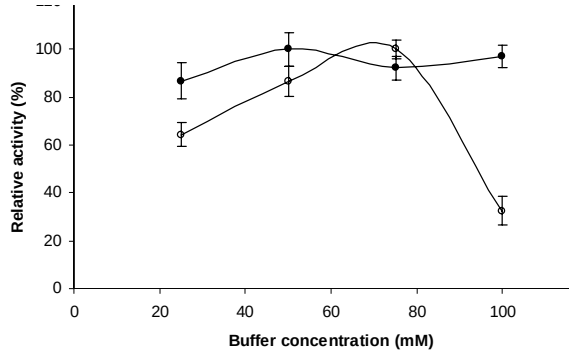

Fig. 4. Effect of buffer concentration on the activity of free catalase (●) and ICATG (○).

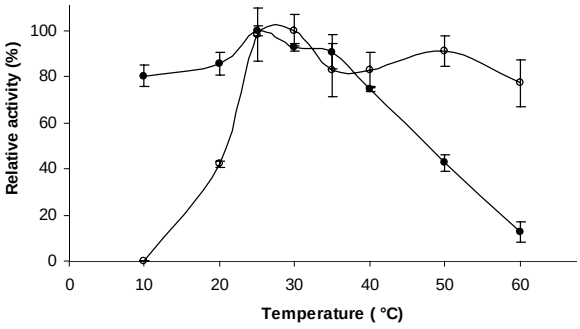

Fig. 5. Effect of temperature on the activity of free catalase (●) and ICATG (○).

Thermal, storage and operational stabilities

Thermal stability. The thermal stability studies were performed by measuring the residual activities of free catalase and ICATG after exposure to 5 different temperatures 30, 35, 40, 50 and 60 °C for 1, 3, 7 and 15 h. The residual activities of free catalase and ICATG are shown in Figs. 6a and 6b, respectively. The activities of the samples were determined under optimum conditions. Generally, as the pre-incubation time increased, the activities of free catalase and ICATG decreased at a constant test temperature. The residual activity of ICATG was 88 % of its original activity at 30 °C after 15 h pre-incubation time, as shown in Fig. 6a. The residual activities of ICATG at 50 and 60 °C were similar for the same incubation time. Free catalase did not show any activity after 15 h at 60 °C. Tükel and Alptekin[8] reported that catalase immobilized on florisil *via* glutaraldehyde showed no activity after 15 h at 60 °C. Betencor *et al.*[5] immobilized *M. lysodeikticus* catalase on agarose and they reported that the residual activity of the immobilized catalase was only 70 % of its initial activity after 10 h at 45 °C.

Storage stability. As shown in Fig. 7, ICATG stored at 5 °C was more stable than when stored at room temperature. After 36 days storage at room temperature, the residual activity of ICATG was 65 % of its initial activity while when stored at 5 ºC for the same time, the residual activity was 96 %. The free catalase completely lost its activity after storage for 11 days at both 5 °C and also at room

temperature. Çetinus *et al.*[22] immobilized catalase on glutaraldehyde-pretreated chitosan films. They reported that the free enzyme had retained about 50 % of its activity after 18 days, immobilized catalase stored wet about 50 % of its activity after 25 days and that stored dry about 50 % of its activity after 5 days at 5 °C. Arıca *et al.*[16] immobilized catalase on poly(2-hydroxyethyl methacrylate)-Cibacron Blue F3GA (poly HEMA-CB) and poly(2-hydroxyethyl methacrylate)-Cibacron Blue F3GA-Fe(III) (poly HEMA-CB-Fe(III)) derivatized membranes by adsorption. They found that the free enzyme lost all its activity within 20 days when stored at 4 °C. Immobilized preparations of poly HEMA-CB-CAT and poly HEMA-CB-Fe(III)-CAT lost 40 and 25 % of their activities during the same period at 4 °C. This decrease in activity was explained as a time-dependent natural loss in enzyme activity and this was prevented to a significant degree upon immobilization. Solas *et al.*[12] immobilized bovine liver catalase on bioskin by ionic adsorption. They reported that the free catalase lost its activity within 3 days and the immobilized catalase retained about 70 % of its activity for 16 days at room temperature.

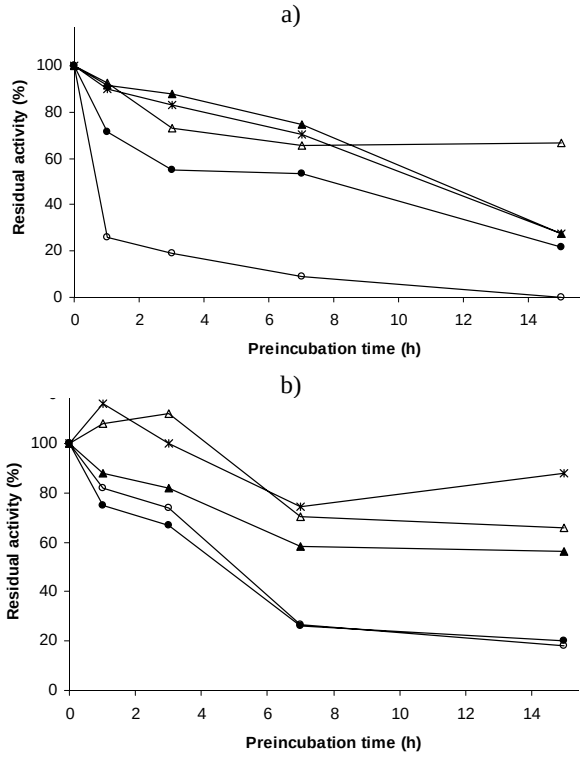

Fig. 6. Thermal stabilities of (a) free catalase and (b) ICATG at 30 (✳), 35 (▲), 40 (△), 50 (●) and 60 °C (○). The free catalase and ICATG activities were measured under their optimum conditions.

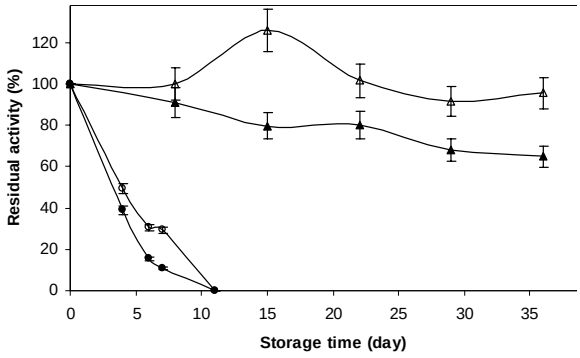

Fig. 7. Storage stabilities of free catalase at room temperature (●) and 5.0 °C (○) and ICATG at room temperature (▲) and 5.0 °C (△).

Operational stability. The operational stability of immobilized enzyme systems is very important for various biotechnological applications; an increased stability could make an immobilized enzyme more advantageous than its free counterpart. The operational stability of ICATG was determined and the results are presented in Fig. 8, from which it may be seen that the activity decays with increasing number of reuses. The remaining activity of ICATG was about 73 % of its initial value after 80 cycles of batch operation. Betancor *et al.*[2] immobilized catalase on dextrane and reported that the immobilized catalase had not lost its activity after 10 cycles. Tükel and Alptekin[8] reported that the remaining activity of catalase immobilized *via* glutaraldehyde on florisil was about 90 % and catalase immobilized *via* glutaraldehyde + spacer was about 30 % after 20 cycles of batch operation.

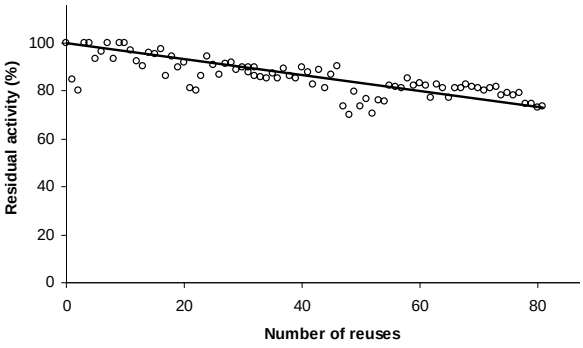

Fig. 8. The residual activity of ICATG in dependence on the number of reuses in a batch type reactor.

Effect of immobilization on the kinetic constants

The K_m and V_{max} values for free catalase and ICATG were determined and are presented in Table I. from which it can be seen that the K_m value of ICATG was smaller than that of the free catalase. However, the V_{max} values and catalytic efficiencies of ICATG were smaller than those of the free catalase. The catalytic efficiencies (k_{cat}/K_m) of free catalase and ICATG were 1.4×10^3 and 2.9 $m^3\ s^{-1}\ mol^{-1}$, respectively. In a previous study,[8] it was found that the K_m value for catalase

immobilized *via* glutaraldehyde on florisil was appreciably higher (10 fold) than that of the free catalase and its V_{max} was about 1 % of the V_{max} of the free catalase. Çetinus *et al.*[22] immobilized bovine liver catalase on glutaraldehyde pretreated chitosan films. They found K_m = 25.16 mM and V_{max} = 24042 min^{-1} μmol H_2O_2/mg of protein for free catalase and K_m = 27.67 mM and V_{max} = 1022 min^{-1} μmol H_2O_2/mg of protein for immobilized catalase. Eberhardt *et al.*[5] immobilized *Aspergillus niger* catalase on cellulose *via* glutaraldehyde and reported K_m and V_{max} values of free and immobilized catalase as 0.02664±0.00674 M and 35120±6762 min^{-1} μmol/mg of enzyme and 0.115±0.0166 M and 3135±203.8 min^{-1} μmol/mg of enzyme, respectively. Thus, a compromise has to be made between immobilized catalase, which is less active but more stable, and free catalase, which although being more active is less stable.

TABLE I. Michaelis–Menten constant and maximal reaction rate values for free and immobilized catalase

Enzyme form	K_m / mM	V_{max} / U (mg protein)$^{-1}$	k_{cat} / 10^4 s^{-1}	$(k_{cat}/K_m)\times10^{-3}$ / m^3 s^{-1} mol^{-1}
Free catalase	49.0±1.6	1.7±0.05×10^4	6.8	1.4
ICATG	41.9±2.7	29.1±1.2	0.012	0.0029

CONCLUSIONS

In this study, the optimal initial amount of catalase for immobilization was determined as 85 mg/g of carrier. Reproducible and reliable results for protein determination could not be obtained with classical methods, probably due to the presence of glutaraldehyde in the filtrate. The amount of catalase bound on the carrier was estimated using the results of induced coupled plasma measurements. ICATG showed its maximum activity in 75 mM, pH 6.0, citrate buffer at 30 °C. The thermal stability of ICATG was higher than that of free catalase at 60 °C. Remaining activity of ICATG was about 73 % of the initial activity after 80 cycles of batch operation. Catalase immobilization onto eggshell is economic and has good reusability. Thus, it can be concluded that eggshell is an efficient carrier for immobilizing catalase.

Acknowledgements. This work was supported by Research Grants FEF 2004 BAP 20, Çukurova University.

И З В О Д

КАРАКТЕРИЗАЦИЈА КАТАЛАЗЕ ИЗ ЈЕТРЕ ГОВЕЧЕТА ИМОБИЛИСАНЕ НА ЉУСЦИ ЈАЈЕТА

ÖZLEM ALPTEKİN, S. SEYHAN TÜKEL и DENİZ YILDIRIM

University of Çukurova, Faculty of Sciences and Letters, Department of Chemistry, Adana 01330, Turkey

Окатрактерисана је каталаза из јетре говечета имобилисана на честицама љуске јајета, док је могућност поновног коришћења имобилисане каталазе испитивана у серијском реактору. За каталазу имобилисану на спрашеној љусци јајета (ICATG) оптимална почетна коли-

чина каталазе износи 85 mg/g спрашене љуске, оптимална pH вредност износи 6,0 (75 mM цитратни пуфер), а температура 30 °C. Одређене су вредности V_{max} и K_m за ICATG од 29,1± ±1,2 U/mg протеина и 41,9±2,7 mM, респективно. Иситивање могућности поновног коришћења ICATG указује на то да активност износи 73 % у односу на почетну активност након 80 циклуса узастопног коришћења. Количина каталазе везане за носач процењена је на основу резултата испитивања методом индуковане купловане плазме. Каталитичка ефикасност (k_{cat}/K_m) слободне каталазе и ICATG износе $1{,}4\times10^6$ и $2{,}8\times10^3$ $dm^3\ s^{-1}\ mol^{-1}$, респективно. Имобилизација каталазе на љусци јајета је економична са великом могућношћу поновног коришћења, па се закључује да је љуска јајета добар носач за имобилизацију каталазе.

(Примљено 12. септембра, ревидирано 21. децембра 2007)

REFERENCES

1. M. M. F. Choi, T. P. Yiu, *Enzyme Microb. Technol.* **34** (2004) 41
2. L. Betancor, A. Hidalgo, G. F. Lorente, C. Mateo, R. F. Lafuente, J. M. Guisan, *Biotechnol. Progr.* **19** (2003) 763
3. S. A. Costa, R. L. Reis, *J. Mater. Sci. Mater. Med.* **15** (2004) 335
4. F. Horst, E. H. Rueda, M. L. Fereira, *Enzyme Microb. Technol.* **38** (2006) 1005
5. A. M. Eberhardt, V. Pedroni, M. Volpe, M. L. Ferreira, *Appl. Catal., B* **47** (2004) 153
6. L. Campanella, R. Roversi, M. P. Sammartino, M. Tomassetti, *J. Pharm. Biomed. Anal.* **18** (1998) 105
7. T. Santoni, D. Santianni, A. Manzoni, S. Zanardi, M. Macsini, *Talanta* **44** (1997) 1573
8. S. S. Tükel, O. Alptekin, *Process Biochem.* **39** (2004) 2149
9. U. Chatterjee, A. Kumar, G. G. Sanwal, *J. Biosci. Bioeng.* **70** (1990) 429
10. S. Akgöl, E. Dinçkaya, *Talanta* **48** (1999) 363
11. S. A. Costa, T. Tzanov, A. Paar, M. Gudelj, G. M. Gübitz, A. C. Paulo, *Enzyme Microb. Technol.* **28** (2001) 815
12. M. T. Solas, C. Vicente, L. Xavier, M. E. Legaz, *J. Biotechnol.* **33** (1994) 63
13. A. Savran, S. Alkan, H. Demir, H. Ceylan, *Asian J. Chem.* **18** (2006) 413
14. S. Alkan, H. Ceylan, O. Arslan, *J. Serb. Chem. Soc.* **70** (2005) 721
15. B. Jiang, Y. Zhang, *Eur. Polym. J.* **29** (1993) 1251
16. M. Y. Arıca, H. A. Öktem, S. A. Tuncel, *Polym. Int.* **48** (1999) 879
17. G. Vemuri, R. Banerjee, B. C. Bhattacharyya, *Bioprocess Biosyst. Eng.* **18** (1998) 111
18. Y. Nys, J. Gautron, J. M. G. Ruiz, M. T. Hincke, *C. R. Palevol.* **3** (2004) 549
19. J. Boratynski, T. Zal, *Anal. Biochem.* **184** (1990) 259
20. S. Lartillot, P. Kedziora, A. Athias, *Prep. Biochem.* **18** (1988) 241
21. H. U. Bergmeyer, *Methods of Enzymatic Analysis*, Academic Press, New York, 1974, p. 438
22. S. A. Çetinus, H. N. Öztop, *Enzyme Microb. Technol.* **26** (2000) 497.

www.shd.org.rs

Journal of the Serbian Chemical Society

JSCS@tmf.bg.ac.yu • www.shd.org.rs/JSCS

J. Serb. Chem. Soc. *73* (6) 619–630 (2008)
JSCS–3744

UDC 546.962+542.913:576+615.9
Original scientific paper

Synthesis, structural characterization and cytotoxic activity of two new organoruthenium(II) complexes

SANJA GRGURIĆ-ŠIPKA[1]*, MOHAMED AL.ARBI M. ALSHTEWI[1], DEJAN JEREMIĆ[1#], GORAN N. KALUĐEROVIĆ[2], SANTIAGO GÓMEZ-RUIZ[3], ŽELJKO ŽIŽAK[4], ZORICA JURANIĆ[4] and TIBOR J. SABO[1]

[1]*Faculty of Chemistry, University of Belgrade, Studentski trg 12–16, 11000 Belgrade,* [2]*Department of Chemistry, Institute of Chemistry, Technology and Metallurgy, Njegoševa 12, 11000 Belgrade, Serbia,* [3]*Departamento de Química Inorgánica y Analítica, E. S. C. E. T., Universidad Rey Juan Carlos, 28933 Móstoles, Madrid, Spain and* [4]*Institute of Oncology and Radiology, 11000 Belgrade, Serbia*

(Received 27 December 2007, revised 4 March 2008)

Abstract: Two new *p*-cymene ruthenium(II) complexes containing as additional ligands *N*-methylpiperazine ([(η^6-*p*-cymene)$RuCl_2(CH_3NH(CH_2)_4NH)$]PF_6, complex **1**) or vitamin K_3-thiosemicarbazone ([(η^6-*p*-cymene)$RuCl_2(K_3tsc)$], complex **2**) were synthesized starting from [(η^6-*p*-cymene)$_2RuCl_2]_2$ and the corresponding ligand. The complexes were characterized by elemental analysis, IR, electronic absorption and NMR spectroscopy. The X-ray crystal structure determination of complex **1** revealed "piano-stool" geometry. The differences in the cytotoxic activity of the two complexes are discussed in terms of the ligand present.

Keywords: ruthenium(II) complexes; *p*-cymene; K_3-thiosemicarbazone; *N*-methylpiperazine; cytotoxic activity.

INTRODUCTION

The field of organoruthenium complexes has been widely explored in recent years with regard to biological activity as well as catalytic activity of these complexes.[1–5] Many of these compounds are soluble in water and display cytotoxicity to cancer cells, including cisplatin-resistant cancer cells.[6,7]

Vitamin K_3, menadione, (2-methylnaphthalene-1,4-dione), is a fat-soluble vitamin and it is necessary for the production of prothrombin and five other blood clotting factors in humans. It also regulates bone calcification.[8] In addition, it was found that vitamin K_3, as well as its water-soluble derivative, menadione sodium bisulfite, has significant antitumor activity *in vitro* and *in vivo*.[9]

* Corresponding author. E-mail: sanjag@chem.bg.ac.yu
# Serbian Chemical Society member.
doi: 10.2298/JSC0806619G

On the other hand, thiosemicarbazones play an important role in research related to biological activity.[10] These ligands form complexes with metals and the influence of chelatation on antitumor activity has been very intensively investigated.[11,12] Thiosemicarbazones are the ligands of choice because thiosemicarbazones themselves exhibit antineoplastic activity. One of the most effective thiosemicarbazone is triapine (3-aminopyridine-2-carboxaldehyde thiosemicarbazone).[13,14] This compound acts as a very strong iron chelator and, consequently, inhibits ribonucleotide reductase (RR) activity.[15] The role of RR in the rate of replication of cancer cells has been well established.[16]

Hitherto, the thiosemicarbazone derivative of vitamin K_3 was used in the preparation of complexes with metals, such as Mn(II), Co(II), Ni(II), Cu(II), Zn(II) and Au(I).[17–19] It should be mentioned that the ruthenium chemistry of thiosemicarbazones has received little attention, especially concerning their potential antitumor activity. Ru(II) formed several complexes with thiosemicarbazones and some of them showed cytotoxic activity.[20–22] In addition, recently a lot of other ruthenium complexes containing the arene moiety have been synthesized and some of them have been evaluated for activity both *in vitro* and *in vivo*.[23–26] Some of the prepared complexes of the type [(η^6-arene)-RuCl(X)(Y)] showed cytotoxic activity to cisplatin-resistant cell lines. Preliminary structure–activity data showed that the hydrophobic arene group, the diamine NH group and the Cl leaving group may all play important roles in the anticancer activity of these complexes.[27]

In this paper, the characterization of two newly synthesized complexes of Ru(II) with *p*-cymene, which contain additional ligands K_3tsc or *N*-methylpiperazine, is described.

EXPERIMENTAL

Materials

Menadione sodium bisulfite (MSB), thiosemicarbazide, α-terpinene and *N*-methylpiperazine were commercially available and used without further purification. MSB thiosemicarbazone (NaK_3tsc) was prepared by treating thiosemicarbazide with menadione sodium bisulfite in an ethanol–water mixture using a published procedure.[17]

The complex $[(\eta^6\text{-}p\text{-cymene})_2RuCl_2]_2$ was prepared following a published protocol.[28]

Synthesis of the complexes

Synthesis of [(η^6-p-*cymene)RuCl*$_2$*(CH*$_3$*NH(CH*$_2$*)*$_4$*NH)]PF*$_6$ ***(1)***. A solution of *N*-methylpiperazine (0.07 ml, 0.50 mmol) in dry methanol (5.0 ml) was added to a solution of $[(\eta^6\text{-}p\text{-cymene})_2RuCl_2]_2$ (120 mg, 0.20 mmol) in dry methanol (10 ml). The resulting mixture was stirred 2 h in dark. Orange solution was then concentrated to half volume and 250 mg (1.5 mmol) of NH_4PF_6 was added. The light orange product that appeared during night was filtered off, washed with ethanol, and ether. Yield: 92.2 mg (42 %).

Synthesis of [(η^6-p-*cymene)RuCl*$_2$*(K*$_3$*tsc)] (**2**)*. A solution of K_3tsc (220 mg, 0.50 mmol) in dry methanol (5.0 ml) was added to a solution of $[(\eta^6\text{-}p\text{-cymene})_2RuCl_2]_2$ (120 mg, 0.20 mmol) in dry methanol (10 ml). The resulting mixture was stirred for 3 h. The obtained

orange solution was then concentrated to half volume and left at 4 °C overnight. The light orange product was filtered off, washed with methanol and then diethyl ether. Yield: 166 mg (67 %).

Physical measurements

Elemental analyses were carried out with an Elemental Vario EL III microanalyser. The infrared spectra were recorded on a Perkin–Elmer FTIR 31725X spectrometer using KBr pellets (4000–400 cm^{-1}). The electronic spectra were obtained using a GBC UV/Vis Cintra 40 spectrophotometer. The NMR spectra were recorded on a Varian Gemini 200 instrument. The chemical shifts for the ^1H and ^{13}C spectra are referenced to the residual ^1H and ^{13}C present in deuterated dimethyl sulfoxide.

X-ray crystal structure determination

A crystal of complex **1** suitable for an X-ray diffraction study was obtained by the slow diffusion of *n*-propanol into an aqueous solution of the complex. The data of complex **1** were collected with a CCD Oxford Xcalibur S ($\lambda(Mo_{K\alpha})$ = 0.71073 Å) using the ω and φ scan modes at 130 K. Semi-empirical correction for absorption was performed with SCALE3 ABSPACK.[29] The structure was solved by direct methods.[30] Structure refinement was performed with SHELXL-97.[31] All non-hydrogen atoms were refined anisotropically and the H atoms were located in ΔF and refined isotropically. Table I lists crystallographic details. The hydrogen atoms from the *N*-methylpiperazine ligand were placed at their calculated positions and refined using the riding model. The PF_6^- anions are disordered as demonstrated by their larger-than-normal mean-square displacement parameters. The structural disorder of the PF_6^- anions explains the relatively high *R* factors. A disordered model for PF_6 with split F-atom positions was introduced. The resultant thermal parameters were better than those without the split of the F-atom positions. Also, the split of the F-atom positions in three parts were examined. In addition, the latter refinement involved severe correlations and the resultant thermal parameters of the F-atoms were still unreasonable. Therefore, the split positions within the PF_6^- anion were introduced into the calculations and a least-squares refinement in the space group $P2_1/c$ with disordered F-atoms was preferred with the present data.

TABLE I. Crystal data, data collection and refinement parameters for **1**

Empirical formula		$C_{15}H_{27}Cl_2N_2RuF_6P$
Formula weight, g mol^{-1}		552.33
Crystal system/space group		monoclinic/$P2_1/c$
a / Å		12.2534(7)
b / Å		7.9458(16)
c / Å		14.0359(8)
β / °		111.114(6)
V / $Å^3$		2082.2(2)
Z		4
ρ / g cm^{-3}		1.762
μ(MoKα) / mm^{-1}		1.142
F(000)		1112
Scan range, °		$2.98 < \theta < 25.51$
Reciprocal lattice segments	h	$-14 \rightarrow 14$,
	k	$-15 \rightarrow 15$,
	l	$-17 \rightarrow 16$
Reflections collected		3860

Table I. Continued

Reflections independent [R_{int}]	2198 [0.078]
Data/restraints/parameters	3860/0/236
Goodness-of-fit on F^2	1.00
R_1, wR_2 [$I > 2\sigma(I)$]	0.074, 0.183
R_1, wR_2 (all data)	0.135, 0.209
Largest differences peak and hole (e Å^{-3})	3.55 and –1.19

Crystallographic data for the structural analyses of **1** have been deposited with the Cambridge Crystallographic Data Centre, CCDC-658171. Copies of this information may be obtained free of charge from The Director, CCDC, 12 Union Road, Cambridge CB2 1EZ, UK (Fax: +44 1223-336033; E-mail: deposit@ccdc.cam.ac.uk; http//www.ccdc.cam.ac.uk).

Cytotoxicity assays

Preparation of the drug solutions. Stock solutions of the investigated ruthenium complexes were prepared in dimethyl sulfoxide (DMSO) at a concentration of 10 mM, filtered through a 0.22 μm Millipore filter before use and diluted with nutrient medium to various working concentrations. DMSO was used due to solubility problems. The nutrient medium was RPMI 1640 medium, without phenol red, supplemented with L-glutamine (3.0 mM), streptomycin (100 μg ml^{-1}), penicillin (100 IU ml^{-1}), 10 % fetal bovine serum (FBS) and 25 mM Hepes, was adjusted to pH 7.2 with bicarbonate solution. MTT, 3-(4,5-dimethylthiazol-2-yl)--2,5-diphenyltetrazolium bromide was dissolved (5.0 mg ml^{-1}) in phosphate buffer saline, pH 7.2, and filtered through a 0.22 μm Millipore filter before use. All reagents were products of Sigma Chemicals.

Cell culture. Human cervix adenocarcinoma HeLa, malignant melanoma Fem-x and human breast carcinoma MDA-MB-361 and MDA-MB-453 cells were cultured as monolayers in the nutrient medium, while human myelogenous leukemia K562 cells were maintained as a suspension culture. The cells were grown at 37 °C in a 5.0 % CO_2 humidified air atmosphere. For the growth of MDA-MB-361 and MDA-MB-453 cells and all subsequent experiments, the complete medium was enriched with 1.11 g dm^{-3} glucose. Peripheral blood mononuclear cells (PBMC) were separated from whole heparinized blood of a healthy volunteer by Lymphoprep (Nycomed, Oslo, Norway) gradient centrifugation. The interface cells, washed three times with Haemaccel (aqueous solution supplemented with 145 mM Na^+, 5.1 mM K^+, 6.2 mM Ca^{2+}, 145 mM Cl^- and 35 g dm^{-3} gelatin polymers, pH 7.4) were counted and resuspended in nutrient medium.

Cell sensitivity analysis. HeLa (2,000 cells per well), Fem-x (2,000 cells per well), MDA-MB-361 (10,000 cells per well), and MDA-MB-453 cells (3,000 cells per well) were seeded into 96-well microtiter plates and 20 h later, after cell adherence, five different concentrations of the investigated compounds were added to the wells. The final concentrations were in the range from 12.5 to 200 μM. Only nutrient medium was added to the cells in the control wells. The investigated compounds were added to a suspension of leukemia K562 cells (3,000 cells per well) 2 h after cell seeding, in the same final concentrations as applied to the HeLa and Fem-x cells. All experiments were performed in triplicate. Nutrient medium with the corresponding concentrations of the compounds but void of cells was used as the blanks. PBMC were seeded (150,000 cells per well) into nutrient medium or into nutrient medium enriched with (5.0 μg ml^{-1}) phytohaemaglutinin (PHA, Welcome Diagnostics, England) in 96-well microtiter plates and 2 h later the investigated compounds were added to the wells, in triplicate, at five final concentrations, except to the control wells where nutrient

medium only was added to the cells. Nutrient medium with the corresponding concentrations of the compounds but void of cells was used as the blanks.

Determination of target cell survival. Cell survival was determined by the MTT test according to the method of Mosmann[32] modified by Ohno and Abe[33] and Drakulić *et al*.,[34] 72 h after drug addition. The concentration IC_{50} of the investigated compounds which diminished the survival of the target cells by 50 % was assessed from graphs of cell survival *vs.* concentration of the investigated compound.

RESULTS AND DISCUSSION

Synthesis of the complexes

The neutral [(η^6-*p*-cymene)$RuCl_2(K_3tsc)$] (**2**) and cationic [(η^6-*p*-cymene)-$RuCl_2(CH_3NH(CH_2)_4NH)]PF_6$ (**1**) organoruthenium complexes were obtained by reaction of K_3tsc and *N*-methylpiperazine, respectively, with [(η^6-*p*-cymene)$_2$-$RuCl_2]_2$ at ambient temperature (Scheme 1). Complex **1** is well soluble in water, ethanol (methanol) and DMSO, whereas complex **2** is less soluble in water and ethanol.

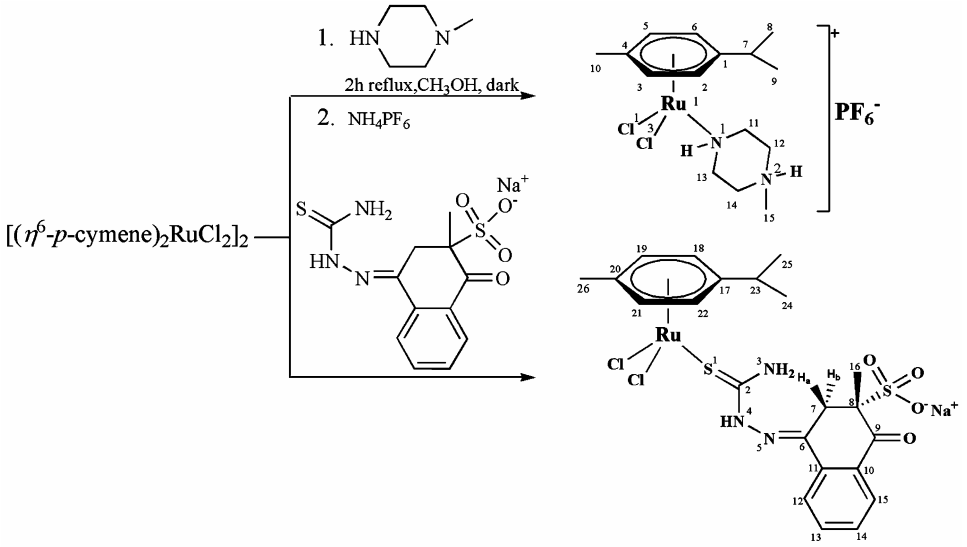

Scheme 1. Preparation of complexes **1** and **2**.

Thiosemicarbazones usually coordinate with a metal ion either in the neutral thione form or, after deprotonation, in the N,S ligand chelating mode. The diversity of coordination can be further increased by the introduction of an additional donor site into the thiosemicarbazone through the donor atom of carbonyl compounds.[11]

*X-ray diffraction study of **1***

The selected bond and angle parameters are listed in Table II. The molecule adopts the usual three-legged "piano-stool" arrangement generally found in

[M(η^6-arene)L_3] units (Fig. 1). Complex **1** is the first structurally characterized mononuclear complex of the [Ru(η^6-*p*-cymene)Cl_2L] type with the Ru atom bonded directly to a heterocyclic amine.

TABLE II. Selected bond lengths (Å) and angles (°) for complex **1**

Ru1–Cg[a]	1.674(5)	Ru1–Cl2	2.401(3)
Ru1–Cl1	2.420(2)	Ru1–N1	2.161(8)
Cg–Ru1–Cl1	127.15(16)	Cg–Ru1–Cl2	127.29(17)
Cg–Ru1–N1	135.0(2)	Cl1–Ru1–Cl2	87.63(9)
Cl1–Ru1–N1	82.2(2)	Cl2–Ru1–N1	80.6(2)

[a]The abbreviation Cg is the centroid of the η^6-arene ligand

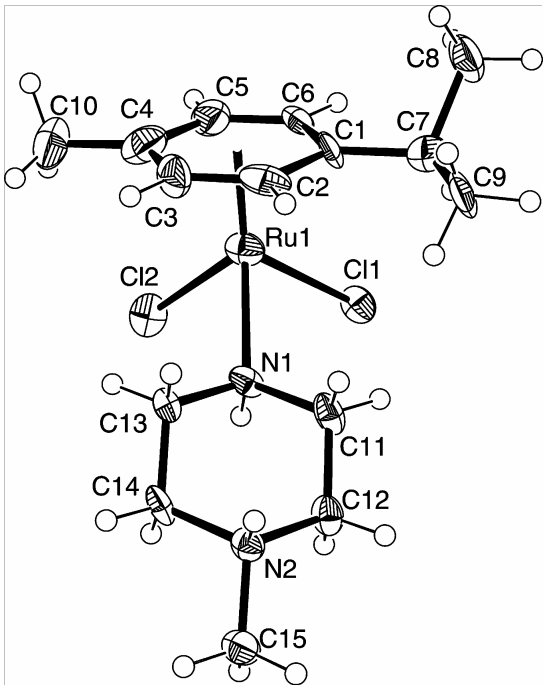

Fig. 1. ORTEP presentation of [(η^6-*p*-cymene)$RuCl_2(CH_3NH(CH_2)_4NH)]^+$ cation in crystals of **1**. Displacement ellipsoids are plotted at the 50 % probability level and H atoms are shown as small spheres of arbitrary radii.

The distance between the metal and the arene centroid, 1.674(5) Å is very similar to that observed in other ruthenium(II) complexes of the [Ru(η^6-*p*-cymene)Cl_2L] class (L/bond distance = dimethylamine/1.666; *sec*-butylamine/1.663–1.664; *p*-toluidine/1.637 Å).[35–37] Similarly to the mentioned complexes, the angles between the "legs" of the stool are slightly less than 90°, due to steric hindrance of the arene ligand. The Ru–N distance (2.161(8) Å) is comparable with the same bond distance in [$RuCl_2$(η^6-*p*-cymene)($NH(CH_3)_2$)] (2.165 Å), but it is significantly longer than those found in compounds of the same type,[36,37] indicating a relatively weaker bond.

An interesting feature of this structure is the protonation of both N atoms of the *N*-methylpiperazine ring, probably originating from NH_4PF_6.

Characterization of the complexes

The analytic and spectroscopic data of the synthesized complexes are as follows.

*[(*η^6-p-*cymene)RuCl$_2$(CH$_3$NH(CH$_2$)$_4$NH)]PF$_6$ (**1**).* Anal. Calcd. for $C_{15}H_{27}Cl_2N_2PF_6Ru$: C, 32.62; H, 4.93; N, 5.07. Found: C, 32.82; H, 4.93; N, 4.94. IR (KBr, cm^{-1}): 3331–3435, 1630, 1467, 841. ^{1}H-NMR (199.97 MHz, DMSO-d_6, δ, ppm): 8.14 (1H, *s*, N**H**), 5.79, 5.51 (4H, *m*, η^6–C$_6$**H**$_4$), 3.06 (4H, *t*, HN(C**H**$_2$)$_2$), 2.86 (4H, *m*, CH$_3$N(C**H**$_2$)$_2$), 2.30 (3H, *s*, NC**H**$_3$), 2.20 − 2.00 (4H, *m*, C**H**(CH$_3$)$_2$, η^6–C$_6$H$_4$–C**H**$_3$), 1.20 (6H, *d*, CH(C**H**$_3$)$_2$). ^{13}C-NMR (50 MHz, DMSO-d_6, δ, ppm): 106.60 (C-1), 100.31 (C-4), 86.58 (C-3,5), 85.73 (C-2,6), 51.46 (C-12,14), 45.60 (C-11,13), 43.14 (C-15), 30.18 (C-7), 21.70 (C-8,9), 18.07 (C-10). Electronic spectrum (H$_2$O) [λ_{max} / nm (ε_{max} / 10^3 dm^3 mol^{-1} cm^{-1})]: 386 (*sh*) (0.4), 306 (*sh*) (0.8), 255 (1.8).

*[(*η^6-p-*cymene)RuCl$_2$(K$_3$tsc)] (**2**).* Anal. Calcd. for $C_{22}H_{26}Cl_2N_3NaO_4S_2Ru$: C, 40.31; H, 4.00; N, 6.41; S, 9.80. Found: C, 40.41; H, 4.12; N, 6.92; S, 10.35; IR (KBr, cm^{-1}): 3363–3437, 1682, 1619, 1224, 1031, 762. ^{1}H-NMR (199.97 MHz, DMSO-d_6, δ, ppm): 10.88 (1H, *s*, N^4**H**), 9.70, 9.06 (2H, *s*, N^3**H**$_2$), 8.52 (1H, *d*, Ph**H**, tsc), 7.86 (1H, *d*, Ph**H**, tsc), 7.57 (2H, *q*, Ph**H**, tsc), 5.79, 6.28 (4H, *m*, η^6–C$_6$**H**$_4$), 3.80 (1H, *d*, **H**a, tsc), 2.87 (1H, *t*, **H**b, tsc), 2.15 (4H, *m*, C**H**(CH$_3$)$_2$, η^6–C$_6$H$_4$–C**H**$_3$), 1.51 (3H, *s*, C**H**$_3$, tsc), 1.23 (6H, *s*, CH(C**H**$_3$)$_2$). ^{13}C-NMR (50 MHz, DMSO-d_6, δ, ppm): 194.94 (C-2), 179.21 (C-9), 144.70 (C-6), 138.19 (C-10), 133.05 (C-12), 132.96 (C-15), 129.17 (C-11), 126.42 (C-14), 124.88 (C-13), 107.98 (C-17), 102.32 (C-20), 85.67 (C-19,21), 83.60 (C-18,22), 65.50 (C-8), 56.25 (C-17), 35.27 (C-7), 30.52 (C-23), 22.26 (C-26), 21.33 (C-16), 18.76 (C-24), 17.98 (C-25). Electronic spectrum (H$_2$O/EtOH, 50/50) [λ_{max} / nm (ε_{max} / 10^3 dm^3 mol^{-1} cm^{-1})]: 275 (*sh*) (15.3), 244 (19.4), 223 (19.3).

NMR spectra

The ^{1}H-NMR spectra of both complexes displayed characteristic resonances which can be attributed to the coordination of *p*-cymene, as well as thiosemicarbazone, or *N*-methylpiperazine. In both complexes the signals corresponding to the phenyl ring of cymene moiety are at δ 5.79 and 5.51 (**1**) and at 6.26 and 5.79 (**2**) ppm. The signals which can be assigned to the two methyl groups of the isopropyl groups are at 1.20 (**1**) and 1.23 (**2**) ppm. The methyl group of the *p*-cymene moiety displays a signal at around δ 2.10 ppm for both complexes. The signals assigned to the CH group of the isopropyl group were centered at δ 2.10 (**1**) and 2.15 (**2**) ppm. Hydrogen resonances due to the CH$_2$ groups of the piperazine ring are located at 2.72–2.97 ppm, appearing as a triplet of triplets ((C**H**$_2$)$_2$NCH$_3$), whereas those attached to the NH part of the heterocycle appear as a triplet centered at 3.06 ppm. The resonance confirming the protonation of the piperazine nitrogen is located at 8.14 ppm. In complex **2**, the signals corresponding to the phenyl ring of the coordinated K$_3$tsc are at δ 7.57 (*q*), 7.86 (*d*) and

8.52 (*d*). Two resonances at 3.80 and 2.87 ppm were assigned to the two diastereotropic protons of the CH_2 group of the thiosemicarbazone moiety. A signal that can be assigned to the methyl group of thiosemicarbazone is at δ 1.51 (*s*) ppm. Two resonances at 9.06 and 9.70 ppm were assigned to the two protons of the N^3H_2 chain, whereas the proton of the azomethine nitrogen appears at 11.88 ppm. The ^{13}C-NMR spectrum of complex **1** shows upfield shifts (51.46 (C-2,6), 45.60 (C-3,5), 43.14 (C-7)) for the piperazine part of the molecule comparing to free piperazine (56.29 (C-2,6), 46.75 (C-3,5) and 45.67 (C-7)), due to coordination *via* the unsubstituted N-4 nitrogen. In the spectrum of complex **2**, a slight upfield shift of C-2 was observed as a consequence of *S*-metallation, while no remarkable shifts of the other carbon atoms were observed.

Infrared spectra

The spectrum of the free ligand, K_3tsc, was compared with those of the complexes to confirm its coordination to metal ion. The ν(CS) vibrations suffer a negative shift from 1278 (**L**) to 1232 cm^{-1} (**2**). Also, the ν(CN) vibration of the C^2–N^4 bond is slightly shifted to lower frequencies due to the partial multiplicity of this bond after coordination. The peaks at 1690 cm^{-1} in the spectrum of the free ligand due to ν(C=O) vibrations and at 1639 cm^{-1} due to ν(CN) vibrations of C^6–N^5 remained unchanged in the complex, confirming the non-coordination of oxygen and the azomethine nitrogen to the metal ion.

This study showed that in complex **2**, K_3tsc acts as a neutral monodentate ligand, which is coordinated to the metal ion *via* the sulfur atom.

UV/Vis spectra

The complexes exhibit intense absorption in the visible region which can be ascribed to high intensity metal-to-ligand charge transfer bands which interfere with the expected d–d transitions, as is observed in low-spin d^6 ruthenium(II) complexes.[38] In general, complexes **1** and **2** exhibit two well resolved bands. The bands at higher wavelengths can be ascribed to a Ru(4dπ) → π*(NH) MLCT transition, whereas the bands at lower wavelengths are attributable to intraligand transitions or a combination of MLCT bands and intraligand transitions.

Cytotoxicity assays

The *in vitro* cytotoxicity of complexes **1** and **2** was determined by an MTT-based assay. The complexes were tested for cytotoxic activity on tumor cell lines: human adenocarcinoma HeLa, human myelogenous leukemia K562, human malignant melanoma Fem-x, human breast carcinoma MDA-MB-361 and MDA-MB-453 cells and on normal immunocompetent cells, *i.e.*, on human peripheral blood mononuclear PBMC cells non-stimulated and stimulated for proliferation with phytohaemaglutinin (PHA). The data are given in Table III and Fig. 2.

TABLE III. IC_{50} (μM) for 72 h of action of the investigated compounds on various tumor cells and on non-stimulated PBMC and PBMC stimulated with PHA, determined by the MTT test

Tumor cell	Compound	
	1	**2**
HeLa	>200	62.50±3.54
K562	>200	71.26±4.22
Fem-x	>200	152.10±5.18
MDA-MB-361	>200	101.84±6.54
MDA-MB-453	>200	62.46±5.98
PBMC-PHA	Not detected	61.10±1.12
PBMC+PHA	Not detected	40.38±1.12

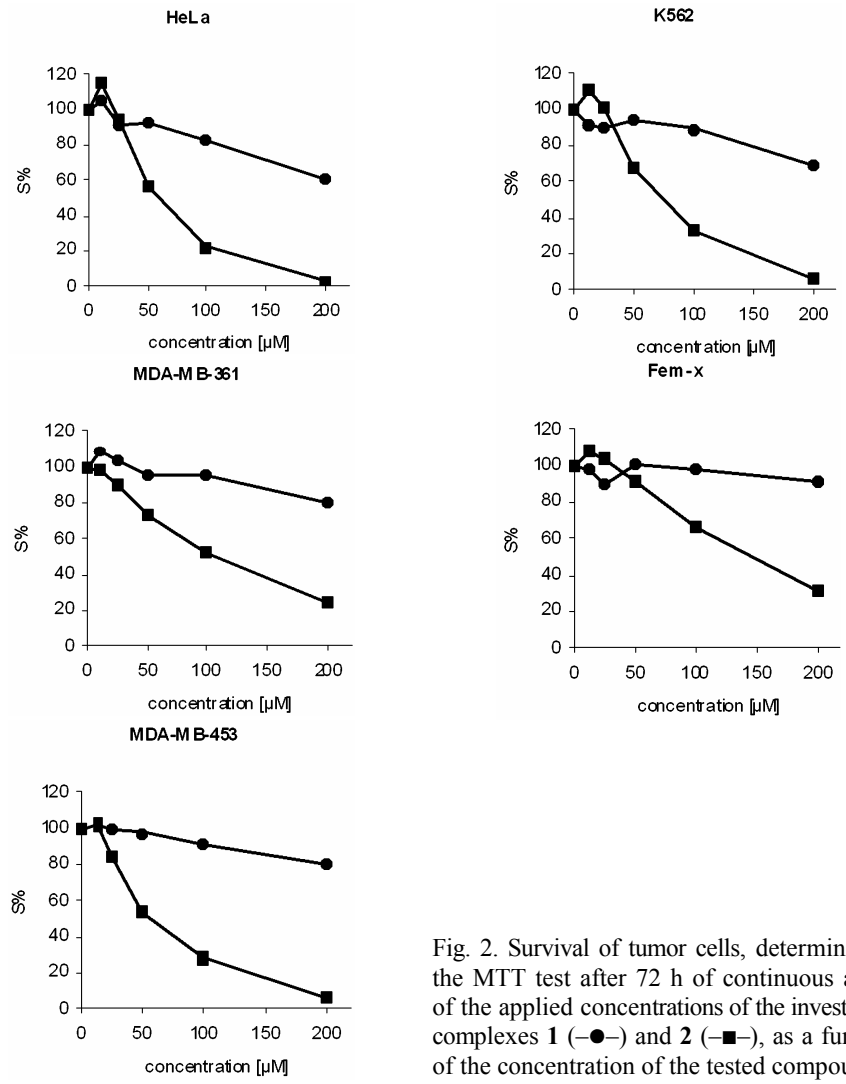

Fig. 2. Survival of tumor cells, determined by the MTT test after 72 h of continuous action of the applied concentrations of the investigated complexes **1** (–●–) and **2** (–■–), as a function of the concentration of the tested compounds.

Complex **1** exerted low activity against all the selected cell lines ($IC_{50} > 200$ μM, Table III and Fig. 2) as determined by the MTT test. This result is consistent with the characteristics of ruthenium compounds which are generally less cytotoxic than platinum compounds. One of two ruthenium complexes that is under clinical investigations, *trans*-[HInd][$RuCl_4(Ind)_2$] (Ind = indazole; KP1019) is only moderately cytotoxic to cancer cells,[39] whereas the other complex, *trans*-[HIm]-[$RuCl_4$(DMSO)(Im)] (Im = imidazole; NAMI-A) is relatively non-toxic to primary cancer cells, but exhibits antimetastatic activity.[40]

Complex **2** showed low to moderate activity with $IC_{50} = 152.10$ μM for Fem-x and $IC_{50} = 101.84$ μM for the slowly proliferating MDA-MB-361 cells. Against HeLa, K562 and the rapidly proliferating MDA-MB-453 cell lines, compound **2** exerted a moderate dose dependent antiproliferative action, with IC_{50} values of 62.50, 71.26 and 62.46 μM, respectively. Complex **2** was more active against the normal control PBMC, with $IC_{50} = 61.10$ μM for non-stimulated resting PBMC and $IC_{50} = 40.38$ μM for PBMC stimulated by PHA. Results from this work are in accordance with many publications which deal with antitumor activity of metal complexes of thiosemicarbazones[13,14,22] and of antileukemia potency of thiosemicarbazones.[41,42] In addition, this compound acted toxically, especially to PBMC which were stimulated for proliferation. This indicates that the mentioned complex might also have a capability for the suppression of autoimmune diseases. Further investigations in this direction need to be performed.

CONCLUSIONS

Two new organoruthenium complexes were synthesized and characterized. The results from this work showed that the ruthenium complex containing vitamin K_3-thiosemicarbazone as the organic part exerted its maximal cytotoxic activity against immunocompetent cells stimulated for proliferation. The higher activity of this complex compared with the complex containing *N*-methylpiperazine is probably related with the presence of vitamin K_3-thiosemicarbazone, itself active. In addition, the obtained data indicate that complex **2** could be further studied regarding its promising action for the control not only of malignant diseases, but also for the control of autoimmune diseases.

Acknowledgement. This work was supported by the Ministry of Science of the Republic of Serbia, Grant Nos. 142010 and 145006. The authors would like to thank Ms. Jelena Lazić and Mr. Aleksandar Savić for their help in the experimental part of this work.

И З В О Д

СИНТЕЗА, СТРУКТУРНА КАРАКТЕРИЗАЦИЈА И ЦИТОТОКСИЧНА АКТИВНОСТ ДВА НОВА ОРГАНОРУТЕНИЈУМ(II) КОМПЛЕКСА

САЊА ГРГУРИЋ-ШИПКА[1], MOHAMED AL.ARBI M. ALSHTEWI[1], ДЕЈАН ЈЕРЕМИЋ[1], ГОРАН Н. КАЛУЂЕРОВИЋ[2], SANTIAGO GÓMEZ-RUIZ[3], ЖЕЉКО ЖИЖАК[4], ЗОРИЦА ЈУРАНИЋ[4] и ТИБОР Ј. САБО[1]

[1]Хемијски факултет, Универзитет у Београду, Студентски трг 12–16, 11000 Београд, [2]Институт за хемију, технологију и металургију – Центар за хемију, Његошева 12, 11000 Београд, [3]Departamento de Química Inorgánica y Analítica, E. S. C. E. T., Universidad Rey Juan Carlos, 28933 Móstoles, Madrid, Spain и [4]Институт за онкологију и радиологију, 11000 Београд

Синтетисана су два нова *p*-цимен-рутенијум(II) комплекса који садрже као додатне лиганде *N*-метилпиперазин ([(η^6-*p*-cimen)$RuCl_2(CH_3NH(CH_2)_4NH)$]PF_6, комплекс **1**) и витамин K_3-тиосемикарбазон ([(η^6-*p*-cimen)$RuCl_2(K_3tsc)$], комплекс **2**). Оба нова комплекса добијена су полазећи од [(η^6-*p*-cimen)$_2RuCl_2]_2$ комплекса и одговарајућег лиганда. Комплекси су окарактерисани елементалном анализом, ИЦ, електронско-апсорпционом и НМР спектроскопијом. Рендгено–структурна анализа комплекса **1** показала је „piano-stool“ геометрију. У зависности од присутног лиганда дискутована је разлика у цитотоксичној активности ова два добијена комплекса.

(Примљено 27. децембра 2007, ревидирано 4. марта 2008)

REFERENCES

1. Y. K. Yan, M. Melchart, A. Habtemariam, P. J. Sadler, *Chem. Commun*. (2005) 4764
2. M. Melchart, P. J. Sadler, in *Bioorganometallics*: *Biomolecules, Labeling, Medicine,* G. Jaouen, Ed., Wiley-VCH, Weinheim, (2006), p. 39
3. C. S. Allardyce, A. Dorcier, C. Scolaro, P. J. Dyson, *Appl. Organomet. Chem*. **19** (2005) 1
4. C. N. Kato, A. Shinohara, N. Moriya, K. Nomiya, *Catal. Commun*. **7** (2006) 413
5. P. Pelagatti, A. Bacchi, F. Calbiani, M. Carcelli, L. Elviri, C. Pelizzi, D. Rogolino, *J. Organomet. Chem*. **690** (2005) 4602
6. R. E. Aird, J. Cummings, A. A. Ritchie, M. Muir, R. E. Morris, H. Chen, P. J. Sadler, D. I. Jodrell, *Br. J. Cancer* **86** (2002) 1652
7. R. E. Morris, R E. Aird, P. del S. Murdoch, H. M. Chen, J. Cummings, N. D. Hughes, S. Parsons, A. Parkin, G. Boyd, D. I. Jodrell, P. J. Sadler, *J. Med. Chem*. **44** (2001) 3616
8. V. Siguret, *Hematologie* **12** (2006) 389
9. S. A. Akman, R. Dietrich, R. Chlebowski, P. Limberg, J. B. Block, *Cancer Res*. **45** (1995) 5257
10. D. X. West, S. B. Padhye, P. B. Sonawane, *Struct. Bonding* **76** (1991) 1
11. J. S. Casas, M.S. García-Tasende, J. Sordo, *Coord. Chem. Rev*. **209** (2000) 197
12. D. C. Greenbaum, Z. Mackey, E. Hensell, P. Doyle, J. Gut, C. R. Caffrey, J. Lehrman, P. J. Rosenthal, J. H. McKerrow, K. Chibale, *J. Med. Chem*. **47** (2004) 3212
13. L. Feun, M. Modiano, K. Lee, J. Mao, A. Marini, N. Savaraj, P. Plezia, B. Almassian, E. Colacino, J. Fischer, S. MacDonald, *Cancer Chemother. Pharmacol*. **50** (2002) 223
14. J. Murren, M. Modiano, C. Clairmont, P. Lambert, N. Savaraj, T. Doyle, M. Sznol, *Clin. Cancer Res.* **9** (2003) 4092
15. E. C. Moore, A. C. Sartorelli, in *Inhibitors of Ribonucleoside Diphosphate Reductase Activity,* J. G. Cory, A. H. Cory, Eds., Pergamon Press, Oxford, 1989, pp. 203
16. H. L. Elford, M. Freese, E. Passamani, H. P. Morris, *J. Biol. Chem*. **245** (1970) 5228
17. Q. Li, H. Tang, Y. Li, M. Wang, L. Wang, C. Xia, *J. Inorg. Biochem*. **78** (2000) 167
18. H. A. Tang, L. F. Wang, L. D. Yang, *Trans. Met. Chem.* **28** (2003) 395

19. J. S. Casas, E. E. Castellano, M. D. Couce, J. Ellena, A. Sánchez. J. Sordo, C. Taboada, *J. Inorg. Biochem*. **100** (2006) 1858
20. U. K. Mazumder, M. Gupta, S. S, Karki, S. Bhattacharya, S. Rathinasamy, S. Thangavel, *Chem. Pharm. Bull.* **52** (2004) 178
21. F. Bregant, S. Pacor, S. Ghosh, S. K. Chattopadhyah, G. Sava, *Anticancer Res.* **13** (1993) 1011
22. S. Grgurić-Šipka, C. R. Kowol, S. M. Valiahdi, R. Eichinger, M. A. Jakupec, A. Roller, S. Shova, V. B. Arion, B. K. Keppler*, Eur. J. Inorg. Chem*. **18** (2007) 2870
23. A. Habtemariam, M. Melchart, R. Fernández, S. Parsons, I. D. H. Oswald, A. Parkin, F. P. A. Fabbiani, J. E. Davidson, A. Dawson, R. E. Aird, D. I. Jodrell, P. J. Sadler, *J. Med. Chem.* **49** (2006) 6858
24. S. M. Guichard, R. Else, E. Reid, B. Zeitlin, R. Aird, M. Muir, M. Dodds, H. Fiebig, P. J. Sadler, D. I. Jodrell, *Biochem. Pharm*. **71** (2006) 408
25. C. Scolaro, A. Bergamo, L. Brescacin, R. Delfino, M. Cocchietto, G. Laurenczy, T.J. Geldbach, G. Sava, P. J. Dyson, *J. Med. Chem.* **48** (2005) 4161
26. B. Serli, E. Zangrando, T. Gianferrara, C. Scolaro, P.J. Dyson, A. Bergamo, E. Alessio, *Eur. J. Inorg. Chem*. **17** (2005) 3423
27. H. Chen, J. A. Parkinson, R. E. Morris, P. J. Sadler, *J. Am. Chem. Soc.* **125** (2003) 173
28. S. B. Jensen, S. J. Rodger, M. D. Spicer, *J. Organomet. Chem*. **556** (1998) 151
29. SCALE3 ABSPACK, Empirical absorption correction, CrysAlis – Software package, Oxford Diffraction Ltd., 2006
30. G. M. Sheldrick, SHELXS-97, Program for Crystal Structure Solution, Gottingen, 1997
31. G. M. Sheldrick, SHELXL-97, Program for the Refinement of Crystal Structures, Gottingen, 1997
32. T. Mosmann*, J. Immunol. Meth*. **65** (1983) 55
33. M. Ohno, T. J. Abe, *J. Immunol. Meth.* **145** (1991) 199
34. B. J. Drakulić, Z. D. Juranić, T. P. Stanojković, I. O. Juranić, *J. Med. Chem*. **48** (2005) 5600
35. D. B. Dell'Amico, F. Calderazzo, L. Labella, F. Marchetti, E. Sbrana, *J. Organomet. Chem.* **651** (2002) 52
36. P. Pertici, E. Pitzalis, G. U. Barretta, F. Marchetti, P. Salvadori, *Gazz. Chim. Ital.* **125** (1995) 27
37. M. J. Begley, S. Harrison, A.H. Wright*, Acta Crystallogr.: C* **47** (1991) 318
38. D. Mishra, S. Naskar, M. G. B. Drew, S. Kumar Chattopadhyah, *Inorg. Chim. Acta* **359** (2006) 585
39. A. Galeano, M. R. Berger, B. K. Keppler, *Arzneim.-Forsch./Drug. Res.* **42** (1992) 821
40. G. Sava, R. Gagliardi, A. Bergamo, E. Alessio, G. Mestroni, *Anticancer Res.* **19** (1999) 969
41. I. Gojo, M. L. Tidwell, J. Greer, N. Takebe, K. Seiter, M. F. Pochron, B. Johnson, M. Sznol, J. E. Karp*, Leuk. Res*. **31** (2007) 1165
42. K. W. L. Yee, J. Cortes, A. Ferrajoli, G. Garcia-Manero, S. Verstovsek, W. Wierda, D. Thomas, S. Faderl, I. King, S.M. O'Brien, S. Jeha, M. Andreeff, A. Cahill, M. Sznol, F. J. Giles, *Leuk. Res*. **30** (2006) 813.

www.shd.org.rs

Journal of the Serbian Chemical Society

JSCS@tmf.bg.ac.yu • www.shd.org.rs/JSCS

J. Serb. Chem. Soc. *73* (6) 631–639 (2008) UDC 544.526.5+542.92+547.56:546.3–386+546.215
JSCS–3745 *Original scientific paper*

Photocatalytic degradation of Phenol Red using complexes of some transition metals and hydrogen peroxide

SAVITRI LODHA, DIPTI VAYA, RAKSHIT AMETA and PINKI B. PUNJABI*

Photochemistry and Solar Energy Laboratory, Department of Chemistry, University College of Science, M. L. Sukhadia University, Udaipur – 313002, Rajasthan, India

(Received 27 July, revised 20 December 2007)

Abstract: The photocatalytic degradation of Phenol Red was investigated using thiocyanate complexes of iron, copper, cobalt and hydrogen peroxide. The rate of photocatalytic degradation of the dye was followed spectrophotometrically. The effect of the variation of different parameters, such as pH, concentration of the complexes and dye, amount of H_2O_2 and light intensity on the rate of photocatalytic degradation was also studied. A tentative mechanism for the photocatalytic degradation of Phenol Red is proposed.

Keywords: photocatalytic degradation; Phenol Red; metal complexes; hydrogen peroxide.

INTRODUCTION

Water is one of the fundamental requirement of life and any undesired addition of chemical substances lead to its contamination and unfit for human use. Generally, various dyes found in industrial effluents, ultimately enter the aquatic ecosystem and can create various environmental hazards. These may have adverse, sometimes irreversible effects on animals and plants, as well. Adsorption, osmosis, flocculation and other methods have been used traditionally to remove dyes from water bodies, but all such methods suffer from various drawbacks. A group of waste treatment methods called AOPs (advanced oxidation processes), such as photo-Fenton and photocatalytic methods, are now widely used for this purpose.

The Fenton reagent is an established reagent for the degradation of dyes but main disadvantage of the reagent is that the reaction ceases after complete consumption of Fe^{2+}, whereas, in the photo-Fenton reaction, Fe^{2+} are regenerated from Fe^{3+} with the additional requirement of light. This makes the process cyclic in nature and the photochemical degradation proceeds smoothly.

Degradation of dyes employing the photo- Fenton reagent provides a newer method for the treatment of wastewater containing dye effluents. This reaction

* Corresponding author. E-mail: pb_punjabi@yahoo.com
doi: 10.2298/JSC0806631L

involves the formation of hydroxyl and perhydroxyl radicals.[1–4]. In addition to the involvement of $^{\bullet}OH$, some results on the mechanism of the Fenton reaction suggests the participation of a ferryl complex.[5] Prousek *et al.*[6] reported the utilization of the Fenton reaction for the degradation of dyes present in collared waste water. Nerud *et al.*[7] investigated the decolourisation of synthetic dyes by the Fenton reagent and the Cu/pyridine/H_2O_2 system. Chen *et al.*[8] observed the electrochemical degradation of Bromopyrogallol Red in the presence of cobalt ions. Verma *et al.*[9] investigated the decolourisation of synthetic dyes using a copper complex with glucaric acid. Lunak *et al.*[10] studied the photocatalytic effects of halogen penta-amine cobalt (III) complexes and H_2O_2. The photochemistry of complexes of a number of metals, such as Cr, Fe, Co, Pt, Mo and W was studied extensively by Zhang *et al.*[11] The photocatalytic effects of Fe (III) compounds were observed to play a dominant role in the degradation of 4-chlorophenoxyacetic acid initiated by polychromatic visible radiation.[12]

In a literature survey, no attention was found to have been paid to the photocatalytic degradation of Phenol Red dye using thiocyanate complexes of iron, copper and cobalt and H_2O_2. Therefore, in the present investigation an attempt was made to carry out photochemical degradation of Phenol Red dye in a homogeneous medium using thiocyanate complexes and H_2O_2, which generates $^{\bullet}OH$.

EXPERIMENTAL

The photochemical degradation of Phenol Red (HIMEDIA) was studied in the presence of a transition metal complex, *i.e.*, $[Fe(SCN)]^{2+}$, $[Cu(SCN)]^{+}$ or $[Co(SCN)]^{+}$, H_2O_2 and light. A stock solution of Phenol Red (1.0×10^{-3} M) was prepared in doubly distilled water. The Complex $[Fe(SCN)]^{2+}$ was prepared by mixing $FeCl_3$ (1.0×10^{-3} M, Himedia) and KSCN (1.0×10^{-3} M, Himedia) in a 1:1 ratio. The $[Cu(SCN)]^{+}$ and $[Co(SCN)]^{+}$ complexes were prepared in a similar manner. H_2O_2 (30 %, Merck) was a commercial product and was used as received. The reaction mixture containing dye (10^{-5} M), complex (10^{-6} M) and hydrogen peroxide was exposed to light for a certain period depending on the employed complex. A 200 W tungsten lamp (Philips) was used for the irradiation. The intensity of light at various distances was measured by a "Suryamapi" (CEL Model 201). The pH of the solution was measured using a digital pH meter (Systronics Model 335). The desired pH of the solution was adjusted by the addition of previously standardised 0.050 M sulphuric acid and 1.0 M sodium hydroxide solutions. A visible spectrophotometer (Systronics Model 106) was used for measuring the absorbance of the reaction mixture at regular time intervals.

RESULTS AND DISCUSSION

A 3.0 ml aliquot was taken from the reaction mixture at regular time intervals and the absorbance measured spectrophotometrically at λ_{max} value of 430 and 560 nm for acidic and basic medium, respectively. The absorbance of the solution was found to decrease with increasing time, which indicates that the concentration of Phenol Red decreased with increasing time of exposure. A plot of 2+log *A vs.* time was linear and followed pseudo-first order kinetics. The rate constant, *k*, was determined using the following expression:

$$k = 2.303 \times \text{slope}$$

The data for typical run are graphically presented in Fig. 1.

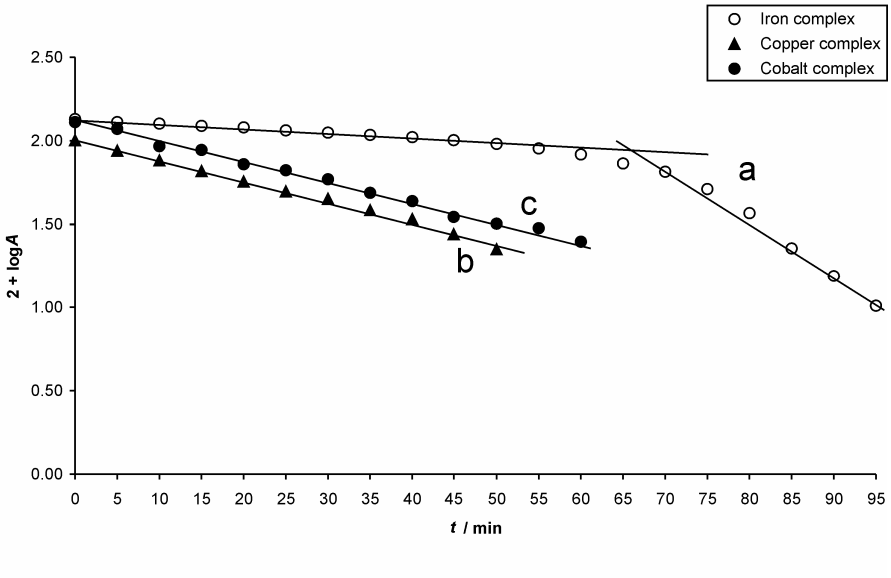

Fig. 1. 2+log *A vs.* time plots for different complexes; $V(H_2O_2)$ = 0.20 ml; complex concentration: 1.75×10^{-5} M; dye concentration: 5.00×10^{-5} (a) and 2.50×10^{-5} M (b and c); pH: 3.0 (a), 8.0 (b) and 9.0 (c); light intensity: 60 (a), 70 (b) and 40 mW cm^{-2} (c). Rate constants, *k*: 1.53×10^{-4} and 11.05×10^{-4} (a), 5.37×10^{-4} (b) and 4.61×10^{-4} s^{-1} (c).

For iron complex/H_2O_2 system, the reaction proceeded in two phases. The first phase was an induction period,[13] in which radicals were generated, whereas the major degradation of the dye occurred in second step, as shown by the sharp decrease in the absorbance.

Effect of pH

The effect of pH on photocatalytic degradation was investigated in the pH ranges 2.0–5.0, 7.0–9.0, 7.5–10.0 for the iron, copper and cobalt complexes, respectively. The results are reported in Table I.

The photochemical degradation of Phenol Red was maximal at pH 3.0, 8.0 and 9.0, with the iron, copper and cobalt complexes, respectively. The photochemical degradation depended strongly on the pH of the reaction medium. This can be explained based on Eqs. (1) and (2), which are part of the mechanism discussed later in the text:

$$Me^{n+} + H_2O_2 \rightarrow Me^{(n+1)+} + OH^- + {}^\bullet OH \quad (1)$$

$$Me^{(n+1)+} + H_2O \xrightarrow{h\nu} Me^{n+} + {}^\bullet OH + H^+ \quad (2)$$

TABLE I. Effect of pH on the degradation rate of Phenol Red. $V(H_2O_2)$ = 0.20 ml; complex concentration: 1.75×10^{-5} M; dye concentration: 5.00×10^{-5} (iron complex) and 2.50×10^{-5} M (copper and cobalt complex); light intensity: 60 (iron complex), 70 (copper complex) and 40 mW cm^{-2} (cobalt complex)

pH	k / 10^{-4} s^{-1}			
	Iron complex		Copper complex	Cobalt complex
	k_1	k_2		
2.0	0.26	0.81	–	–
2.5	0.75	2.1	–	–
3.0	1.5	11.0	–	–
3.5	0.10	0.16	–	–
4.0	0.040	0.13	–	–
4.5	0.030	0.10	–	–
5.0	0.020	0.060	–	–
7.0	–	–	2.82	–
7.5	–	–	4.80	3.65
8.0	–	–	5.37	3.94
8.5	–	–	3.96	4.27
9.0	–	–	3.66	4.61
9.5	–	–	–	3.61
10.0	–	–	–	1.97

In case of the iron complex, it was observed that rate of degradation of the dye increased on decreasing the pH from 5.0 to 3.0. This may be due to the dominance of Eq. (1) over Eq. (2), where OH^- are generated. These OH^- are removed on increasing the H^+ concentration with decreasing pH. This will facilitate *via* Eq. (1) the formation of more $^{\bullet}OH$, which are utilized for the oxidative degradation of Phenol Red and thiocyanate radicals. On decreasing the pH further, *i.e.*, below 3.0, the reaction rate decreased again. This may be attributed to the fact that Eq. (2) commences to dominate over Eq. (1), as $Fe(OH)_3$ is less soluble than $Fe(OH)_2$ and the generation of $^{\bullet}OH$ *via* Eq. (2) is retarded at pH values lower than 3.0.[14]

In cases of the copper and cobalt complexes, the reaction proceeds faster in basic media. The rate of degradation of dye increased on increasing the pH from 7.0 to 8.0 and from 7.5 to 9.0 for copper and cobalt complexes, respectively. This may be due to the dominance of Eq. (2) over Eq. (1), in which H^+ are generated. These H^+ are removed by increasing the concentration of OH^-. This will facilitate Eq. (2), forming more $^{\bullet}OH$, which are utilized for the oxidative degradation of Phenol Red as well as the thiocyanate radical. Above pH 8.0 and 9.0 for the copper and cobalt system, respectively, increasing the pH further resulted in a decrease in the rate of degradation, which can be attributed as the dominance of Eq. (2) over Eq. (1), in which H^+ are generated.

Effect of hydrogen peroxide

The effect of amount of H_2O_2 on the rate of photocatalytic degradation of Phenol Red was also investigated. The results are reported in Table II.

TABLE II. Effect of the concentration of H_2O_2 on the degradation rate of Phenol Red. Complex concentration: 1.75×10^{-5} M; dye concentration: 5.00×10^{-5} (iron complex) and 2.50×10^{-5} M (copper and cobalt complex); pH: 3.0 (iron complex), 8.0 (copper complex) and 9.0 (cobalt complex); light intensity: 60 (iron complex), 70 (copper complex) and 40 mW cm^{-2} (cobalt complex)

$V(H_2O_2)$ / ml	k / 10^{-4} s^{-1}			
	Iron complex		Copper complex	Cobalt complex
	k_1	k_2		
0.0	0.060	0.16	0.66	0.38
0.10	0.45	0.81	1.4	2.3
0.20	1.5	11.0	3.1	2.9
0.30	1.4	10.2	3.4	3.1
0.40	1.4	10.0	3.7	3.3
0.50	1.3	9.8	3.8	3.4
0.60	1.2	9.4	4.0	4.2
0.70	1.1	7.4	5.4	4.6

The rate of photochemical degradation of Phenol Red was maximal with 0.20 ml H_2O_2 for the iron complex, This may be explained because increasing the amount of H_2O_2 would result in more $^{\bullet}OH$, responsible for the oxidative degradation of Phenol Red, being formed. However, after a certain amount of H_2O_2 (0.20 ml), a further increase in the amount of H_2O_2 would produce more OH^- ions together with $^{\bullet}OH$ and, as a result, the pH of the medium would increase, resulting in a decrease in the rate of degradation.

A different kind of behaviour was observed for the copper and cobalt complex systems. In these cases, a continuous increase in the rate of degradation of Phenol Red was observed with increasing amount of H_2O_2 in the range from 0.0 to 0.70 ml. This may be attributed to the fact that Eq. (1) does not dominate over Eq. (2) in these cases and hence no decrease in the rate was observed with increasing amount of H_2O_2.

Effect of the concentration of the complexes

The effect of the concentration of the complexes on the rate of photocatalytic degradation of Phenol Red was studied by keeping all other factors identical. The results are given in Table III.

It is clear from the data that the rate of photocatalytic degradation increases with increasing concentration of the complexes. The rates were determined up to concentrations of 1.75×10^{-5}, 4.37×10^{-5}, 1.75×10^{-5} M for the iron, copper and cobalt complexes, respectively. Above these limits, the rates were extremely fast and it was not possible to study the rates satisfactorily due to experimental limitations. This increasing trend may be explained by more molecules of the com-

plexes being available to participate in the reaction. This results in an enhanced generation of •OH and, therefore, the rate of photocatalytic degradation of the dye increases.

TABLE III. Effect of complex concentration on the degradation rate of Phenol Red. $V(H_2O_2)$ = 0.20 ml; dye concentration: 5.00×10^{-5} (iron complex) and 2.50×10^{-5} M (copper and cobalt complex); pH: 3.0 (iron complex), 8.0 (copper complex) and 9.0 (cobalt complex); light intensity: 60 (iron complex), 70 (copper complex) and 40 mW cm^{-2} (cobalt complex)

Complex concentration $\times10^5$ M	k / 10^{-4} s^{-1}			
	Iron complex		Copper complex	Cobalt complex
	k_1	k_2		
0.0	0.22	0.25	0.83	0.85
0.25	0.38	0.80	–	2.3
0.50	0.46	0.90	–	2.9
0.62	–	–	2.9	–
0.75	0.75	3.0	–	3.4
1.0	1.1	6.0	–	4.0
1.2	1.5	7.0	3.3	4.3
1.5	1.5	9.0	–	4.4
1.8	1.5	11.0	–	4.6
1.9	–	–	4.1	–
2.5	–	–	4.3	–
3.1	–	–	4.5	–
3.8	–	–	4.7	–
4.4	–	–	5.4	–

Effect of the Phenol Red concentration

The effect of the Phenol Red concentration on the rate of photocatalytic degradation was also examined and the results are given in Table IV.

TABLE IV. Effect of the dye concentration on the degradation rate of Phenol Red. $V(H_2O_2)$ = = 0.20 ml; complex concentration: 1.75×10^{-5} M; pH: 3.0 (iron complex), 8.0 (copper complex) and 9.0 (cobalt complex); light intensity: 60 (iron complex), 70 (copper complex) and 40 mW cm^{-2} (cobalt complex)

Dye concentration $\times10^5$ M	k / 10^{-4} s^{-1}			
	Iron complex		Copper complex	Cobalt complex
	k_1	k_2		
1.50	–	–	4.02	1.03
2.00	1.42	7.66	4.70	3.07
2.50	–	–	5.37	4.61
3.00	1.48	9.68	5.04	4.10
3.50	–	–	4.76	3.94
4.00	1.53	10.1	4.56	3.85
4.50	–	–	4.35	3.58
5.00	1.53	11.0	4.23	3.07
6.00	1.02	10.2	–	–
7.00	0.760	10.9	–	–
8.00	0.500	10.1	–	–

The rate of degradation was found to increase with increasing concentration of Phenol Red up to 5.00×10^{-5}, 2.50×10^{-5} and 2.50×10^{-5} M for the $[Fe(SCN)]^{2+}$, $[Cu(SCN)]^{+}$, $[Co(SCN)]^{+}$ complexes, respectively. Further increasing of the concentration beyond these limits decreases the rate of degradation. This may be explained on the basis that, on increasing the concentration of Phenol Red, the reaction rate increases as more molecules of the dye were available for degradation. Further increase in the concentration causes a retardation of the reaction because at higher concentrations, the dye molecules themselves act as a filter for the incident light, thus the full intensity of the light was not employed in the photodegradation, which resulted in a decrease in the rate of degradation. Moreover, at the higher concentration, the number of collisions between dye molecules increases whereas the number of collisions between dye molecules and $^{\bullet}OH$ decreases. Consequently, the rate of the reaction is retarded. An unsuitable steric orientation is also another factor for a decrease in the rate of reaction.[15,16]

Effect of light intensity

The effect of the light intensity on the photocatalytic degradation of Phenol Red was also investigated and the results are reported in Table V.

TABLE VI. Effect of the light intensity on the degradation rate of Phenol Red. $V(H_2O_2)$ = = 0.20 ml; dye concentration: 5.00×10^{-5} (iron complex) and 2.50×10^{-5} M (copper and cobalt complex); complex concentration: 1.75×10^{-5} M; pH: 3.0 (iron complex), 8.0 (copper complex) and 9.0 (cobalt complex)

Light intensity mW cm^{-2}	k / 10^{-4} s^{-1}			
	Iron complex		Copper complex	Cobalt complex
	k_1	k_2		
10.0	0.43	0.57	3.87	3.86
20.0	0.65	8.1	4.19	4.04
30.0	0.87	8.2	4.48	4.32
40.0	1.1	8.4	4.65	4.61
50.0	1.3	9.6	4.78	4.43
60.0	1.5	11.0	5.07	4.32
70.0	1.3	10.9	5.37	4.20
80.0	1.3	8.8	4.78	4.04

The data indicate that an increase in the light intensity increases the rate of reaction and maxima were found at 60, 70 and 40 mW cm^{-2} for the iron, copper and cobalt complexes, respectively. This may be explained by an increase in the number of photons striking per unit area as the light intensity was increased. A further increase in the intensity beyond the maximum limits resulted in a decreease in the rate of reaction, which may be due to thermal side reactions.

MECHANISM

Based on the experimental observations and corroborating existing literature, a tentative mechanism is proposed for the degradation of Phenol Red in presence of iron and copper complexes, H_2O_2 and light:[17]

$$[Me(SCN)]^{n+} \xrightarrow{h\nu} Me^{n+} + {}^{\bullet}SCN \quad (3)$$

$$Me^{n+} + H_2O_2 \rightarrow Me^{(n+1)+} + OH^- + {}^{\bullet}OH \quad (1)$$

$$Me^{(n+1)+} + H_2O \xrightarrow{h\nu} Me^{n+} + {}^{\bullet}OH + H^+ \quad (2)$$

$${}^{\bullet}SCN + 8{}^{\bullet}OH \rightarrow SO_4^{2-} + NH_4^+ + CO_2 + 2H_2O \quad (4)$$

$$Dye + {}^{\bullet}OH \rightarrow Products \quad (5)$$

$${}^{\bullet}OH + {}^{\bullet}OH \rightarrow H_2O_2 \quad (6)$$

$$2H_2O_2 \rightarrow 2H_2O + O_2 \quad (7)$$

where Me denotes iron or copper.

In case of cobalt complex, the following mechanism is proposed:

$$[Me(SCN)]^{n+} \xrightarrow{h\nu} Me^{(n+1)+} + SCN^- \quad (8)$$

$$Me^{(n+1)+} + H_2O \xrightarrow{h\nu} Me^{n+} + {}^{\bullet}OH + H^+ \quad (2)$$

$$Me^{n+} + H_2O_2 \rightarrow Me^{(n+1)+} + OH^- + {}^{\bullet}OH \quad (1)$$

$${}^{\bullet}SCN + 8{}^{\bullet}OH \rightarrow SO_4^{2-} + NH_4^+ + CO_2 + 2H_2O \quad (4)$$

$$Dye + {}^{\bullet}OH \rightarrow Products \quad (5)$$

$${}^{\bullet}OH + {}^{\bullet}OH \rightarrow H_2O_2 \quad (6)$$

$$2H_2O_2 \rightarrow 2H_2O + O_2 \quad (7)$$

The photo-Fenton reaction is one of the examples of classical photocatalytic process in homogeneous system that involves H_2O_2, iron(III) and visible radiation. The thiocyanate complex of Fe^{3+} gives Fe^{2+} and the thiocyanate radical on exposure to light. The Fe^{2+} decomposes hydrogen peroxide into ${}^{\bullet}OH$, OH^- and Fe^{3+}. The Fe^{3+} decomposes water photochemically to give ${}^{\bullet}OH$ and Fe^{2+}. The thiocyanate radical and the dye are decomposed by hydroxyl radicals to simpler ions/molecules, such as sulphates and ammonium ion, carbon dioxide, water, *etc*.

The above-proposed mechanism for the iron complex is also applicable for the copper complex.

The mechanism for the cobalt complex differs from that for the iron and copper complexes in that the iron and copper complexes involve thiocyanate radicals, whereas in the case of the cobalt complex, thiocyanate ions are involved. The release of thiocyanate ion from its cobalt complex was ascertained by its spot test,[18] however, the negative spot test for thiocyanate ions in the case of the iron and copper complexes indicates that ${}^{\bullet}SCN$ was involved in this reaction and not SCN^-.

CONCLUSIONS

The rate of photocatalytic degradation of Phenol Red was enhanced by metal complexes. The following order of the degradation rate with different metal complexes was found:

$$[Fe(SCN)]^{2+} > [Cu(SCN)]^+ > [Co(SCN)]^+$$

Hydroxyl radicals photocatalytically degrade Phenol Red. The participation of $^{\bullet}OH$ as active oxidising species was confirmed by using hydroxyl radical scavengers, where the rate of photodegradation was drastically reduced.

Further, this method is more advantageous over other methods, since it does not add further to pollution. The active oxidising species, the hydroxyl radicals, dimerise to give hydrogen peroxide, which degrades ultimately to water and oxygen.

Acknowledgement. We are thankful to Prof. S. C. Ameta for valuable critical discussions. SL is thankful to the UGC for the award of JRF.

И З В О Д

ФОТОКАТАЛИТИЧКА РАЗГРАДЊА ФЕНОЛ-ЦРВЕНОГ КОМПЛЕКСИМА НЕКИХ ПРЕЛАЗНИХ МЕТАЛА И ВОДОНИК-ПЕРОКСИДОМ

SAVITRI LODHA, DIPTI VAYA, RAKSHIT AMETA и PINKI B. PUNJABI

Photochemistry and Solar Energy Laboratory, Department of Chemistry, University College of Science, M. L. Sukhadia University, Udaipur – 313002, Rajasthan, India

Фотокаталитичка разградња фенол-црвеног испитивана је помоћу тиоцијанатних комплекса гвожђа, бакра и кобалта и водоник-пероксида. Брзина фотокаталитичке разградње обојеног једињења праћена је спектрофотометријски. Такође је испитивана и утицај разних параметара на брзину фотокаталитичке разградње, као што су pH, концентрација комплекса и обојеног једињења, количина H_2O_2 и интензитет светлости. Предложен је механизам реакције фотокаталитичке разградње фенол-црвеног.

(Примљено 27. јула, ревидирано 20. децембра 2007)

REFERENCES

1. W. G. Barb, J. H. Baxendale, P. George, K. R. Hargrave, *Trans. Faraday Soc.* **47** (1951) 591
2. C. Walling, *Acc. Chem. Res.* **8** (1975) 125
3. R. G. Zepp, B. C. Faust, J. Hoigue, *J. Environ. Sci. Technol.* **26** (1992) 313
4. J. J. Pignatello, G. Chapa, *Environ. Toxicol. Chem.* **13** (1994) 423
5. J. J. Pignatello, D. Liu, P. Huston, *Environ. Sci. Technol.* **33** (1999) 1832
6. J. Prousek, E. Ivanova, M. Kochmanikova, *Chem. List.* **91** (1997) 48
7. F. Nerud, P. Baldrian, J. Gabriel, D. Ogbeifun, *Chemosphere* **44** (2001) 957
8. J. Chem, M. Liu, J. Zhang, Y. Xian, L. Jin, *Chemosphere* **53** (2003) 1131
9. P. Verma, V. Shah, P. Baldrian, J. Gabriel, P. Stopka, T. Trnka, F. Nerud, *Chemosphere* **54** (2004) 291
10. S. Lunak, P. Sedlak, P. Lederer, *J. Photochem. Photobiol.* **72A** (1993) 169
11. Q. H. Wu, B. W. Zhang, Y. Cao, J. W. Bai, *J. Photochem. Photobiol.* **106** (1999) 170
12. S. Lunak, J. Brodilova, J. Muzart, *Collect. Czech. Commun*. **62** (1997) 1843
13. F. Chem, W. Ma, J. He, J. Zhao, *J. Phys. Chem. A* **106** (2002) 9485
14. *Lange's Handbook of Chemistry*, J. A. Dean, Ed., McGraw-Hill, New York, 1978, Ch. 5
15. K. J. Laidler, *Chemical Kinetics*, Tata McGraw Hill Publishing Co. Ltd., New York, 1994, p. 65
16. A. Jain, P. B. Punjabi, V. K. Sharma, S. C. Ameta, *J. Indian Chem. Soc.* **84** (2007) 996
17. K. Lang, S. Lunak, *Photochem. Photobiol. Sci.* **1** (2002) 588
18. F. Feigl, V. Anger, *Spot Tests in Inorganic Analysis*, Elsevier, Amsterdam, 2005, p. 432.

www.shd.org.rs

Journal of the Serbian Chemical Society

JSCS@tmf.bg.ac.yu • www.shd.org.rs/JSCS

J. Serb. Chem. Soc. *73* (6) 641–654 (2008) UDC 544.032.4:66.094.1:546.92+544.478+546.26
JSCS–3746 *Original scientific paper*

Temperature dependence of the kinetics of oxygen reduction on carbon-supported Pt nanoparticles

NEVENKA R. ELEZOVIĆ[1]*#, BILJANA M. BABIĆ[2], NEDELJKO V. KRSTAJIĆ[3], SNEŽANA LJ. GOJKOVIĆ[3] and LJILJANA M. VRAČAR[3]

[1]*Institute for Multidisciplinary Research, P. O. Box 33, Belgrade,* [2]*Vinča Institute of Nuclear Sciences, P. O. Box 522, 11001 Belgrade and* [3]*Faculty of Technology and Metallurgy, University of Belgrade, Karnegijeva 4, 11120 Belgrade, Serbia*

(Received 11 July, revised 20 November 2007)

Abstract: The temperature dependence of oxygen reduction reaction (ORR) was studied on highly dispersed Pt nanoparticles supported on a carbon cryogel. The specific surface area of the support was 517 m^2 g^{-1}, the Pt particles diameter was about 2.7 nm and the loading of the catalyst was 20 wt. %. The kinetics of the ORR at the Pt/C electrode was examined in 0.50 mol dm^{-3} $HClO_4$ solution in the temperature range from 274 to 318 K. At all temperatures, two distinct E–log j regions were observed; at low current densities with a slope of $-2.3RT/F$ and at high current densities with a slope of $-2.3\times2RT/F$. In order to confirm the mechanism of oxygen reduction previously suggested at a polycrystalline Pt and a Pt/Ebonex nanostructured electrode, the apparent enthalpies of activation at selected potentials *vs.* the reversible hydrogen electrode were calculated in both current density regions. Although $\Delta H^{\neq}_{a,l} > \Delta H^{\neq}_{a,h}$, it was found that the enthalpies of activation at the zero Galvani potential difference were the same and hence it could be concluded that the rate-determining step of the ORR was the same in both current density regions. The synthesized Pt/C catalyst showed a small enhancement in the catalytic activity for ORR in comparison to the polycrystalline Pt, but no change in the mechanism of the reaction.

Keywords: oxygen reduction reaction; platinum catalyst; carbon support; temperature dependence; enthalpy of activation.

INTRODUCTION

Platinum is the most active electrocatalyst for the oxygen reduction reaction (ORR) and it is still the only electrode material that can fulfill the demands for fuel cells working in acidic media. The kinetics of this reaction was extensively studied on smooth polycrystalline[1–8] and monocrystalline[6,9–14] Pt surfaces and on supported Pt nanoparticles,[15–22], as well as on Pt-based alloys[23–25] and Pt-al-

* Corresponding author. E-mail: nelezovic@tmf.bg.ac.yu
# Serbian Chemical Society member.
doi: 10.2298/JSC0806641E

loy nanoparticles.[19,26] Investigations on supported Pt nanoparticles are especially important because this type of electrocatalyst is employed for the fabrication of gas-diffusion electrodes in fuel cells with a solid polymer electrolyte (SPEFC). Most of the research was focused on the effects of loading,[17,21] particle size,[15–17] supporting material[17,22] and the influence of the alloying metal.[19,26] However, there has been little systematic research on the temperature dependence of the ORR on Pt nanoparticles, although SPEFCs operate at elevated temperatures. Paulus *et al.*[18] investigated the ORR on a Pt/Vulcan rotating disk electrode and found good agreement of both the Tafel slopes and the activation energy with the corresponding values on a single crystal[13] and polycrystalline Pt surfaces.[8] Yano *et. al.*[20] used a channel flow double electrode cell operating as a closed system in to order to eliminate any influence of temperature on the concentration of oxygen in the electrolyte. The activities of Pt/Carbon black and a bulk Pt film with and without a Nafion coating were investigated at temperatures in the range 30 to 110 °C. At all three electrodes, the current densities per real surface area and the apparent energy of activation agreed quite well, with the last being close to the results of Paulus *et al*.[18]

The temperature dependence of the ORR is not only important from the practical point of view, but it can also be used as a diagnostic tool for the elucidation of the mechanism of the reaction. A well established fact about the ORR on Pt is that the Tafel slopes differ at low and high current densities.[3,5,8–13,18–22] It was postulated that this is not caused by a change in the rate determining step but in the surface coverage by adsorbed intermediates. Šepa *et al.*[8] proved this by comparing the enthalpy of activation at zero Galvani potential difference for these two current density regions.

In this study, the temperature dependence of the ORR on Pt nanoparticles supported on a carbon cryogel was investigated in order to determine the mechanism of the reaction and to compare it with that of a polycrystalline Pt surface.

EXPERIMENTAL

Preparation of the catalyst

The catalyst used in the experiments was platinum nanoparticles supported on a carbon cryogel powder. The carbon cryogel was synthesized by a sol–gel polycondensation and freeze-drying; its BET surface area was 517 $m^2\ g^{-1}$.[27] The platinum was deposited on the support by a modified ethylene glycol method. The details of the preparation are given elsewhere.[28] The Pt loading of the catalyst was 20 wt. %.

Characterization of the catalyst

The Pt/C catalyst was characterized by X-ray diffraction (XRD) analysis and transmission electron microscopy (TEM). The XRD measurements were performed on a Siemens D500 X-ray diffractometer using CuKα radiation with a Ni filter. The 2θ angular region between 5 and 80° was explored at a scan rate of 0.02° s^{-1} with an angular resolution of 0.02° for all XRD tests.

The transmission electron microscopy (TEM) measurements were performed at the National Center for Electron Microscopy, USA, (NCEM) using an FEI (Phillips electronic instruments). The catalyst powder was suspended in ethanol, dropped onto a clean holey carbon grid and dried in air. The particle size distribution was determined from images of 20 different regions containing 10–20 particles each. The particle shape was determined by real space crystallography using high-resolution images taken from particles near or on the edge of the carbon black substrate and/or by numerical Fourier filtering of the digitized image intensity spectrum of particles on the top of the carbon.

Electrode preparation

The catalyst was applied to a gold substrate (6 mm diameter) in the form of a thin film. One milligram of Pt/C catalyst was mixed with 1.0 ml of water and 50 μl of Nafion solution (5 wt. %, Aldrich). The suspension was agitated in an ultrasonic bath for 60 min and 12.5 μl of it was placed on the gold electrode using a micro-pipette. After volatilization of the solvent, the electrode was heated at 80 °C for 10 min. The amount of Pt on the electrode was 2.5 μg, *i.e.*, 8.8 μg cm^{-2}.

Electrochemical measurements

A conventional three-compartment all-glass cell was used. The gold working electrode covered with a thin film of the Pt/C catalyst was in the form of rotating disk. The counter electrode was a platinum sheet of 5.0 cm^2 geometric area. A reversible hydrogen electrode in the same solution, maintained at room temperature in a compartment separated from the working electrode, was used as the reference electrode. All potentials are referred to the reversible hydrogen electrode (RHE). The electrolyte was 0.50 mol dm^{-3} $HClO_4$ solution (Spectrograde, Merck), prepared with high purity water (Millipore, 18 MΩ cm resistivity) at 293 K. The measurements were performed in the temperature range from 273 to 318 K.

Cyclic voltammetry was carried out in the electrolyte saturated with high purity nitrogen in the potential range from 0.03 to 1.40 V, at a sweep rate of 100 mV s^{-1}. Polarization curves of the ORR were recorded in the same solution saturated with O_2, bubbled continuously at 10^5 Pa pressure through the working electrode compartment. A slow linear sweep (1.0 mV s^{-1}) and a potentiostatic steady-state technique were applied. The electrode was rotated at 1600 rpm. An EG&G 273 potentiostat and a Philips PM 8143 X–Y recorder were employed in all the electrochemical experiments.

RESULTS AND DISCUSSION

Structure and particle size of the Pt/C catalyst

The XRD pattern of the Pt/C catalyst, given in Fig. 1, shows three characteristic reflection peaks: a peak at 2θ = 44.2°, corresponding to the hexagonal graphite structure (100) and peaks at about 39 and 46°, corresponding to the Pt (111) and Pt (200) plane, respectively. The first peak suggests good graphite characteristics of the carbon cryogel and the diffraction peaks of fcc Pt demonstrate a successful reduction of the Pt precursor to metallic Pt.

The low magnification TEM micrograph, presented in Fig. 2a, shows a very uniform Pt nanoparticles distribution. The mean particle size was determined as 2.7±0.7 nm. The atomically resolved image in Fig. 2b shows Pt atomic rows, with a spacing corresponding to the (200) and (111) planes of the fcc Pt nano-

particles, as indicated in the corresponding digital diffractogram also given in Fig. 2b. The Pt particles have the common cubo-octahedral shape. Occasionally twinned particles were observed with the same (111) twinning plane, as was observed with some other Pt-based catalysts.[29]

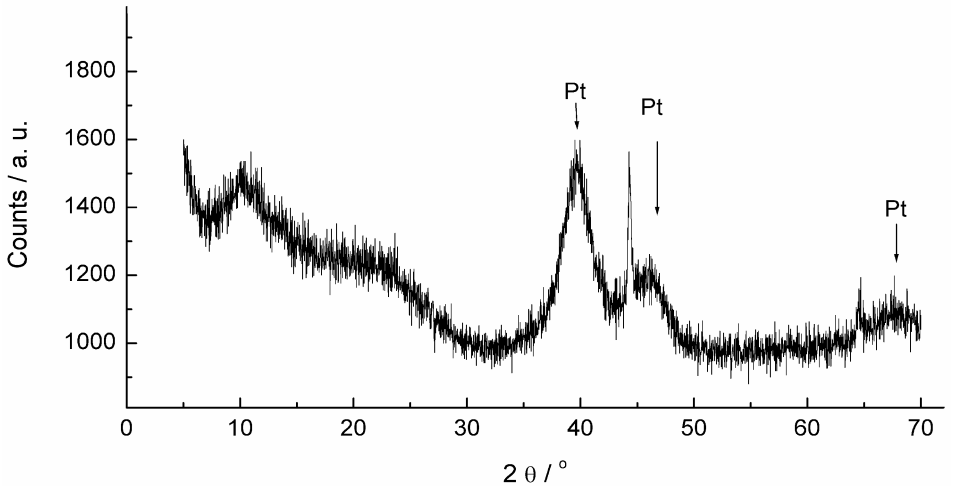

Fig. 1. X-Ray diffraction pattern of the Pt/C catalyst.

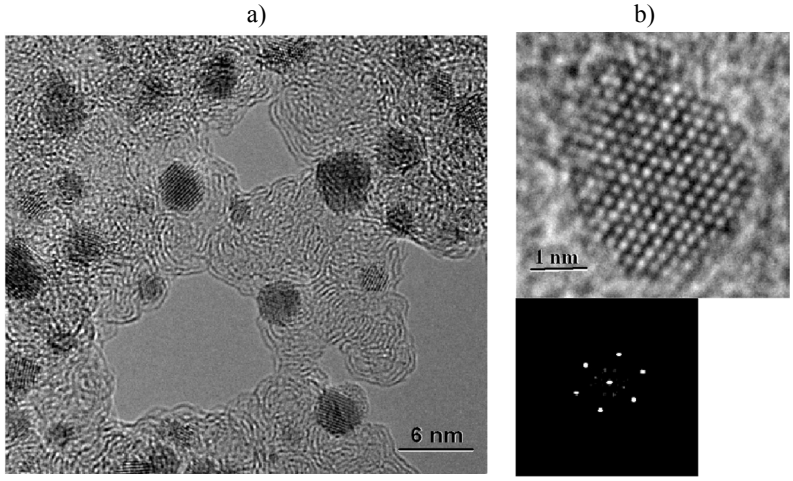

Fig. 2. TEM Images of the Pt nanoparticles on the carbon substrate; a) low magnification overview showing the spread of the Pt particles distribution on the carbon support; b) high resolution image showing the cubo-octahedral shape of a Pt particle.

Cyclic voltammetry of the Pt/C catalyst

The electrochemically active surface area is an implicit factor in the determination of the current density for any electrochemical reaction. This parameter

was determined from the steady-state cyclic voltammogram of Pt/C electrode in a 0.50 mol dm^{-3} $HClO_4$ electrolyte, shown in Fig. 3. The anodic part of the voltammogram, corresponding to hydrogen desorption, was integrated and the double-layer charging current subtracted. Assuming that 210 μC cm^{-2} corresponds to a monolayer coverage of adsorbed hydrogen, the surface area of the Pt nanoparticles was determined and the current densities for oxygen were calculated with respect to the surface area of that particular layer of the catalyst. The average value of the specific surface area of Pt particles was found to be 76 m^2 g^{-1}. Approximating the cubo-octahedral Pt particles as ideal spheres, a particle diameter of 3.7 nm was calculated. This value is larger that that obtained by TEM but this is to be expected because the surface of the supported catalyst particles in a thin film on the electrode is never completely accessible in the electrochemical experiments. However, taking into account also the fact that the carbon support material was also of high porosity, it is to be expected that some of the Pt particles were located in the inner part of the carbon support (micropores) and, consequently, were not electrochemically active (utility efficiency).

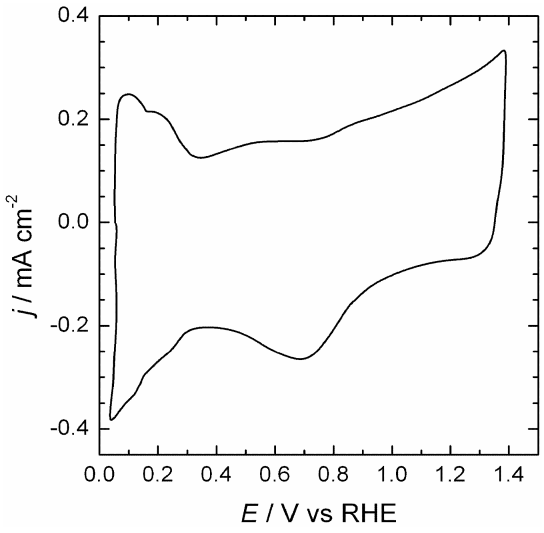

Fig. 3. Cyclic voltammetry curve for the Pt/C electrode at a sweep rate of 100 mV s^{-1} in a N_2-saturated 0.50 mol dm^{-3} $HClO_4$ solution at 298 K.

It should also be stressed that the current associated with the double layer is not constant with potential, meaning that the evaluation of the charge associated with UPD H would carry a certain error and this might explain the discrepancies between the average value of specific surface area found from integration of the UPD H peaks and average particle size from TEM images.

Kinetics of oxygen reduction

Since the ORR depends on the hydrodynamic conditions, a rotating Pt/C disk electrode was employed to measure the current densities of the reaction. The po-

larization curves for the ORR at different temperatures recorded with a slow potential sweep at an electrode rotating at 1600 rpm are shown in Fig. 4. The limiting current densities increased with temperature, indicating that the increase of the oxygen diffusion coefficient with temperature was higher than the decrease of oxygen solubility. A similar temperature dependence of the limiting current between 20 and 40 °C was reported in the literature.[18]

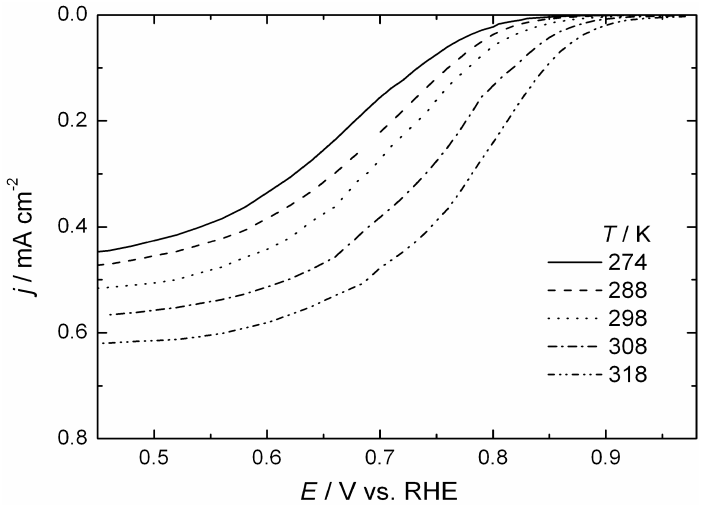

Fig. 4. Potentiodynamic (1.0 mV s^{-1}) polarization curves for the ORR at a Pt/C disk electrode rotating at 1600 rpm in a 0.50 mol dm^{-3} $HClO_4$ solution as a function of temperature.

For the kinetic analysis, the ORR current densities were determined by potentiostatic steady-state measurements because this technique corresponds better to real fuel cell conditions than linear sweep voltammetry. Also, a correction for the double layer charging current is avoided in steady-state measurements, which is important since the carbon cryogel support had a large surface area. After 30 min stabilization of the open circuit potential of the Pt/C electrode, potential steps of 30 s were applied in the ascending direction of overpotentials. These currents were corrected for the diffusion effects using the equation for the kinetic current density:

$$j_{\mathrm{kin}} = \frac{I_{\mathrm{L}} I}{I_{\mathrm{L}} - I} \times \frac{1}{S_{\mathrm{Pt}}} \tag{1}$$

where I is the measured current, I_{L} is the limiting current and S_{Pt} is the surface area of the Pt nanoparticles on the electrode, determined by cyclic voltammetry. The polarization curves, given as E *vs*. $\log j_{\mathrm{kin}}$ plots, at temperatures in the range from 273 to 318 K are shown in Fig. 5. In the whole examined temperature range, two distinct linear regions were observed, with Tafel slopes, b, increasing with temperature from 57 to 74 mV dec^{-1} at low current densities, and from 113 to 133 mV dec^{-1} at high current densities. In order to determine the transfer coeffi-

cients, the Tafel slopes were plotted as a function of temperature. Figure 6 shows the linear dependence on temperature in both current density regions. At high current densities, the *b vs*. *T* line follows the conventional dependence of–2.3*RT*/*βF,* with β being constant and close to 0.5. Such a conventional dependence, with β = = 1/2, is indicated in Fig. 6 by a broken line. At low current densities, the slope of *b vs*. *T* is close to –2.3*RT*/*F*. The Tafel slopes are similar to those on polycrystalline Pt.[3,5,9]

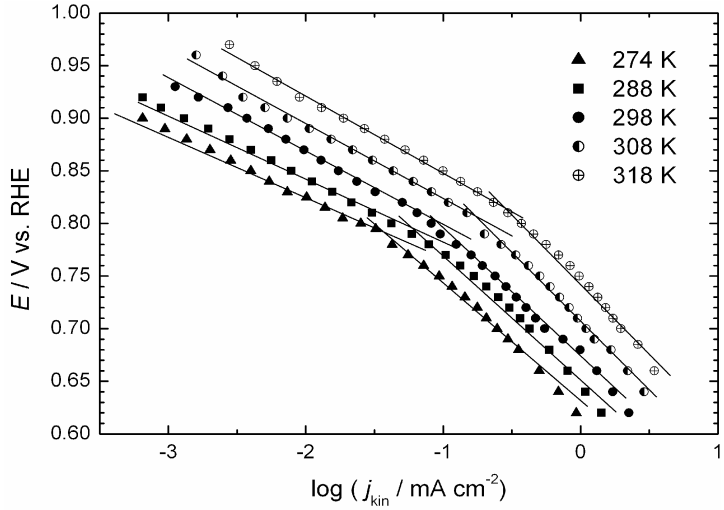

Fig. 5. Mass transfer corrected Tafel plots for the ORR on a Pt/C electrode in a 0.50 mol dm^{-3} $HClO_4$ solution for the temperature range 274–318 K.

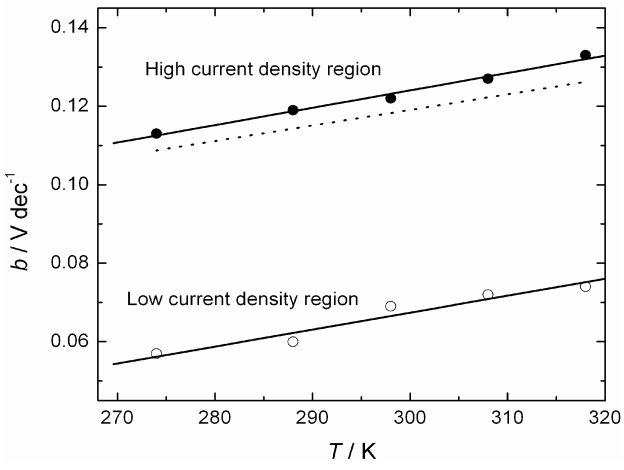

Fig. 6. Temperature dependence of the Tafel slope in low and high current density regions for the ORR at a Pt/C electrode in a 0.50 mol dm^{-3} $HClO_4$. The conventional dependence for β = 0.5 is indicated by the broken line.

The apparent enthalpy of activation of the oxygen reduction can be determined from the Arrhenius plot log j_{kin} *vs*. T^{-1}. However, since the concentration of dissolved oxygen in the electrolyte depends on the temperature, the kinetic

currents were normalized with respect to oxygen concentration at the given temperature.[30] The data for the potentials in low and high current density regions are presented in Fig. 7. The apparent enthalpies of activation were determined to be 69 kJ mol^{-1} at 0.900 V and 46 kJ mol^{-1} at 0.700 V. These values are higher than those reported in the literature,[18,20] which is probably the result of the different techniques employed for recording the polarization curves, *i.e.*, in this study, the steady-state technique was employed while in the others, the linear potential sweep technique was applied.

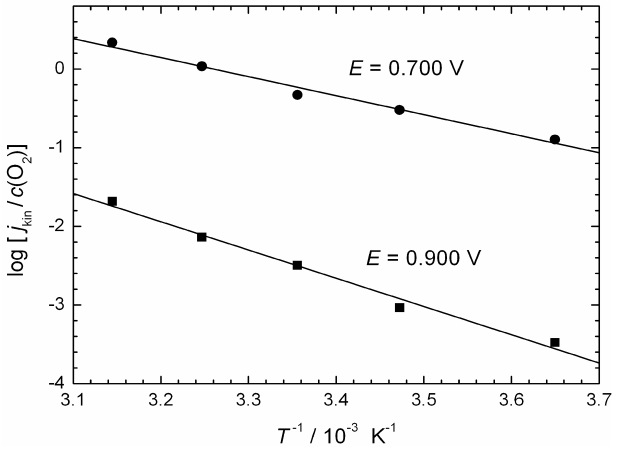

Fig. 7. Arrhenius plots for the ORR in a 0.50 mol dm^{-3} $HClO_4$ at a Pt/C electrode at potentials in the low and high current density regions. The mass transfer corrected currents were normalized with the respect to the concentration of dissolved oxygen.

The activity of the Pt/C catalyst for the ORR is compared with that of polycrystalline Pt in Fig. 8. For both electrodes, the current densities were calculated using the Pt surface area determined by cyclic voltammetry. As can be seen, the ORR current densities are higher on Pt/C catalyst than on polycrystalline Pt at more positive potentials while they are almost the same at potentials closer to the limiting current. The higher activity of Pt nanoparticles is probably the result of their surface structure. According to Sattler and Ross,[31] surface (111) and rough (110) regions dominate for particles of less than 3.5 nm. The TEM image of a Pt particle in the Pt/C catalyst used in this work (Fig. 2b) confirms that the (111) structure prevails in small particles. On the other hand, Marković *et al.*[12] showed that the activity for the ORR increased in the order (100) < (110) ≈ (111) in $HClO_4$ solutions.

Mechanism of the oxygen reduction reaction and apparent enthalpies of activation

A change in Tafel slopes with potential for an electrochemical reaction is usually explained by a change in the mechanism of the reaction. However, in the case of oxygen reduction, where adsorbed intermediates are involved, there is another possibility. For oxygen reduction on polycrystalline Pt, this was explained[5,8] by a change in the adsorption conditions of the adsorbed intermediates from

Temkin to Langmuirian. The same analysis as on polycrystalline Pt will be applied for oxygen reduction on the Pt/C nanostructured catalyst employed in this study.

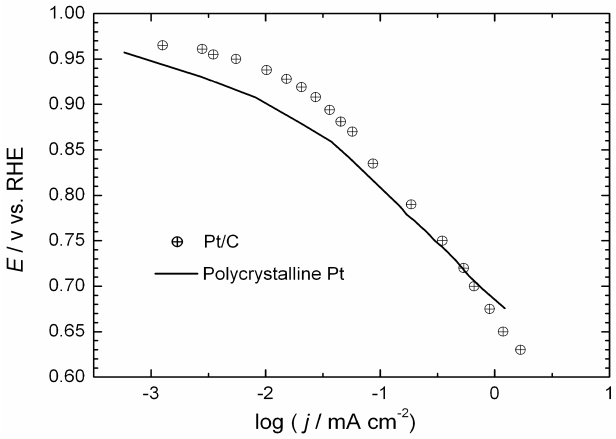

Fig. 8. Mass transfer corrected Tafel plots for the ORR at a Pt/C and a polycrystalline Pt electrode in a 0.50 mol dm^{-3} $HClO_4$ solution at 298 K.

According to Šepa *et al.*[5] the first step in oxygen reduction is the adsorption of molecular oxygen, which is followed by the slow transfer of an electron with or without the participation of an H_3O^+:

$$M + O_2 \rightleftarrows M\cdots O_2 \quad (2)$$

$$M\cdots O_2 + H_3O^+ + e^- \rightarrow \text{products} \quad (3)$$

or

$$M\cdots O_2 + e \rightarrow \text{products} \quad (4)$$

The rate equation for the proposed mechanism is:

$$j = k \exp(-\frac{\Delta G_0^*}{RT}) \exp[-\frac{\beta F(E - E_{\text{zop}})}{RT}] \quad (5)$$

where ΔG_0^* is the Gibbs energy of activation for the rate determining step at the zero Galvani potential difference, E_{zop} is the potential on the hydrogen electrode scale, at which the Galvani potential difference at the working electrode is zero[32] and k is the rate constant containing pH and oxygen partial pressure dependences of the individual rate equations as required for the steps (3) or (4).

Taking that the surface coverage by the adsorbed intermediates at high current densities is low, as was shown to be the case for both polycrystalline Pt[5] and Pt nanoparticles supported on Ebonex,[22] Langmuirian conditions prevail and ΔG_0^* is independent of the coverage, meaning that the reaction rate is:

$$j_{\text{h}} = k_{\text{h}} \exp(-\frac{\Delta G_{0,\text{h}}^*}{RT}) \exp[-\frac{\beta F(E_{\text{h}} - E_{\text{zop}})}{RT}] \quad (6)$$

where the subscript "h" denotes the high current density region.

In the low current density region, the coverage with the reaction intermediates is appreciable[5,22] and Temkin adsorption conditions must be considered. Since the adsorption energy of the reaction intermediate decreases with increasing coverage of oxygen species, the chemical part of the Gibbs energy of activation increases with the coverage:

$$\Delta G_\theta^* = \Delta G_0^* + \alpha r(\theta - \theta_\Gamma) \tag{7}$$

where θ_Γ is the transition level of surface coverage above which ΔG^* is affected by the coverage and where Langmuirian conditions change to Temkin conditions of adsorption, ΔG_0^* is the Gibbs energy of activation at low coverage ($\theta < \theta_\Gamma$), r is an energy parameter and α is a symmetry factor, usually taken to be 0.5. In the potential region where the Tafel slope is $-2.3RT/F$, the surface coverage θ was found to be linearly dependent on the electrode potential,[5] according to the relation:

$$\theta - \theta_\Gamma = \frac{F}{r}(E - E_\Gamma) \tag{8}$$

where E_Γ is the transition potential at which θ_Γ is reached, and the Tafel slope changed to $-2.3\times2RT/F$. Substituting Eq. (8) into Eq. (7), the Gibbs energy of activation is related to the electrode potential by:

$$\Delta G_\theta^* = \Delta G_0^* + \alpha F(E - E_\Gamma) \tag{9}$$

When Eq. (9) is introduced into the rate law (4), it takes the form:

$$j_l = k_l \exp(-\frac{\Delta G_{0,l}^*}{RT}) \exp[-\frac{F(\alpha E_l + \beta E_l - \alpha E_\Gamma - \beta E_{zop})}{RT}] \tag{10}$$

where the subscript "l" denotes the low current density region.

If rate determining step in the low and high current densities regions is the same, then the enthalpies of activation in these two regions will also be the same. Since the enthalpy of activation is a function of the electrode potential, the values at the same potential, *e.g.*, at the zero Galvani potential difference, are to be compared. In order to do this, Eqs. (9) and (10) have to be differentiated with respect to temperature. If it is assumed that the variation of the entropy of activation over the narrow temperature range of 40 °C is small and can be ignored, the enthalpies of activation at given potentials (E_h and E_l) *vs*. RHE, are given by the following equations:

$$\Delta H_{a,E_h}^* = -R(\frac{d\, ln\, j_h}{d(1/T)})_{E_h} = \Delta H_{0,h}^* + \beta F E_h - F E_{zop} + \frac{\beta F}{T} \times \frac{d(E_h - E_{zop})}{d(1/T)} \tag{12}$$

and

$$\Delta H^*_{\mathrm{a},E_\mathrm{l}} = -R\left(\frac{\mathrm{d}\,ln\,j_\mathrm{h}}{\mathrm{d}(1/T)}\right)_{E_\mathrm{l}} = \Delta H^*_{0,\mathrm{l}} + F(\beta E_\mathrm{l} + \alpha(E_\mathrm{l} - E_\mathrm{T})) - \beta F E_\mathrm{zop} + \\ + \frac{F}{T} \times \frac{\mathrm{d}(\alpha(E_\mathrm{l} - E_\mathrm{T}) + \beta(E_\mathrm{l} - E_\mathrm{zop}))}{\mathrm{d}(1/T)} \quad (13)$$

where $\Delta H^*_{0,\mathrm{h}}$ and $\Delta H^*_{0,\mathrm{l}}$ are the enthalpies of activation for the high and low current density regions at the zero Galvani potential difference. They cannot be experimentally determined because of the unknown E_zop, but their difference can be calculated using the apparent enthalpies of activation at the constant potential, $\Delta H^*_{\mathrm{a},E_\mathrm{h}}$ and $\Delta H^*_{\mathrm{a},E_\mathrm{l}}$:

$$\Delta^\mathrm{h}_\mathrm{l}(\Delta H^*_0) = \Delta H^*_{0,\mathrm{l}} - \Delta H^*_{0,\mathrm{h}} = \\ = \Delta H^*_{a,E_\mathrm{l}} - \Delta H^*_{a,E_\mathrm{h}} - F(\alpha E_\mathrm{l} + \beta E_\mathrm{l} - \beta E_\mathrm{h} - \beta E_\mathrm{T}) + \frac{\alpha F}{T} \times \frac{\mathrm{d}E_\mathrm{T}}{\mathrm{d}(1/T)} \quad (14)$$

It should be noted that the difference in the enthalpies at the zero Galvani potential depends neither on the position of the zero Galvani potential nor on the choice of the reference electrode.

Calculation of $\Delta^\mathrm{h}_\mathrm{l}(\Delta H^*_0)$ according to Eq. (14) requires the temperature dependence of the transition potential, E_T. The transition potentials were determined from the intersections of the Tafel lines in the low and high current density regions (Fig. 6) and plotted as a function of temperature in Fig. 9. All the data necessary for the calculation of $\Delta^\mathrm{h}_\mathrm{l}(\Delta H^*_0)$ at 298 K are given in Table I. As a result, $\Delta^\mathrm{h}_\mathrm{l}(\Delta H^*_0) \approx 1$ kJ mol^{-1} was obtained. Such a small difference can be ignored taking that $\Delta H^*_{0,\mathrm{l}} \approx \Delta H^*_{0,\mathrm{h}}$. This is the proof that oxygen reduction on the Pt/C catalyst followed the same mechanism in both the low and high current density regions. The difference in the Tafel slopes was not caused by different rate determining steps but by the change in the surface coverage and the adsorption conditions.

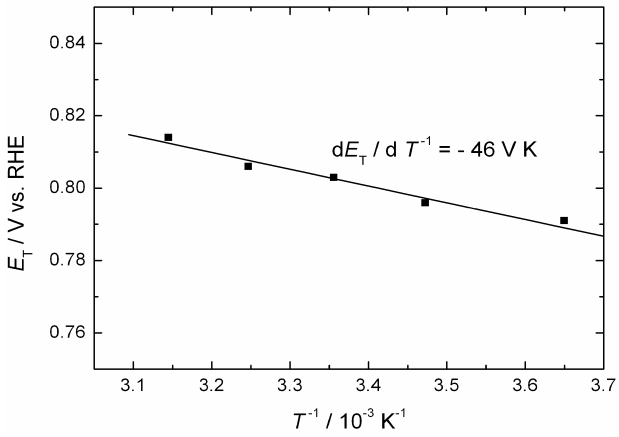

Fig. 9. Dependence of the transition potential on temperature for the ORR at a Pt/C electrode in a 0.50 mol dm^{-3} $HClO_4$ solution.

TABLE I. Data for the calculation of the difference in the enthalpies of activation at the zero Galvani potential for oxygen reduction on a Pt/C catalyst at 298 K: the apparent enthalpies of activation in the low and high current density region, the transition potential and its variation with temperature

$\Delta H^*_{\mathrm{a},E_\mathrm{l}=0.70\,\mathrm{V}}$ kJ mol^{-1}	$\Delta H^*_{\mathrm{a},E_\mathrm{h}=0.70\,\mathrm{V}}$ kJ mol^{-1}	$F\alpha E_\mathrm{T}$ kJ mol^{-1}	$\frac{\alpha F}{T}\times\frac{dE_\mathrm{T}}{d(1/T)}$ kJ mol^{-1}	$\Delta^\mathrm{h}_\mathrm{l}(\Delta H^*_0)$ kJ mol^{-1}
69±4	46±3	39	7.5	1

CONCLUSIONS

Platinum nanoparticles supported on a carbon cryogel showed activities for the ORR which was higher than that of polycrystalline Pt in the low current density region but the same in the high current density region. This is in accordance with literature data about preferential (111) and (110) faces on Pt nanoparticles smaller than 3.5 nm[31] and the higher activity of these planes for the ORR than the (100) plane.[12]

The Tafel slope values were $-2.3RT/F$ in the low current density region and $-2.3\times2RT/F$ in the high current density region, which is the same as on polycrystalline Pt. Therefore, an analysis of the apparent enthalpies of activation based on the proposed mechanism for oxygen reduction on polycrystalline Pt was performed. It was confirmed that the enthalpies of activation at the zero Galvani potential difference in both current density regions were the same, meaning that the same rate determining step of the ORR on Pt/C was operative in all potential regions, despite the changes in the Tafel slopes. The change in kinetics with potential arose from the different adsorption conditions of the reaction intermediates with potential. The values of the apparent enthalpies of activation, higher than those reported by applying linear potential sweep, could be the result of the steady-state technique used in the present experiments, which corresponds better to the real fuel cell conditions than linear sweep voltammetry.

Acknowledgement. This work was financially supported by the Ministry of Science of the Republic of Serbia, under Contact No. 142038.

И З В О Д

ТЕМПЕРАТУРНА ЗАВИСНОСТ ЕЛЕКТРОХЕМИЈСКЕ РЕДУКЦИЈЕ КИСЕОНИКА НА НАНОЧЕСТИЦАМА ПЛАТИНЕ НА УГЉЕНИЧНОМ НОСАЧУ

НЕВЕНКА. Р. ЕЛЕЗОВИЋ[1], БИЉАНА. М. БАБИЋ[2], НЕДЕЉКО. В. КРСТАЈИЋ[3], СНЕЖАНА. Љ. ГОЈКОВИЋ и ЉИЉАНА. М. ВРАЧАР[3]

[1]Институт за мултидисциплинарна истраживања, Београд, [2]Институт за нуклеарне науке "Винча", Београд и [3]Технолошко–металуршки факултет Универзитета у Београду, Београд

Кинетика реакције редукције кисеоника је испитивана на наночестицама платине дисперговaним на угљеничном носачу, у 0,50 mol dm^{-3} $HClO_4$, у температурном интервалу од 278 до 318 K. За синтезу Pt катализатора (Pt/C) је примењена модификована полиол метода

из раствора етилен гликола, док је као носач коришћен угљенични криогел. Катализатор је окарактерисан применом BET методе, дифракције X-зрака (XRD) и трансмисионе електронске микроскопије (TEM). Кинетика реакције редукције кисеоника испитивана је коришћењем стационарне поларизационе методе и методе цикличне волтаметрије. Област малих густина струје, на свим тепературама, на кривој поларизације, карактерише вредност Tafel-овог нагиба од $-2.3RT/F$, док је у области високих густина струје вредност овог нагиба $-2.3\times2RT/F$. Одређене су вредности привидне енталпије активације на константним потенцијалима, за обе области густина струја, и њихова разлика исказана за нулу Галванијеве разлике потенцијала. Потврђено је да је механизам редукције кисеоника, као и ступањ који одређује укупну брзину реакције исти у обе области густина струја, а да је разлика у кинетици реакције последица разлике у зависности адсорпције реакционих интермедијара од потенцијала. Поређењем каталитичке активности, изражене преко густине струје по реалној површини катализатора, констатована је нешто већа активност Pt/C катализатора у односу на поликристалну Pt.

(Примљено 11. јула, ревидирано 20. новембра 2007)

REFERENCES

1. A. Damjanović, M. A. Genshaw, J. O'M. Bockris, *J. Electrochem. Soc.* **114** (1967) 466
2. A. Damjanović, V. Brusić, *Electrochim. Acta* **12** (1967) 615
3. M. R. Tarasevich, *Elektrokhimiya* **9** (1973) 599 (in Russian)
4. M. R. Tarasevich, A. Sadkovski, E. Yeager in *Comprehensive Treatise of Electrochemistry, Vol. 7,* B. E. Conway, J. O'M. Bockris, S. V. M. Khan, R. E. White, Eds., Plenum Press, New York, 1983
5. D. B. Šepa, M. V. Vojnović, A. Damjanović, *Electrochim. Acta* **26** (1981) 781
6. R. Adžić, in *Electrocatalysis*, J. Lipkowski, P. N. Ross, Eds., Wiley, New York, 1998, p. 197
7. N. Wakabayashi, M. Takeichi, M. Itagaki, H. Uchida, M. Watanabe, *J. Electroanal. Chem.* **574** (2005) 339
8. D. B. Šepa, M. V. Vojnović, Lj. M Vračar, A. Damjanović, *Electrochim. Acta* **31** (1986) 1105
9. P. N. Ross, *J. Electrochem. Soc.* **126** (1979) 78
10. N. M. Marković, R. R. Adzić, B. D. Cahan, E. B. Yeager, *J. Electroanal. Chem.* **377** (1994) 249
11. N. M. Marković, H. A. Gasteiger, P. N. Ross, *J. Phys. Chem.* **99** (1995) 3411
12. N. Marković, H. Gasteiger, P. N. Ross, *J. Electrochem. Soc.* **144** (1997) 1591
13. B. N. Grgur, N. M. Marković, P. N. Ross, *Can. J. Chem.* **75** (1997) 1465
14. M. D. Maciá, J. M. Campiña, E. Herrero, J. M. Feliu, *J. Electroanal. Chem.* **564** (2004) 141
15. M. Watanabe, S. Saegusa, P. Stonehart, *Chem. Lett.* (1988) 1487
16. K. Kinoshita, *J. Electrochem. Soc.* **137** (1990) 845
17. S. Lj. Gojković, S. K. Zečević, R. F. Savinell, *J. Electrochem. Soc.* **145** (1998) 3713
18. U. A. Paulus, T. J. Schmidt, H. A. Gasteiger, R. J. Behm, *J. Electroanal. Chem.* **495** (2001) 134
19. U. A. Paulus, A. Wokaun, G. G. Scherer, T. J. Schmidt, V. Stamenković, N. M. Marković, P.N. Ross, *Electrochim. Acta* **47** (2002) 3787
20. H. Yano, E. Higuchi, H. Uchida, M. Watanabe, *J. Phys. Chem. B.* **110** (2006) 16544
21. E. Higuchi, H. Uchida, M. Watanabe, *J. Electroanal. Chem.* **583** (2005) 69
22. Lj. M. Vračar, N. V. Krstajić, V. R. Radmilović, M. M. Jakšić, *J. Electroanal. Chem.* **587** (2006) 99

23. V. Stamenković, T. J. Schmidt, P. N. Ross, N. M. Marković, *J. Phys. Chem. B.* **106** (2002) 11970
24. V. Stamenković, T. J. Schmidt, P. N. Ross, N. M. Marković, *J. Electroanal. Chem.* **554–555** (2003) 191
25. M. D. Obradović, B. N. Grgur, Lj. M. Vračar, *J. Electroanal. Chem.* **548** (2003) 69
26. U. A. Paulus, A. Wokaun, G. G. Scherer, T. J. Schmidt, V. Stamenković, N. M. Marković, P. N. Ross, *J. Phys. Chem. B.* **106** (2002) 4181
27. B. Babić, D. Đokić, N. Krstajić, *J. Serb. Chem. Soc.* **70** (2005) 21
28. B. M. Babić, Lj. M. Vračar, V. Radmilović, N. V. Krstajić, *Electrochim. Acta* **51** (2006) 3820
29. V. Radmilović, T. J. Richardson, S. J. Chen, P. N. Ross, *J. Catal.* **232** (2005) 99
30. D. Tromans, *Hydrometallurgy* **50** (1998) 279
31. M. L. Sattler, P. N. Ross, *Ultramicroscopy* **20** (1986) 21
32. A. J. Appleby, in *Modern Aspects of Electrochemistry*, *Vol. 9*, J. O′M. Bockris, B. E. Conway, Eds., Plenum Press, New York, 1974.

www.shd.org.rs

Journal of the Serbian Chemical Society

JSCS@tmf.bg.ac.yu • www.shd.org.rs/JSCS

J. Serb. Chem. Soc. 73 (6) 655–659 (2008)
JSCS–3747

UDC 543.551/.552+547–36:546.11'98+541.135.5
Short communication

SHORT COMMUNICATION

Coulometric–potentiometric determination of pK_A of several organic bases in propylene carbonate

LJILJANA N. JAKŠIĆ[1]*# and RADMILA M. DŽUDOVIĆ[2#]

[1]*Faculty of Mining and Geology, University of Belgrade, Đušina 7, 11000 Belgrade and* [2]*Faculty of Sciences, University of Kragujevac, Radoja Domanovića 12, 34000 Kragujevac, Serbia*

(Received 30 November 2007, revised 4 February 2008)

Abstract: The pK_A values of protonated triethylamine, pyridine and 2,2'-dipyridyl in propylene carbonate (PC) were determined by applying the coulometric–potentiometric method and a hydrogen/palladium generator anode (H_2/Pd). The investigated and reference base were titrated to 50 % with protons electrogenerated from hydrogen-saturated palladium, in the presence of sodium perchlorate as the supporting electrolyte. The half-neutralization potentials $E_{1/2(x)}$ and $E_{1/2(st.)}$ of the investigated and standard base, respectively, were measured using a glass–SCE pair. The obtained pK_A values were compared with those reported in the literature.

Keywords: coulometry; pK_A of base; propylene carbonate; hydrogen/palladium electrode.

INTRODUCTION

There are only a few papers in the literature concerning the determination of the pK_A of bases in PC.[1–3] The presented procedures for the determination of pK_A values are based on the potentiometric titrations of bases with a standard solution of perchloric or hydrochloric acid. The pK_A values for protonated amines reported in the literature differ considerably between one another.[2,3]

PC is an aprotic dipolar solvent which has some advantages ("environmental friendly" solvent) over other protophobic solvents such as acetone or acetonitrile. This solvent has been recommended as a medium for electrochemical investigations[4] and acid base titrations.[5–8] The principal disadvantage of PC, is that it hydrolyzes fairly rapidly in the presence of strong acids. In previous papers[7,8] it was shown that the use of a standard perchloric acid solution for titration of bases

* Corresponding author. E-mail: nikola66@net.yu
# Serbian Chemical Society member.
doi: 10.2298/JSC0806655J

in PC can be avoided by generating perchloric acid coulometrically at a H_2/Pd electrode. Furthermore, a H_2/Pd electrode was applied as a generator electrode for the determination of the autoprotolysis constant of PC[9] and other aprotic solvents,[10] as well of protonization constants of electrolytes in ketones.[11–12] The aim of this work was to confirm whether the coulometric–potentiometric method and a hydrogen/palladium generator electrode can be employed for the determination the pK_A values of some organic bases in PC.

EXPERIMENTAL

Apparatus and electrodes

The apparatus and electrodes used in this study were described earlier.[10]

Reagents and solutions

All chemicals were of p.a. purity (Merck and Fluka). Propylene carbonate was distilled under reduced pressure (b.p. about 80 °C) before use. The supporting electrolyte was a 0.10 mol dm^{-3} solution of sodium perchlorate in PC. The liquid bases triethylamine and pyridine were dried over fused potassium hydroxide and then distilled under reduced pressure. An appropriate amount of a base was weighed into a volumetric flask, dissolved in PC and then diluted to the mark. The base concentration (0.010 mol dm^{-3}) was checked by titration with protons generated at a H_2/Pd electrode, with potentiometric detection of the equivalence point.

Procedure

A base solution (2.00 ml) and the sodium perchlorate solution (18.00 ml) were put into the anode compartment of the electrolytic vessel. The sodium perchlorate solution was put into the cathode compartment to the same level. The auxiliary electrode (a platinum wire) was immersed in the catholyte. The generator H_2/Pd anode and the electrode pair glass-modified SCE were immersed in the anolyte. The current was switched on, and H^+ ions were generated at the H_2/Pd anode in the amount required to half-neutralize the reference base (investigated base) solution. Titration of the base (0.0010 mol dm^{-3}) was performed at a constant current (3.0 mA). After thermostating at 25.0±0.1 °C, the potential was read.

RESULTS AND DISCUSSION

The dissociation constants of protonated triethylamine, 2,2'-dipyridyl and pyridine in PC were determined in the following cells:

$$\text{SCE} \parallel \text{B}_{st}, c_M, \text{BH}^+_{st}, c_M \mid \text{glass electrode}$$

$$\text{SCE} \parallel \text{B}_{x}, c_M, \text{BH}^+_{x}, c_M \mid \text{glass electrode}$$

The standard and investigated base at the same concentration c_M were titrated coulometrically to half-neutralization with protons generated by the anodic oxidation of hydrogen dissolved in palladium in presence of sodium perchlorate as the supporting electrolyte. The half-neutralization potentials $E_{1/2(st.)}$ and $E_{1/2(x)}$ of the standard and investigated base, respectively, were measured by a glass–SCE electrode pair. The pK_A value of the studied base was calculated according to the following equation:

$$pK_{A(x)} = pK_{A(st)} + (E_{1/2(x)} - E_{1/2(st)})/0.059$$

where $pK_{A(st.)}$ represents the dissociation constant of the standard base 1,3-diphenylguanidine ($pK_{A(st.)} = 16.98$).

The pK_A values of the investigated bases determined coulometrically using a H_2/Pd anode and a 0.10 mol dm^{-3} sodium perchlorate as the supporting electrolyte, as well as the literature data obtained by other experimental techniques, are summarized in Table I.

TABLE I. Dissociation constants of protonated organic bases obtained by coulometry at 25.0±0.1 °C (supporting electrolyte, 0.10 mol dm^{-3} sodium perchlorate in propylene carbonate; generation current 3.0 mA)

Base	pK_A±SD[a]	pK_A, literature data[2]
Triethylamine	17.28±0.09	17.94
2,2'-Dipyridyl	13.20±0.07	–
Pyridine	11.32±0.10	11.92

[a]Standard deviation; number of determinations: 5

No data have been published in the literature for 2,2'-dipyridyl. The experimental pK_A value for 2,2'-dipyridyl obtained in this study by coulometry is 13.20±0.07. The pK_A values for pyridine and triethylamine determined by the herein proposed procedure are lower by approximately 0.60 pK units than those obtained by the classic potentiometric method.[1] This can be explained by the different conditions of the investigation in the present work in comparison with those applied by other authors.

In the herein proposed procedure, the use of a H_2/Pd anode as the source of hydrogen ions in the coulometric determination of the dissociation constants of bases in PC makes this simpler than the classical method. The oxidation of hydrogen generates "dry" hydrogen ions, hence, as the introduction of a titrant into the solution is avoided, the titrated volume and the ionic strength remain unchanged. Particularly, since the ionic strength of the solution in PC cannot be calculated, the coulometrically determined acid dissociation constants of protonated bases are only valid for the applied supporting electrolyte, sodium perchlorate at a concentration of 0.10 mol dm^{-3} and thus represent conditional dissociation constants.

Based on the values of the dissociation and homoconjugation constants of acids in PC and acetonitrile, it was shown that an enhanced polarity of the aprotic solvent is favorable for the dissociation of the cationic acids and that PC is a somewhat stronger base than acetonitrile.[1] In accordance with this consideration, the pK_A values of bases in PC determined either by coulometry or the classic method are smaller than those obtained in acetonitrile.[2]

PC has a small autoprotolysis constant, a relatively high permittivity and dipole moment, as well as a pronounced differentiating effect, relative to many electrolytes. On account of these properties, PC is suitable for the determination of mixtures of bases. A differential titration of bases in this solvent is only pos-

sible if the difference between the pK values of the bases in the employed solvent is sufficiently high. From this point of view, the conditional dissociation constants of protonated bases in PC are important physico–chemical parameters, which can be used for predicting the conditions for the differential coulometric–potentiometric titration of bases in mixtures in this solvent.

CONCLUSIONS

The conditional dissociation constants of triethylamine, pyridine and 2,2'-dipyridyl in propylene carbonate were determined by applying the coulometric–potentiometric method and a hydrogen/palladium generator anode. Employing this procedure, the preparation of a standard solution of perchloric acid, which is unstable in this solvent, is avoided and the effect of dilution of the solution in the course of the titration is eliminated. This method is simpler than the classical potentiometric method.

Acknowledgments. The authors are grateful to the Serbian Ministry of Science for financial support (Grant No. 142060)

ИЗВОД

КУЛОНОМЕТРИЈСКО–ПОТЕНЦИОМЕТРИЈСКО ОДРЕЂИВАЊЕ pK_A НЕКИХ ОРГАНСКИХ БАЗА У ПРОПИЛЕНКАРБОНАТУ

ЉИЉАНА Н. ЈАКШИЋ[1] и РАДМИЛА М. ЏУДОВИЋ[2]

[1]*Природно–математички факултет, Универзитет у Крагујевцу, Радоја Домановића 12, 34000 Крагујевац и* [2]*Рударско–геолошки факултет, Универзитет у Београду, Ђушина 7, 11000 Београд*

Применом кулонометријско–потенциометријске методе и водоник–паладијумове генераторске електроде одређене су pK_A вредности протонисаног триетиламина, пиридина и 2,2'-дипиридила у пропиленкарбонату. Испитивана и референтна база титрисане су кулонометријски до 50 % протонима добијеним анодном оксидацијом водоника раствореног у паладијуму у присуству натријум-перхлората као основног електролита. Полу-неутрализациони потенцијали ($E_{1/2(x)}$ and $E_{1/2(st.)}$) испитиване и стандардне базе мерени су применом електродног пара стаклена електрода–ЗКЕ. На основу вредности полу-неутрализационих потенцијала и p$K_{A(st)}$ вредности стандардне базе израчунате су константе дисоцијације испитиваних база. Добијене pK_A вредности упоређене су са литературним подацима.

(Примљено 30. новембра 2007, ревидирано 4. фебруара 2008)

REFERENCES

1. K. Izutsu, I. M. Kolthoff, T. Fujinaga, M. Hattori, M. K. Chantoni, *Anal. Chem*. **49** (1977) 503
2. K. Izutsu, T. Nakamura, I. Iijima, *Bull. Chem. Soc. Japan* **52** (1979) 2721
3. J. Talarmin, M. L'her, J. Courtot-Coupezz, C. R. Hebd, *Sci. Acad, Sci. Ser. C* **287** (1978) 105
4. V. Vojinović, S. Mentus, V. Komnenić, *J. Elactroanal. Chem*. **547** (2003) 109
5. N. A. Baranov, N. A. Vlasov, L. P. Potehina, O. F. Shopot'ko, *Zhur. Anal. Khim*. **25** (1970) 2069
6. R. Mihajlović, V. Vajgand, Lj. Jakšić, M. Manetović, *Anal. Chim. Acta* **229** (1990) 287
7. R. P. Mihajlović, V. J. Vajgand, Lj. N. Jakšić, *Talanta* **39** (1992) 1587

8. Lj. N. Jakšić, R. M. Džudović, R. P. Mihajlović, Z. D. Stanić, *J. Serb. Chem. Soc.* **65** (2000) 587
9. R. M. Džudović, R. P. Mihajlović, Lj. N. Jakšić, in *Proceedings of XV Yugoslav Symposium on Electrochemistry*, Palić, Yugoslavia, (2001), *Book of Abstracts*, Serbian Chemical Society, Belgrade, (2001), p. 97 (in Serbian)
10. V. J. Vajgand, R. P. Mihajlović, R. M. Džudović, *Talanta* **36** (1989) 1154
11. R. Mihajlović, Z. Simić, Lj. Mihajlović, M .Vukićević, *Talanta* **43** (1996) 2131
12. R. P. Mihajlović, Lj. N. Jakšić, R. M. Džudović, *Anal. Chim. Acta* **557** (2006) 37.

www.shd.org.rs

Journal of the Serbian Chemical Society

JSCS@tmf.bg.ac.yu • www.shd.org.rs/JSCS

J. Serb. Chem. Soc. 73 (6) 661–664 (2008)
JSCS–3748

UDC 62–405.8.004.12:544.6–188
Extended abstract

EXTENDED ABSTRACT

Supercapacitive characteristics of electrochemically active porous materials§

VLADIMIR V. PANIĆ*#

Institute of Chemistry, Technology and Metallurgy, Center for Electrochemistry, Njegoševa 12, 11000 Belgrade, Serbia

(Received 27 March 2008)

Abstract: The results of an investigation of the capacitive characteristics of sol–gel-processed titanium- and carbon-supported electrochemically active noble metal oxides, as representatives of porous electrode materials, are presented in the lecture. The capacitive properties of these materials were correlated to their composition, the preparation conditions of the oxides and coatings, the properties of the carbon support and to the composition of the electrolyte. The results of the electrochemical test methods, cyclic voltammetry and electrochemical impedance spectroscopy, were employed to resolve the possible physical structures of the mentioned porous materials, which are governed by the controlled conditions of the preparation of the oxide by the sol–gel process.

Keywords: porous electrodes; sol–gel procedure; oxide sols; supercapacitors; dimensionally stable electrodes.

High surface area porous materials, applied as electrodes in many electrochemical processes and in energy-storage devices, are comprehended as so-called quasi-3D electrochemical systems.[1] Opposed to planar smooth electrode surfaces, the electrochemical and capacitive properties of porous electrodes are characteristic functions of their morphology and physical structure.[2] Due to the ever-growing interest for the investigation of dispersed Pt-based electrocatalysts[3–5] and electrochemical supercapacitors[1,6] of highly extended surfaces, it is extremely important to develop powerful tools which model in detail the applicative behavior of disperse electrodes, taking into account their physical state.[7–9]

Carbon black[10] supercapacitors and carbon black-supported noble metal oxides pseudo-supercapacitors, as well as porous coatings, consisting of noble metal

§ Lecture at the Meeting of the Electrochemical Division of the Serbian Chemical Society, 19 February 2008.

* E-mail: panic@ihtm.bg.ac.yu

Serbian Chemical Society member.

doi: 10.2298/JSC0806661P

oxides on activated titanium anodes are typical examples of porous electrochemical systems. It is known that the capacitive properties of these materials are strongly influenced by the real surface area, porosity and particle size and distribution, due not only to diffusion limitations of the pseudocapacitive redox transitions but also to the difficult double layer charging/discharging transients at the inner surfaces of the porous material.[1,11–13] Electrocatalytic activity and electrolytic stability of titanium anodes activated by sol–gel processed RuO_2–TiO_2 in chlorine and oxygen evolution were found to be sensitive to particle size and distribution owing to so-called geometric factor, related to real surface area changes.[14–16] The above-mentioned structure-related electrochemical characteristics of porous electrode materials emerge if they are subjected to a time-dependent input signal – the electrode potential, in most cases. Hence, a variety of information related to porous electrode system can be obtained using the methods of cyclic voltammetry (CV), with changeable potential ramp input signal, and electrochemical impedance spectroscopy (EIS), with a sinusoidal potential signal of adjustable frequency.

In this lecture, a survey of the results of an investigation of the capacitive properties of carbon blacks (CB) and two types of RuO_2-based porous materials is presented. Two commercial CBs, with a near 10-fold difference in BET surface area, and the from them obtained C/RuO_2 composite materials (first type of RuO_2-based porous materials), with different particle sizes of the sol–gel processed RuO_2, were investigated as supercapacitive materials in the form of a thin layer over an appropriate current collector. The influence of the amount of Ti-supported RuO_2 coating (second type of RuO_2-based porous materials) on its capacitive properties in H_2SO_4 and NaCl solution was examined for RuO_2 coatings prepared by an alkoxide ink procedure.

For all the investigated porous materials, the capacitive response can be interpreted by a layer (coating) in-depth distribution of the capacitance. From CV measurements, the response of the external layer (coating) surface, directly exposed to the bulk electrolyte, and the internal one, exposed to the electrolyte only through the pores, can be resolved. More detailed in-depth capacitance profiling is available from EIS measurements, since these materials were found to be electrically equivalent to the transmission line circuit.[1] This electrical circuit comprises n parallel branches with $R_{p,n}$ and C_n, being the pore resistance and associated capacitance, respectively, in series in each branch. In comparison to CV data, EIS profiling offers refined distributions of R_p and C with respect to the layer (coating) depth, qualitatively reflected through the value of n. An analysis of the capacitance in-depth profile thus aids in resolving whether a certain porous electrode would be suitable for a certain electrochemical process and/or charging/discharging regime.

The results for the CBs showed that the larger surface area the internal surface is less available for charging/discharging processes. In the case of CBs with

a surface area of the order of 1000 m^2 g^{-1}, the internal surface participates almost 90 % to the overall capacitive response, while for low surface area CBs (several hundreds of m^2 g^{-1}), this participation is below 50 %. Analysis of the EIS data by fitting to the transmission line model showed that high surface area CBs, as a rule, require higher n values than low surface area ones. In addition, the EIS data indicated that the pore resistance increases by up to two orders of magnitude in going from the external towards the internal surface (from the first to the n^{th} branch of transmission line).

Depending on the particle size of the oxide, CB-supported RuO_2 composite supercapacitors can behave twofold. In the case of small oxide particles combined with a high surface area CB, the total layer capacitance could be even smaller than that of the pure CB. The detailed in-depth capacitance profile by EIS indicates the hindered response of the internal CB surface, since small oxide particles block the pores required for the electrolyte to penetrate to the internal surface of the CB, which appears not to be impregnated by the oxide due to steric difficulties. The oxide pseudocapacitance superimposed on the CB double layer capacitance is not high enough to replace the capacitance of the blocked internal surface. However, if the oxide particle size is greater, the pores become partially unblocked, which manifests itself as an increase in the capacitance of the composite with respect to the CB-supported small oxide particles, due to the contribution of the internal surface of the CB. Similar observations also hold for composites involving a low surface area CB but, in this case, the composite capacitance is considerably higher in comparison to the CB, irrespective of the particle size of the oxide.

A similar behavior was also registered for RuO_2 coatings on Ti prepared by the alkoxide ink procedure.[17] A thick coating required a higher n value than a thin one, hence a more refined capacitance in-depth distribution was obtained for the thick coating. Additionally, the distribution was dependent on the composition of the electrolyte; a higher n value was required for a NaCl solution of rather high concentration than for a 1.0 M H_2SO_4 solution. This effect can be explained by the different ion mobility in electrolytes of different composition and concentration, bearing in mind the diffusion limitation of oxide redox transitions, as well as the slow response of the ions to a fast perturbation of the input charging/discharging signal.

Generally, an increase in surface area and a decrease in the particle size of electroactive porous materials (for composites, these features are not straightforwardly interconnected!) should lead to an improvement of the electrochemical characteristics, but the regime in which the material is to operate should be considered carefully.

Acknowledgements. The results presented in the lecture were realized due to the financial support of the Ministry of Science of the Republic of Serbia, Projects No. 142048B and 142061B.

И З В О Д

СУПЕРКОНДЕНЗАТОРСКЕ КАРАКТЕРИСТИКЕ ЕЛЕКТРОХЕМИЈСКИ АКТИВНИХ ПОРОЗНИХ МАТЕРИЈАЛА

ВЛАДИМИР В. ПАНИЋ

Институт за хемију, технологију и металургију, Центар за електрохемију, Његошева 12, 11000 Београд

У оквиру предавања су приказани резултати испитивања капацитивних карактеристика електрохемијски активних превлака оксида племенитих метала формираних на титанском носачу и композитних угљенично–оксидних материјала као најчешћих типова планарних порозних електрода. Капацитивна својства ових електрода испитивана су у функцији њиховог састава, услова под којима су добијени оксиди и превлаке, карактеристика угљеничног носача и састава електролита, методама цикличне волтаметрије и спектроскопије електрохемијске импеданције. Резултати електрохемијских метода корелисани су са могућом структуром ових материјала коју дефинише контолисани процес добијања оксида сол–гел поступком.

(Примљено 27. марта 2008)

REFERENCES

1. B. Conway, *Electrochemical Supercapacitors: Scientific Fundamentals and Technological Applications*, Plenum Publishers, New York, 1999
2. Yu. Chizmadzev, Yu. Chirkov, in *Comprehensive Threatise of Electrochemistry Vol. 6*, E. Yeager, J. Bockris, B. Conway, S. Sarangapani, Eds., Plenum press, New York, 1983, Ch. 5
3. T. D. Jarvi, E. M. Stuve, in *Electrocatalysis*, J. Lipkowski, P. N. Ross, Eds., Wiley, New York, 1998
4. N. R. Elezović, B. M. Babić, Lj. M. Vračar, N. V. Krstajić, *J. Serb. Chem. Soc*. **72** (2007) 699
5. A. V. Tripković, S. Lj. Gojković, K. Dj. Popović, J. D. Lović, *J. Serb. Chem. Soc*. **71** (2006) 1333
6. B. M. Babić, B. V. Kaludjerović, Lj. M. Vračar, V. Radmilović, N. V. Krstajić, *J. Serb. Chem. Soc*. **72** (2007) 773
7. N. S. Marinković, R. R. Adžić, *J. Serb. Chem. Soc*. **71** (2006) 945
8. S. Buller, E. Karden, D. Kok, R. W. De Doncker, *IEEE Trans. Ind. Appl*. **38** (2002) 1622
9. N. D. Nikolić, *J. Serb. Chem. Soc*. **71** (2007) 1083
10. K. Kinoshita, *Carbon – Electrochemical and Physicochemical Properties*, Wiley, New York, 1988
11. F. Raimondi, G. G. Scherer, R. Kötz, A. Wokaun, *Angew. Chem. Int. Ed.* **44** (2005) 2190
12. V. Panić, A. Dekanski, S. Gojković, V. Mišković-Stanković, B. Nikolić, *Mater. Sci. Forum* **453-454** (2004) 133
13. V. Panić, A. Dekanski, S. Gojković, S. Milonjić, V. B. Mišković-Stanković, B. Nikolić, *Mater. Sci. Forum* **494** (2005) 235
14. V. Panić, A. Dekanski, S. Milonjić, V. B. Mišković-Stanković, B. Nikolić, *J. Serb. Chem. Soc.* **71** (2006) 1173
15. V. Panić, A. Dekanski, S. Milonjić, R. Atanasoski, B. Nikolić, *Electrochim. Acta* **46** (2000) 415
16. V. V. Panić, B. Ž. Nikolić, *J. Serb. Chem. Soc.* **72** (2007) 1393
17. V. V. Panić, T. R. Vidaković, A. B. Dekanski, V. B. Mišković-Stanković, B. Ž. Nikolić, *J. Electroanal. Chem.* **609** (2007) 120.

www.shd.org.rs

Journal of the Serbian Chemical Society

JSCS@tmf.bg.ac.yu • www.shd.org.rs/JSCS

J. Serb. Chem. Soc. 73 (6) 665–671 (2008)
JSCS–3749

UDC 615.33:543.544.5:543–76
Original scientific paper

A rapid and reliable determination of doxycycline hyclate by HPLC with UV detection in pharmaceutical samples

SNEŽANA S. MITIĆ[1], GORDANA Ž. MILETIĆ[1], DANIJELA A. KOSTIĆ[1]*, DANIELA Č. NASKOVIĆ-ĐOKIĆ[2], BILJANA B. ARSIĆ[1#] and IVANA D. RAŠIĆ[1]

[1]*Department of Chemistry, Faculty of Natural Sciences and Mathematics, Višegradska 33, 18000 Niš and* [2]*D. D. "Zdravlje–Actavis" – Pharmaceutical and Chemical Company, 16000 Leskovac, Serbia*

(Received 14 September, revised 7 November 2007)

Abstract: An accurate, sensitive and reproducible high performance liquid chromatographic (HPLC) method for the quantification of doxycycline hyclate in pharmaceutical samples has been developed and validated. The drug and the standard were eluted from a Lichrosorb RP-8 (250 mm×4.6 mm, 10 μm particle size) at 20 °C with a mobile phase consisting of methanol, acetonitrile and 0.010 M aqueous solution of oxalic acid (2:3:5, v/v/v). The flow rate was 1.25 ml min^{-1}. A UV detector set at 350 nm was used to monitor the effluent. Each analysis required no longer than 4 min. The limits of detection and quantification were 1.15 and 3.84 μg ml^{-1}, respectively. Recoveries for different concentrations ranged from 99.58 to 101.93 %.

Keywords: high performance liquid chromatography; doxycycline hyclate; ultraviolet detection.

INTRODUCTION

Doxycycline ($C_{22}H_{24}N_2O_8 \cdot H_2O$, molecular mass 462.5 g mol^{-1}, CAS number: 17086-28-1), is the monohydrate of (4*S*,4a*R*,5*S*,5a*R*,6*R*,12a*S*)-4-(dimethylamino)-1,4,4a,5,5a,6,11,12a-octahydro-3,5,10,12,12a-pentahydroxy-6-methyl-1,11-dioxonaphthacene-2-carboxamide, a substance obtained from oxytetracycline or metacycline or by other means.[1] It is a broad spectrum anti-bacterial tetracycline derivative with a wide range of activity against gram positive and gram negative organisms, including *Spirochetes, Actinomyces* sp., and *Mycoplasma* sp.[2] It is the drug of choice in the treatment of sexually transmitted diseases.[3] Doxycycline is preferred to other tetracyclines in the treatment of specific infections because of its fairly reliable absorption and its long half-life, which permits less frequent dosage. Doxycycline hyclate ($C_{22}H_{24}N_2O_8 \cdot HCl \cdot 0.5C_2H_5OH \cdot 0.5\ H_2O$, molecular

* Corresponding author. E-mail: dan69@bankerinter.net
# Serbian Chemical Society member.
doi: 10.2298/JSC0806665M

mass 512.94 g mol^{-1}, CAS number: 24390-14-5) is the hydrochloride hemiethanol hemihydrate of doxycycline. The synonym for doxycycline hyclate is doxycycline hydrochloride. Doxycycline hyclate is much more soluble than doxycycline monohydrate, which is one of the main reasons for it more frequent use in pharmaceutical samples. One of the broadly used and important veterinary pharmaceuticals is Tiadox powder. It is a complex powder with doxycycline hyclate as the main component.

Various methods for determination of doxycycline *in vitro* and *in vivo* have been reported. These include microbiology,[4] fluorimetry,[5] TLC-fluorescence scanning densitometry[6] and HPLC[7–17] for the determination of doxycycline in biological materials. HPLC was also applied for the determination of doxycycline in pharmaceutical formulations.[18] Various chromatographic methods have also been reported for the determination of doxycycline in human tissues[19] and foods.[20,21] Derivative spectrophotometry (pharmaceuticals, urine and honey)[22] and sequential injection chromatography (SIC) methods (pharmaceutical preparations)[23] for the determination of doxycycline have also been developed. Reviewing literature data, it was concluded that there are a few methods reported for the determination of doxycycline hyclate in pharmaceutical samples (spectrophotometric methods[24–26] and HPLC methods[27,28]). The standard procedure is given in the British Pharmacopoeia.[29]

HPLC offers several advantages over other techniques, including minimal sample manipulation before chromatography, rapid analysis and the simultaneous analysis of multiple compounds with good specificity, precision and accuracy. For this reason, a fast, simple method for the determination of doxycycline hyclate in the mentioned veterinary powder (Tiadox powder) was developed and is presented in this paper. The proposed method is reproducible, reliable and permits more samples to be analyzed in a short period of time.

EXPERIMENTAL

Reagents and chemicals

Doxycycline was obtained from PromoChem, Teddington, United Kingdom. All the employed solvents were of HPLC grade, while other chemicals were of spectroscopic grade and were obtained from Merck (Darmstadt, Germany). The Pharmaceutical Industry "Actavis", Leskovac, supplied the Tiadox powder. It consists of various ingredients, among them doxycycline hyclate (10.0 g doxycycline hyclate per 100 g of Tiadox powder) represents the only active component.

HPLC apparatus and conditions

The HPLC system consisted of an Agilent 1100 series isocratic LC system, an Agilent 1100 series variable wavelength detector SL and a Hewlett Packard 1000 data system (Agilent Technologies, Inc., Santa Clara, CA, USA). The detector wavelength was set at 350 nm. The mobile phase consisted of methanol:acetonitrile:0.010 M oxalic acid (2:3:5, v/v/v). Routine degassing of the mobile phase was performed by passing it through a 0.45 μm membrane filter (Millipore, Bedford, MA, USA). The mobile phase was pumped isocratically at a flow rate of 1.25 ml min^{-1} at 20 °C. The injection volume was 50 μl.

Stock solutions

Doxycycline hydrochloride (25 mg) was dissolved in 25 ml of mobile phase. The working solution was obtained by dilution of 1.0 ml of the stock solution to 10 ml with mobile phase.

Assay procedure

Tiadox powder (250 mg) was dissolved in 25 ml of mobile phase. This solution (1.0 ml) was diluted to 10 ml with mobile phase.

RESULTS

Assay validation

A high performance liquid chromatographic method for the quantification of doxycycline hyclate concentrations in a pharmaceutical sample (Tiadox powder) was developed. The active ingredients were monitored by measurement of the peak area of both doxycycline hyclate from Tiadox powder and the standard, and the ratio of the peak areas was calculated. The specificity of the chromatographic method was determined by the screening of a placebo solution and the assay solution. The placebo solution was prepared in the same manner as the investigated solution but without doxycycline hyclate. Typical chromatograms of the standard and assay solution are presented in Figs. 1 and 2, respectively.

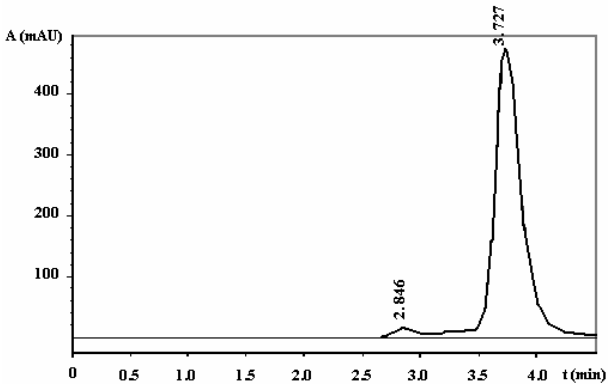

Fig. 1. Representative chromatogram of a standard solution of doxycycline hyclate.

Linearity

The linearity was checked on samples of standard doxycycline hydrochloride at five different concentrations (25.2–252.0 μg ml^{-1}).

A regression curve was constructed:

$$y = 77498x - 72.455, \text{ with } R^2 = 0.9997$$

where x represents concentration in μg ml^{-1}, y represents the HPLC peak area, which was automatically measured by an integrator of the HPLC instrument, and R is the correlation coefficient. The calculations were performed on a personal computer using the Microsoft Excel program (Version 2003, Microsoft Co., Redmond, USA, 2003).

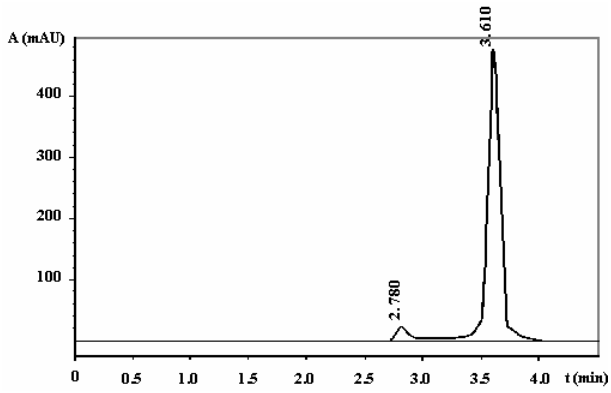

Fig. 2. Representative chromatogram of an assay solution – – Tiadox powder.

Accuracy

The accuracy of the method was checked by determining recovery values. Series of solution were made containing 80, 100 and 120 % of doxycycline hyclate regarding the declared content. The results are presented in Table I.

TABLE I. Accuracy of the method

Concentration g/100g	Recovery %	*N*	x_{sr}	*SD*	*RSD* %
8.00	101.7	3	101.5	0.1819	0.1809
	101.4				
	101.4				
10.00	101.8	3	100.5	1.108	1.102
	100.2				
	99.6				
12.00	100.8	3	101.6	0.6264	0.6167
	101.9				
	101.9				

Limit of detection and quantification

The limit of detection (*LOD*) and quantification (*LOQ*) were calculated according to the following formula:

$$LOD = 3S_{do}/b_{sr} = 1.15 \text{ μg ml}^{-1}$$

$$LOQ = 10S_{do}/b_{sr} = 3.84 \text{ μg ml}^{-1}$$

where S_{do} is the standard deviation of the response and b_{sr} is the mean value of the slope of the calibration curve constructed during the linearity determination.

Precision

The precision was determined by measuring five sample probes under the same experimental conditions. The obtained results are given in Table II, together with the calculated values of their standard deviation, *SD*, and relative standard deviation, *RSD*.

TABLE II. Precision of the method

N	Content of doxycycline hyclate in Tiadox powder, g/100g	x_{sr}	*SD*	RSD %
5	9.98 9.71 9.81 9.78 9.82	9.82	0.0992	1.01

The method is precise since $RSD < RSD_{max}$. RSD_{max} is 2 %, which represents the maximum allowed value of the *RSD* for HPLC methods according to the Pharmacopoeias.

DISCUSSION

A comparison of the proposed method with other methods is given in Table III. The results obtained by the proposed method have an *RSD* of 1.01 %, better than that reported by Šatínský *et al.*[22], Salinas *et al.*[23] and Lopez-Paz and Martinez Calatayud.[24] The first two methods[22,23] have relatively high *RSD* values, higher than RSD_{max}. This suggests that the proposed method is more precise than some of the previously published methods. The *LOD* values[22,23] were also a little higher than in the method described in this paper. Mahrous and Abdel-Khalek[25] described a long pre-treatment of the drug through mixing with acetic acid and sodium cobalt nitrite, then boiling the mixture, followed by cooling. In addition, the same author[26] described a determination employing ammonium vanadate. On the other hand, Hoogmartens *et al.*[27] revealed a method for the determination of doxycycline hyclate by HPLC using poly(styrene–divinylbenzene) packing materials. Estimates for the repeatability and reproducibility of the method, expressed as relative standard deviations of the results of the determination of doxycycline hyclate, were found to be 0.90 and 1.20 %, respectively. The authors[27] used a complex mobile phase, consisting of 2-methyl-2-propanol, 0.2 M potassium hydrogen phosphate buffer, tetrabutylammonium hydrogen sulfate and 0.10 M Na_2EDTA. Using this mobile phase system, the analysis time is about 20 min, which is 5 times longer, compared to the method proposed in this paper.

TABLE III. Comparison of the proposed method with other methods for the determination of doxycycline hyclate in pharmaceutical preparations

Ref.	Concentration range, μg ml^{-1}	*RSD*[a] %	Recovery %	*LOD* μg ml^{-1}	Comments, conditions
This paper	25.20–252.00	1.01	100.2	1.15	HPLC, UV detection
22	2.00–100.00	5.05	99.3 102.8	2.00	Sequential injection chromatography
23	–	0.78–5.00[b]	95	0.6-3.00[b]	Derivative spectrophotometry
24	10.00–80.00	1.40[d]	2.3[c]	–	FIA-spectrophotometry

Table III. Continued

Ref.	Concentration range, μg ml^{-1}	*RSD*[a] %	Recovery %	*LOD* μg ml^{-1}	Comments, conditions
25	10.00–30.00	–	100.3	–	Spectrophotometry
26	20.00–100.00	–	99.6	–	Spectrophotometry
28	–	0.1–1.7[e]	92–107[e]	–	HPLC, UV detection

[a]*RSD* values were taken and compared for concentrations of ≈ 10 μg ml^{-1} of doxycycline; [b]ranges of *RSD* and *LOD* values at different first-derivative signals; [c]relative error; [d]*RSD* for samples containing 2.5 μg ml^{-1} of doxycycline; [e]recovery range for different pharmaceuticals

CONCLUSION

The proposed HPLC method provides a rapid, sensitive, accurate, and reproducible determination of doxycycline hyclate in pharmaceutical samples, without sample derivatization.

Acknowledgements. The presented study is a part of the grant number 142015, supported by the Ministry of Science of the Republic of Serbia.

И З В О Д

БРЗО И ПОУЗДАНО ОДРЕЂИВАЊЕ ДОКСИЦИКЛИН-ХИКЛАТА МЕТОДОМ HPLC СА UV ДЕТЕКЦИЈОМ У ФАРМАЦЕУТСКИМ УЗОРЦИМА

СНЕЖАНА С. МИТИЋ[1], ГОРДАНА Ж. МИЛЕТИЋ[1], ДАНИЈЕЛА А. КОСТИЋ[1], ДАНИЕЛА Ч. НАСКОВИЋ-ЂОКИЋ[2], БИЉАНА Б. АРСИЋ[1] И ИВАНА Д. РАШИЋ[1]

[1]Одсек за хемију, Природно–математички факултет, Вишеградска 33, 18000 Ниш и
[2]Д. Д. "Здравље–Актавис" – Фармацеутска и хемијска компанија, 16000 Лесковац

Тачна, осетљива и репродуктивна метода високо ефективне течне хроматографије (HPLC) за квантификацију доксициклин-хиклата у фармацеутским узорцима је развијена и потврђена. Лек и стандард су елуирани са колоне Lichrosorb RP-8 (250 mm×4,6 mm, величине честице од 10 μm) на 20 ºC са мобилном фазом која се састојала од метанола, ацетонитрила и 0,010 M воденог раствора оксалне киселине (2:3:5, v/v/v). Брзина протока је била 1,25 ml min^{-1}. За праћење ефлуента коришћен је UV детектор подешен на 350 nm. Свака анализа је трајала не дуже од 4 минута. Граница детекције је 1,15, док је граница квантификације 3,84 μg ml^{-1}. Ефикасност за различите концентрације се креће од 99,6 до 101,9 %.

(Примљено 14. септембра, ревидирано 7. новембра 2007)

REFERENCES

1. *British Pharmacopoeia*, The Stationary Office Ltd., London, 2001, pp. 526, 527
2. A. L. Cinquina, F. Longo, G. Anastasi, L. Giannetti, R. Cozzani, *J. Chromatogr. A* **987** (2003) 227
3. N. Joshi, D. Q. Miller, *Arch. Intern. Med.* **157** (1997) 1421
4. O. Cars, D. M. Ryan, *Scand. J. Infect. Dis. Suppl.* **53** (1988) 18
5. C. Van den Bogert, A. M. Kroon, *J. Pharm. Sci.* **70** (1981) 186
6. H. Z. Xie, C. Dong, Y. L. Fen, C. S. Liu, *Anal. Lett.* **30** (1997) 79
7. A. Zarghi, A. Kebriaeezadeh, R. Ahmadkhaniha, *Bll. Chim. Farm.* **140** (2001) 112
8. J. Klimes, M. Dohnalova, J. Sedlacek, *J. Chromatogr. A* **846** (1999) 181

9. M. Lavda, C. E. Clausnitzer, J. D. Walters, *J. Periodontol.* **75 (2**004) 1663
10. J. M. Prevosto, B. Beraud, V. Cheminel, Y. Gaillard, C. Mounier, J. F. Chaulet, *Ann. Biol. Clin.* **53** (1995) 29
11. J. L. Riond, K. M. Hedeen, K. Tyczkowska, J. E. Riviere, *J. Pharm. Sci.* **78** (1989) 44
12. N. Ruz, M. Zabala, M. G. Kramer, M. A. Campanero, M. C. Dios-Vieitez, M. J. Blanco--Prieto, *J. Chromatogr. A* **1031** (2004) 295
13. D. Farin, G. Piva, I. Gozlan, R. Kitzes, *Chromatographia* **47** (1998) 547
14. B. Axisa, A. R. Naylor, P. R. F. Bell, M. M. Thompson, *J. Chromatogr. B* **744** (2000) 359
15. M. D. Santos, H. Vermeersch, J. P. Remon, M. Schelkens, P. De Backer, R. Ducatelle, F. Haesebrouck, *J. Chromatogr. B* **682** (1996**)** 301
16. I. A. Alsarra, E. M. Niazy, Y. M. Al-Sayed, K. I. Al-Khamis, M. El-Awad Ibrahim, *Saudi Pharm. J*. **13** (2005) 42
17. P. N. Newton, J.-F. Chaulet, A. Brockman, W. Chierakul, A. Dondorp, R. Ruangveerayuth, S. Looareesuwan, C. Mounier, N. J. White, *Antimicrob. Agents Chemother.* **49** (2005) 1622
18. L. Monser, F. Darghouth, *J. Pharm. Biomed. Anal.* **23** (2000) 353
19. H. J. C. F. Nelis, A. P. De Leenheer, *Clin. Chim. Acta* **103** (1980) 209
20. H. Oka, Y. Ito, H. Matsumoto, *J. Chromatogr. A* **882** (2000) 109
21. X. Ding, S. Mou, *J. Chromatogr. A* **897** (2000) 205
22. F. Salinas, J. J. Berzas Nevado, A. Espinosa, *Analyst* **114** (1989) 1141
23. D. Šatínský, L. M. L. Dos Santos, H. Sklenářová, P. Solich, M. C. B. S. M. Montenegro, A. N. Araújo, *Talanta* **68** (2005) 214
24. J. L. Lopez Paz, J. Martinez Calatayud, *J. Pharm. Biomed. Anal.* **11** (1993) 1093
25. M. S. Mahrous, M. M. Abdel-Khalek, *Talanta* **31** (1984) 289
26. M. M. Abdel-Khalek, M. S. Mahrous, *Talanta* **30** (1983) 792
27. J. Hoogmartens, N. H. Khan, H. Vanderhaeghe, A. L. Van der Leeden, M. Oosterbaan, G. L. Veld-Tulp, W. Plugge, C. Van der Vlies, D. Mialanne, R. Melamed, *J. Pharm. Biomed. Anal.* **7** (1989) 601
28. K. Dihuidi, M. J. Kucharski, E. Roets, J. Hoogmartens, H. Vanderhaeghe, *J. Chromatogr. A* **325** (1985) 413
29. *British Pharmacopoeia 98/34/EEC*, The Stationary Office, London, 2005.

www.shd.org.rs

Journal of the Serbian Chemical Society

JSCS@tmf.bg.ac.yu • www.shd.org.rs/JSCS

J. Serb. Chem. Soc. 73 (6) 673–680 (2008)
JSCS–3750

UDC 553.492.004.54:504.53:58.051
Original scientific paper

Methods for the determination of the form of aluminium: Pseudogley soils

VESNA MRVIĆ[1]*, MIODRAG JAKOVLJEVIĆ[2], DRAGI STEVANOVIĆ[2], DRAGAN ČAKMAK[1] and MIRJANA ZDRAVKOVIĆ[1]

[1]*Institute of Soil Science, Teodora Drajzera 7, Belgrade and* [2]*Faculty of Agriculture, Nemanjina 6, Zemun, Serbia*

(Received 26 November 2007, revised 18 March 2008)

Abstract: Exchangeable aluminium (Al_{KCl}) and $CaCl_2$-extractable aluminium (Al_{CaCl_2}) have approximately the same value in the prognosis of detrimental effect on plants. Additional, more in-depth research should show which of the two applied methods of exchangeable Al determination is more suitable (after Sokolov or using aluminon). The contents of total Al and amorphous Al increase with depth and percentage clay. Crystalline Al oxides and $CuCl_2$-extractable aluminium (Al_{CaCl_2}) and EDTA-extractable aluminium (Al_{EDTA}) represent the more mobile reserves of Al and they depend mostly on changes in the acidity parameters of the soil. Exchangeable Al is on average 4.3–4.7 times lower than the contents of Al_{CaCl_2} and Al_{EDTA}, 8 times lower than crystalline Al and 35 times lower than amorphous Al. Some methods are not sufficiently selective, hence further research is required to achieve more favourable methods for the determination of the different forms of Al.

Keywords: exchangeable Al; Al oxalate; Al dithionate; $CuCl_2$ extractable Al; organic Al.

INTRODUCTION

Aluminium is the most represented metal in rocks and soil; on average it accounts for about 7–8 %. In soil, it is found in primary and secondary alumino--silicates, hydrated Al oxides, in the form of compounds with inorganic ligands, bound to organic matter, in allophanes, imogolites, various forms of short-range order materials, exchangeably adsorbed and fixed (in interstratified three-layered minerals), as well as in the soil solution.[1–3]

Knowledge of the total Al and other forms not readily available to plants is significant in order to determine, primarily, the paedogenetic processes and the reserves of mobile aluminium. Paedological research usually deals with the contents of crystalline and amorphous Al oxides (along with Fe oxides). These are

* Corresponding author. E-mail: vesnavmrvic@yahoo.com
doi: 10.2298/JSC0806673M

determined by various methods: Al and Fe organic, most often by the method using pyrophosphate; total non-siliceous using the dithionate method and amorphous oxides by the oxalate method.[4,5] However, the applied methods are less specific to Al than to Fe, hence they often render unreal results.[6] More recent studies include the distinction between non-crystalline and different quasi-crystalline forms of Al in vermiculite interlayers and other non-crystalline forms, as well as the determination of crystalline oxides (sodium citrate–dithionate) and non-crystalline oxides (acid NH_4 oxalate in the dark).[2] Employing the above methods, some authors studied the contents of different forms of Al in several soil types, their correlations and the relation with toxic forms of Al.[7–9]

The content of available Al (exchangeable and in the soil solution) is essential for the evaluation of the risk of plant production on acid soils, in which it can occur in toxic concentrations for plants and micro-organisms.[10] Exchangeable Al (active, mobile) is plant-available Al and it is extracted using non-buffered solutions of neutral salts (mainly 1.0 M KCl). This form is usually determined employing the standard method with titration (Sokolov), but some authors also recommended a colorimetric method with aluminon.[1] In addition to extraction using a highly ionic reagent, such as 1.0 M KCl, phytotoxic Al can be determined by extraction using a 0.010 M solution of $CaCl_2$,[11] which is advantageous because it has an ionic dependence comparable to that of natural soil and is in more direct relation with Al in the soil solution, because it extracts a smaller part of the exchangeable Al.[12]

There have only been a few studies on the different forms of Al and their inter-relationship in Serbian soils. The aim of this study was to determine the content and relations of different forms of Al (available and non-available) in acid soils, type pseudogley (occupying 6 % of the area of Serbia), using some relatively novel chemical methods, taking into account their significance both in paedological research and in the field of soil chemistry and environmental protection.

EXPERIMENTAL

The soil samples were taken at 30 sites under lowland Pseudogleys in Nortwest Serbia (Jabučje, Bajevac, Debrc, Varna, Lipolist, Brankovina, Klašnić), East Serbia (Salaš, Kladovo, Karbulovo) and in the valley of the river Zapadna Morava (Samaila, Čibukovac, Podunavci, Globoder, Kruševac), from three characteristic horizons (Ah, Eg, EBtg and Btg). The basic characteristics of the soil samples were determined by standard methods: pH in H_2O and 1.0 M KCl – potentiometrically; humus – after Kotzman; available P and K–Al method of Egner–Riehm; adsorptive complex of soil (H, T, S) – after Kappen; soil texture – combined method of sieving and the pipette method. Exchangeable Al (Al_{KCl}) was determined by two methods: after Sokolov – extraction with 1.0 M KCl (1:2.5), shaken for 1 h, titration and spectrophotometrically with aluminon[1] – extraction with 1.0 M KCl (1:10), shaken for 30 min and using an aluminon–acetate buffer.

In selected samples phytotoxic Al was also determined – extraction with 0.010 M $CaCl_2$, (1:5), shaken for 1 h using aluminon (Al_{CaCl_2}).[8,11]

At 15 sites, soil samples from three characteristic horizons were taken and in them less available forms of Al were determined with different reagents:

− Na citrate-dithionite solution (Al_{dit}, crystalline oxide): 5.0 g soil was shaken for 1 h with 50 ml of a solution containing 0.15 M Na citrate, 0.050 M citric acid and 2 g dm^{-3} Na dithionite;[7]

− ammonium oxalate solution in the dark (Al_{oxa}, amorphous oxide): 1.0 g soil was shaken in the dark for 4 h with 50 ml of acidified 0.20 M NH_4 oxalate at pH 3.25;[7]

− $CuCl_2$ (Al_{Cu}): 3.0 g soil was shaken for 2 h with 30 ml 0.50 M $CuCl_2$;[13,14]

− EDTA (Al_{EDTA}): 5.0 g soil was shaken for 1 h with 50 ml 0.25 M EDTA (pH 7.0, modification as in the original method 0.50 M EDTA was used).[15]

All the suspensions were centrifuged for 20 min at 2500 relative centrifugal force and filtered (Whatman 42) and the content of Al was determined by AAS with a N_2O–C_2H_2 flame.

The total Al was determined by digestion with HF and perchloric acid and then by AAS.[1]

The results were processed by mathematical–statistical methods of regression analysis and descriptive statistics (program SPSS 10.0.).

RESULTS

The characteristics of pseudogleys are very variable depending on the site and profile depth. Pseudogleys are characterised by lighter soil texture of the eluvial horizons and clay accumulation in the hardly permeable illuvial horizon (Table I). The soils were acidic, except the pseudogleys in Debrc and Kladovo, which were neutral, thanks to the application of liming. Of the total number of samples, 60 % were in the category of very acid soils (pH in KCl ≤ 4.5) and acidity increased slightly with depth. The content of humus in the Ah horizon was below 2 % in about half the samples. The values of cation adsorption capacity (*T*) and of the composition of adsorbed cations (*S* and *H*) varied depending on the pH value, the quantity and composition of organic and mineral colloid particles. Despite their acid reaction, most pseudogleys were rich in base cations, according to other investigations.[16] Only the most acid pseudogleys at two sites in West Serbia (Samaila and Klašnić) were dystric.

The exchangeable Al was determined by two methods. The method with aluminon was preferable because the Al is read directly (not with the total exchangeable acidity) and the uncertainty of detecting the discoloration which occurs in titration was avoided.

The values of exchangeable Al determined by the Sokolov method (non-multiplication with 1.75) ranges from 0–32.4 mg/100g (average 5.93) and by the method with aluminon, the average content Al was 5.26 mg/100g (88.4 % of the values determined by the Sokolov method). Their correlation is high but there are some variations, therefore more in-depth research would show an appropriate method (Fig. 1).

The exchangeable Al increased with depth, especially sharply in the illuvial horizon. The method of simple correlation (quadratic function) shows that the changes of exchangeable Al are maximally affected by the parameters of soil

acidity: pH in H_2O (R = –0.78), pH in KCl (R = –0.86), hydrolytic acidity H (R = 0.85) and V (R = –0.63).

TABLE I. Statistical parameters of the basic characteristics of the pseudogley soils

Horizon	Stat. param.	Total sand	Silt	Clay	pH		Humus %	*H*	*S*	*T*	*V* / %	Al mg/100g	
		%			H_2O	KCl		meq/100g				Sok.	Alum.
Aoh	Min	31.40	17.40	15.50	4.75	3.45	1.17	1.30	4.83	15.42	18.80	0.0	0.0
	Max	67.10	42.20	34.30	7.30	6.80	4.13	20.88	36.52	37.83	96.55	19.80	23.76
	Aver.	41.64	32.80	25.56	5.62	4.63	2.34	8.70	14.91	23.61	62.93	2.05	2.49
	Sd	9.81	7.24	4.48	0.47	0.64	0.79	4.11	5.32	4.35	14.70	4.82	6.27
Eg	Min	26.10	16.50	14.90	4.85	3.60	0.12	2.27	8.04	13.64	31.34	0.09	0.0
	Max	68.60	40.10	43.40	6.40	5.70	3.51	17.62	22.84	34.68	88.22	23.13	19.91
	Aver.	40.38	31.68	27.94	5.54	4.40	1.41	8.59	14.66	23.24	63.48	2.85	2.90
	Sd	9.95	7.00	6.10	0.32	0.45	0.81	3.63	3.75	4.41	12.75	5.21	5.21
EBtg or	Min	24.00	15.20	21.3	4.70	3.20	0.01	2.57	10.05	15.35	38.12	0.0	0.0
Btg	Max	61.40	38.10	49.50	6.40	5.80	1.60	18.92	25.29	36.59	87.28	32.04	26.70
	Aver.	36.44	28.19	35.31	5.57	4.37	0.50	9.35	16.87	26.23	65.28	5.61	4.82
	Sd	9.94	6.31	8.44	0.42	0.68	0.44	4.22	3.57	5.31	11.38	8.80	6.93

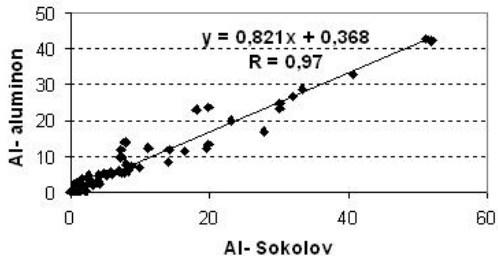

Fig. 1. Exchangeable Al determined by two methods (n = 90).

The release of Al from the reserves commences mainly at pH values ≤ 4.5 in KCl and is well explained by a linear function (Fig. 2).

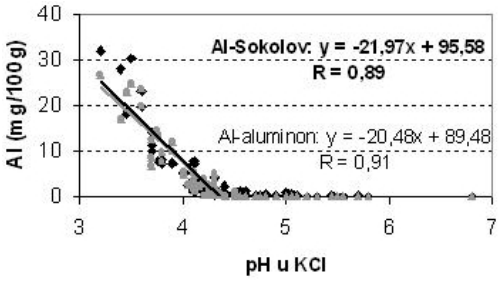

Fig. 2. Relation between pH of the KCl and the exchangeable Al.

The correlation of the exchangeable Al (Al_{KCl}, aluminon) and Al extracted with $CaCl_2$ (Al_{CaCl_2}) is high (Fig. 3). They have approximately the same value in the prognosis of detrimental effect on plants. The average values of the exchangeable Al were about 12 times higher than Al_{CaCl_2}.

The sources of available Al in soil are the less available forms. The content of these forms depends on the composition of the parent rock, the intensity of the leaching processes of clay and other colloids, on the destruction process, the content of organic matter and other soil characteristics.

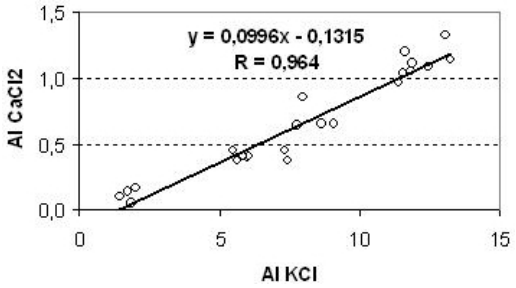

Fig. 3. Relation between Al_{KCl} and Al_{CaCl_2}.

The content of total and amorphous Al increased with depth, which is related to the leaching of colloid particles and Fe and Al oxides in the illuvial horizon (Figs. 4a and 4b). Amorphous Al accounts for on average 1.8 % of the total Al and in the Eg and Btg horizons and a significant, medium correlation between these two forms exists (R = 0.58 and 0.66, respectively).

The concentrations of crystalline Al oxides were less, ranging from 17–51 mg/100 g and had a medium correlation with Al_{oxa} (R = 0.60). The values were changed under the effect of the acidity parameters: pH in H_2O (R = –0.66), pH in KCl (R = –0.53), hydrolytic acidity (R = 0.71) and V (R = –0.54).

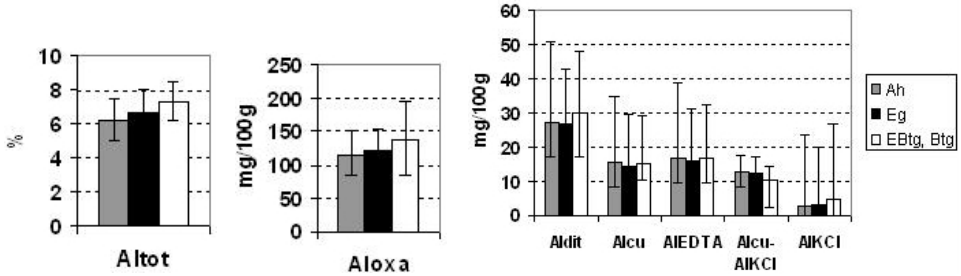

Fig. 4. Content of less available forms of Al per horizon (average, minimum and maximum).

The Al extracted with 0.50 M $CuCl_2$ is Al which forms low and medium stable complexes with organic matter,[13] and this reagent and pyrophosphate are suitable for the determination of organic Al in organic-rich mineral horizons.[9] The aluminium extracted with 0.50 M EDTA is also in good correlation with the organic matter in the soil.[7]

The values of the $CuCl_2$-extractable Al (Al_{Cu}) and EDTA-extractable aluminium (Al_{EDTA}) represent the more mobile reserves of Al and they depend mostly on the changes of the soil acidity parameters.

The average content $CuCl_2$-extractable Al (Al_{Cu}) was 15.02 mg/100g, *i.e.*, 92 % of the Al_{EDTA}, and their correlation is very high (R = 0.96). These forms show good correlation with Al_{dit} and the soil acidity parameters but also not with humus. A better correlation with humus was obtained if the Al_{KCl} was subtracted from Al_{Cu}, according to other authors,[8] and in this manner, the so-called unavailable exchangeable Al is obtained. This correlation was higher in the Ah horizon (values obtained with Al_{KCl} – aluminon, Fig. 5), and also in the Eg horizon (values obtained with Al_{KCl} – Sokolov: R_{ah} = 0.725, R_{Eg} = 0.740 and R_{Btg} = 0.510).

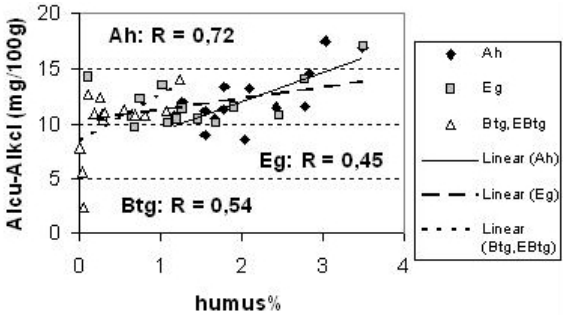

Fig. 5. Relation between humus content, %, and AlCu–AlKCl.

The relation between the available Al and the less available Al forms show that the values of the exchangeable Al are in low correlation with the total and amorphous Al, with Al_{dit} (crystalline) and Al_{EDTA} the correlation is medium (R = 0.71 and 0.73, respectively) and with Al_{Cu} it is high (R = 0.82). The exchangeable Al was on average 4.3–4.7 times lower than the content of Al_{Cu} and Al_{EDTA}, 8 times lower than the crystalline Al and 35 times lower than the amorphous Al. The inclusion also of other soil parameters, using the method of multiple linear regression, did not explain the changes in the exchangeable Al better.

DISCUSSION

The results of this study show that the content of exchangeable Al in pseudogleys is very variable depending on the locality and profile depth and its dynamics depends mostly on the change of the soil pH (active, exchangeable and hydrolytic acidity).

Compared to 1.0 M KCl, on using 0.50 M $CuCl_2$, 6–7 times more Al was on average extracted in the humus horizon, 5 times more in the eluvial horizon and about 3 times more in the illuvial horizon. $CuCl_2$ extracts potentially reactive organic and inorganic Al reserves, because Cu^{2+} is a strong complexation agent, hence it replaces Al from the organic matter and the acidity of the $CuCl_2$ solution can cause depolymerisation of hydroxyl–Al polymers.[13] In this study, it was shown that the value Al_{Cu}−Al_{KCl} in the more humus horizons represents Al bound to organic matter, while in the deeper horizons, $CuCl_2$ probably also extracts the polymerised hydroxyl–Al and the more soluble amorphous Al in the inorganic

phase of the soil, as also reported by the above authors for soil types Ultisol, Oxisol and Histosol.

According to the literature, amorphous Al is a more reactive reserve of Al than crystalline Al.[7,17,18] The present study showed a higher correlation of exchangeable Al with Al_{EDTA} and Al_{Cu} but also with Al_{dit} (crystalline). This could be explained by the fact that exchangeable Al contributes to a considerable extent to the Al reserves, which were shown to be potentially more mobile (especially in the deepest horizon): Al_{dit} on average 7–19 %, Al_{Cu} and Al_{EDTA} 13–37 %. Moreover, as already stated, some amorphous Al forms can also be extracted using EDTA and $CuCl_2$. The issue of selectiveness of the applied methods (also reported by other authors)[14] still remains, which draws attention to the need for further research of methods suitable for individual Al forms.

И З В О Д

МЕТОДЕ ЗА ОДРЕЂИВАЊЕ ОБЛИКА Al: ПСЕУДОГЛЕЈНА ЗЕМЉИШТА

ВЕСНА МРВИЋ[1], МИОДРАГ ЈАКОВЉЕВИЋ[2], ДРАГИ СТЕВАНОВИЋ[2], ДРАГАН ЧАКМАК[1] и МИРЈАНА ЗДРАВКОВИЋ[1]

[1]Институт за земљиште, Теодора Драјзера 7, Београд и [2]Пољопривредни факултет, Немањина 6, Земун

Размењиви алуминијум (Al_{KCl}) и Al екстрахован са $CaCl_2$ (Al_{CaCl_2}) имају приближно исту вредност у прогнози штетног дејства на биљке. Накнадна детаљнија испитивања треба да покажу која је од две примењене методе за одређивање размењивог Al (по Соколову и алуминоном) погоднија. Садржај укупног и аморфног Al се повећава са дубином и садржајем глине. Кристални Al и Al екстрахован са $CuCl_2$ (Al_{Cu}) и EDTA (Al_{EDTA}) представљају мобилније резерве Al и највише зависе од промена параметара киселости земљишта. Размењиви Al је просечно 4.3–4.7 пута мањи од садржаја Al_{Cu} и Al_{EDTA}, 8 пута мањи од Al кристалног и 35 пута од аморфног. Поједине методе нису довољно селективне, па је потребно даљим истраживањем доћи до погоднијих метода за облике Al.

(Примљено 26. новембра 2007, ревидирано 18. марта 2008)

REFERENCES

1. R. Barnhisel, P. M. Bertsch, *Methods of Soil Analysis – Chemical and Microbiological Properties*, SSSA and ASA, Madison, WI, 1982, p. 275
2. V. C. Farmer, *Eur. J. Soil Sci.* **50** (1999) 713
3. J. Choroverer, M. Amistad, O. Chadwik, *Geochem. Cosmochim. Acta* **68** (2004) 4859
4. J. A. McKeague, *Can. J. Soil Sci.* **47** (1967) 95
5. O. P. Mehr, M. L. Jackson, *National Conferention on Clays and Clay Minerals*, A. Swineford, Ed., Pergamon Press, London, 1958, p. 100
6. W. Mahaney, K. Sanmugadas, *Catena* **17** (1990) 563
7. S. C. Jarvis, *J. Soil Sci.* **37** (1986) 211
8. M. J. McLaughlin, T. G. Baker, T. R. James, J. A. Rundle, *Aust. J. Soil Res.* **28** (1990) 371
9. E. Garcia-Rodeja, J. C. Novos, X. Ponteverdra, A. Martiney-Cortiyas, P. Buurman, *Catena* **56** (2004) 155
10. T. Mossor-Pietrasyewska, *Acta Biochim. Pol.* **48** (2001) 673

11. P. B Hoyt, M. Nyborg, *Can. J. Soil Sci*. **52** (1972) 163
12. V. C. Baligar, G. V. E. Pitta, E. E. G. Gama, R. E. Schaffert, A. F. Bahia Filho, R. B. Clark, *Plant and Soil* **192** (1997) 9
13. A. S. R. Juo, E. J. Kamprath, *Soil Sci. Soc. Am. J.* **43** (1979) 35
14. P. M. Bertsch, P. R. Bloom, *Methods of Soil Analysis – Chemical Methods*, SSSA and ASA, Madison, WI, 1996, p. 518
15. V. C. Farmer, J. D. Russell, M. L. Berrow, *J. Soil Sci.* **31** (1980) 673
16. M. Jakovljević, N. Kostić, S. Antić-Mladenović, *Proceedings of Matica Srpska for natural sciences* **104** (2003) 11 (in Serbian)
17. M. Zysset, P. Blaser, J. Luster, A. U. Gehring, *Soil Sci. Soc. Am. J.* **63** (1999) 1106
18. Y. Yagasaki, J. Mulder, M. Okayaki, *Geoderma* **137** (2006) 40.

J. Serb. Chem. Soc. 73 (6) 681 (2008)

Errata

1. Issue No. 5 (2008), Vol. **73**, Contents (back cover):
   – Title of the paper by *V. V. Glodjović* and *S. R. Trifunović* should read: Stereospecific ligands and their complexes. Synthesis and characterization of the *s*-*cis*-K[Ru(*S,S*-eddp)Cl_2]·3H_2O